

# Diglyme as an electrolyte solvent for sodium-ion batteries

Deciphering degradation mechanisms and redox behaviour

Master's thesis in Applied Physics

KASPER WESTMAN



MASTER'S THESIS 2016

# Diglyme as an electrolyte solvent for sodium-ion batteries

Deciphering degradation mechanisms and redox behaviour

KASPER WESTMAN



**CHALMERS**  
UNIVERSITY OF TECHNOLOGY

Department of Physics  
*Division of Condensed Matter Physics*  
CHALMERS UNIVERSITY OF TECHNOLOGY  
Gothenburg, Sweden 2016

Diglyme as an electrolyte solvent for sodium-ion batteries  
Deciphering degradation mechanisms and redox behaviour  
KASPER WESTMAN

© KASPER WESTMAN, 2016

Supervisor: Romain Dugas, Chimie du solide et énergie, Collège de France, Paris  
Examiner: Patrik Johansson, Department of Physics, Chalmers University of Technology,  
Gothenburg

Department of Physics  
Division of Condensed Matter Physics  
Chalmers University of Technology  
SE-412 96 Gothenburg  
Telephone +46 31 772 1000

Typeset in L<sup>A</sup>T<sub>E</sub>X  
Gothenburg, Sweden 2016

Diglyme as electrolyte solvent for sodium-ion batteries  
Deciphering degradation mechanisms and redox behaviour  
Kasper Westman  
Department of Physics  
Chalmers University of Technology

## Abstract

For storing energy in future sustainable energy systems, sodium-ion batteries (SIB) have emerged as an alternative to the current state-of-the-art lithium-ion batteries (LIBs), since SIBs are potentially cheaper. For LIBs and SIBs alike, the development of stable systems depends on employing stable or metastable electrolytes, forming a SEI. Ether compounds have earlier been investigated for use in electrolytes, due to a presumed high reductive stability. In this project diglyme, an ether solvent, mixed with 1 M NaPF<sub>6</sub> has been evaluated for use with Na-metal reference electrodes and a SIB electrode platform comprising Na<sub>3</sub>V<sub>2</sub>(PO<sub>4</sub>)<sub>2</sub>F<sub>3</sub> (NVPF) and hard carbon (HC), and with a model system using Na<sub>3</sub>V<sub>2</sub>(PO<sub>4</sub>)<sub>3</sub> (NVP) at both electrodes. Furthermore, this electrolyte has been investigated for electrochemical stability, and for possible degradation mechanisms. Techniques used are galvanostatic cycling (GCPL), cyclic voltammetry (CV) and electrical impedance spectroscopy (EIS), coupling these to *ab-initio* calculations and physico-chemical characterisation methods. Using these techniques, Na-metal is shown to provide a stable reference electrode. In spite of the electrochemical stability of 1 M NaPF<sub>6</sub> in diglyme appearing promising when conducting CV, cells of NVPF|HC are shown to exhibit a  $\eta_c$  of 99.13 %, a high initial irreversibility (30 %), and an inferior capacity retention, when compared to equivalent cells using a EC<sub>50</sub>:DMC<sub>50</sub>-based electrolyte. NVP|NVP cells, on the other hand, show outstanding capacity retention and low initial irreversibility. The problems experienced in NVPF|HC cells are proposed to arise due to a set of different mechanisms: binder degradation, vanadium dissolution-deposition, and possibly reduction of the electrolyte. No coherent indications are given for the formation of an SEI. However, reduction schemes drawn still allow for undetectable reduction products. By independently exploring different voltage regions of the active materials the oxidative stability of 1 M NaPF<sub>6</sub> in diglyme is put to question despite earlier indications of stability. Future studies should aim to change the type of binder to avoid losses. NVP should be tested separately with both the active materials NVPF/HC to determine where most of the loss occurs along with further investigations to confirm if there is a reduction of the electrolyte at sodiated HC, since any lack thereof could point towards a future SEI-free system.

Keywords: Sodium-ion Batteries, Electrolytes, Diglyme, Electrolyte Degradation, Galvanostatic Cycling, Electrochemistry

## Acknowledgements

Firstly: my heartfelt thanks to Prof. Jean-Marie Tarascon and the group of Chimie du solide et énergie at Collège de France, both for accepting me in the lab, and for providing a warmhearted social context away from home. Relating to this, I am especially grateful for the invaluable support of Romain Dugas for being my supervisor and for teaching me the ways of battery research. Without his patience and pedagogy, I would not have been able to conduct this project. Yet another person deserving of special mention is my examiner Patrik Johansson, who took time to arrange this scientific exchange and who has given me continuous feedback on how to improve my work. Furthermore, I would like to acknowledge Rosa Palacín, Alexandre Ponrouch and Enrique Jiménez for valuable discussions and for taking care of me in Barcelona. I direct a special thanks to Enrique for helping me conduct FTIR-spectroscopy and to Alexander for helping me with the ionic conductivity-measurements.

I gratefully wish to acknowledge Grégory Gacuhot for helping me conduct GS/MS analysis and for teaching me about the basics of electrolyte reduction. I also wish to acknowledge Piotr Jankowski for providing me with DFT-calacualtion data regarding solvent reduction. Finally, I am thankful for the economical support received from Chalmers Master-Card Foundation, helping me cover my living-costs while in Paris.

Kasper Westman, Gothenburg, June 2016

# Contents

<b>List of Figures</b>	<b>xiii</b>
<b>List of Tables</b>	<b>xiv</b>
<b>List of Abbreviations</b>	<b>xv</b>
<b>1 Introduction</b>	<b>1</b>
1.1 Importance of Stable SIBs for a Future Energy System . . . . .	2
1.2 Aim . . . . .	4
1.3 Limitations . . . . .	4
<b>2 Batteries and SIBs</b>	<b>5</b>
2.1 Batteries–Primary and Secondary Galvanic Cells . . . . .	6
2.2 Electrolyte Fundamentals - Salts and Solvents . . . . .	9
2.3 Electrode-Electrolyte Interfaces and Interphases . . . . .	10
2.4 Sodium-ion Batteries . . . . .	11
2.4.1 SIB Anode Materials . . . . .	12
2.4.2 SIB Cathode Materials . . . . .	12
2.4.3 SIB Binders and Current Collectors . . . . .	14
2.4.4 SIB Electrolytes . . . . .	15
2.5 The Glyme Family of Solvents . . . . .	16
2.5.1 Metal Complexing Properties of Glymes . . . . .	17
2.5.2 Electrochemistry of Glymes . . . . .	17
2.5.3 Toxicity and Cost of Glymes . . . . .	18
<b>3 Description of Experiments</b>	<b>19</b>
3.1 Theory of Main Methods Employed . . . . .	20
3.1.1 Galvanostatic Cycling with Potential Limitation-GCPL . . . . .	20
3.1.2 Cyclic Voltammetry–CV . . . . .	21
3.1.3 Electrical Impedance spectroscopy–EIS . . . . .	21
3.1.4 Gas Chromatography, Mass spectrometry–GC/MS . . . . .	21
3.1.5 FTIR Spectroscopy . . . . .	22
3.2 Experimental Techniques–General Considerations . . . . .	22
3.2.1 Choice of Electrode Materials . . . . .	22
3.2.2 Tape-Cast Electrodes . . . . .	23
3.2.3 Powdered Electrodes . . . . .	24
3.2.4 Electrolyte Preparation . . . . .	24
3.2.5 Cell Assembly . . . . .	24
3.2.6 Coin Cells . . . . .	24

3.2.7	Swagelok Cells . . . . .	24
3.3	Electrolyte Stability with Na-metal . . . . .	26
3.3.1	Investigating Film Growth on Na Surfaces . . . . .	26
3.3.2	Investigating Gas Release from Electrolyte Decomposition . . . . .	26
3.3.3	Storage Experiment . . . . .	26
3.4	Ionic Conductivity and Viscosity . . . . .	26
3.5	Electrolyte Stability Window . . . . .	27
3.6	Galvanostatic Cycling Experiments . . . . .	28
3.6.1	Half-cell Capacity Tests of Diglyme Electrolytes . . . . .	28
3.6.2	Full Cell Capacity Tests of Diglyme Electrolyte - Galvanostatic Cycling . . . . .	28
3.6.3	Cycling Different Voltage-regions of the Active Materials . . . . .	29
3.6.4	Cycling of NVP/NVP Cells . . . . .	29
3.7	Physico-chemical Characterisation of Capacity Fade . . . . .	30
3.7.1	GC/MS of Cycled Cell Separators . . . . .	30
3.7.2	SEM and EDX Analysis of Cycled Anodes . . . . .	30
3.7.3	FTIR-Spectroscopy of Cycled Cells . . . . .	31
3.7.4	Binder Stability . . . . .	32
<b>4</b>	<b>Results and Discussion</b>	<b>33</b>
4.1	Stability of Na Electrodes . . . . .	34
4.1.1	Gas Evolution from Na Surfaces . . . . .	34
4.1.2	Impedance Evolution of Na Electrodes diglyme electrolyte . . . . .	34
4.1.3	Storing Na Metal in Electrolyte . . . . .	35
4.2	Ionic Conductivity of Diglyme-based Electrolyte . . . . .	36
4.3	ESW of the Diglyme-based Electrolyte . . . . .	36
4.3.1	Oxidative Stability of Diglyme-based Electrolyte . . . . .	37
4.3.2	Reductive Stability of Diglyme Electrolyte . . . . .	38
4.4	Characterising Loss and Performance . . . . .	39
4.4.1	Half Cell Capacity/Voltage Profiles . . . . .	40
4.4.2	Full Cell Capacity/Voltage Profiles . . . . .	40
4.4.3	Comparing Full and Half Cell Capacity Retention . . . . .	42
4.4.4	Comparing Efficiency and Irreversibility of Full and Half Cells . . . . .	44
4.4.5	Performance at Different Voltage Regions of the Cathode and Anode . . . . .	45
4.4.6	Another voltage range–NVP NVP-cells . . . . .	46
4.5	Investigating Degradation Mechanisms . . . . .	48
4.5.1	GC/MS Analysis of Degradation Products in Cycled Cells . . . . .	48
4.5.2	Reduction Schemes for Diglyme . . . . .	49
4.5.3	FTIR of Cycled HC Anodes . . . . .	50
4.5.4	Surface Structure of Pristine and Cycled HC . . . . .	52
4.5.5	EDX of Anodes from cycled Full Cells . . . . .	53
4.6	Test of Binder Defluorination . . . . .	55
4.7	Visual Summary of Degradation Mechanisms . . . . .	56
<b>5</b>	<b>Conclusions and Outlook</b>	<b>57</b>
	<b>Bibliography</b>	<b>59</b>
<b>A</b>	<b>Industrial Uses of Glymes With R=Me and n=1-4</b>	<b>I</b>
<b>B</b>	<b>Details of CVs From Half Cells</b>	<b>III</b>

<b>C Full Cell Reconstructions</b>	<b>IV</b>
<b>D Reduction Schemes for PVDF Binder</b>	<b>V</b>
<b>E Ionic Conductivity and Viscosity Data</b>	<b>VI</b>
<b>F Images of Swagelok Insulating Polymers After Cycling</b>	<b>VII</b>



# List of Figures

1.1	Map of world's most Li producing countries and the total mining output during 2015 [1]. . . . .	2
2.1	The fundamental principles of a galvanic cell. . . . .	6
2.2	Conventional components of an electrode coated on a metal current collector. . . . .	6
2.3	Molecular structure of some common solvents used in alkaline metal batteries. . . . .	10
2.4	Decomposition scheme taking a range of different Li-ion battery processes into account when using carbonate electrolytes. Reprinted with permission from [2]. Copyright 2011 American Chemical Society. . . . .	11
2.5	Intercalation of Na-atoms in turbostratic graphitic regions of HC and of Li-atoms between ordered layers of graphite . . . . .	12
2.6	The polyanionic NVPF. Each vanadium atom is in the middle of an octahedra bonding $\text{PO}_4^{3-}$ and $\text{F}^-$ speices. In the interlayer Na is intercalated. Rendered using VESTA [3]. . . . .	13
2.7	Schematic of the NVPF Na extraction mechanism looking down into the intercalation plane of Na : Showing 1) Extraction of the first sodium, 2) internal reorganisation into a 3) meta-stable phase and finally 4) extraction of the second reversible sodium. For each sodium extraction a vanadium changes oxidation state. Associated potentials of extraction are given vs. $\text{Na}^+/\text{Na}^\circ$ . Based on [4]. . . . .	13
2.8	Molecular structure of binders used in SIB electrodes. . . . .	14
2.9	Number of publications until 2015 of the different parts of a SIB. Light green bar is projection for 2015. Reproduced under the CC-BY licence from [5]. . . . .	15
2.10	Molecular structure of some salts used in SIBs. . . . .	16
2.11	General structure of glymes. "n" denotes chain length. . . . .	16
3.1	Principle of a three electrode setup. A current is measured between the counter and working electrodes. Voltages are, instead measured against a third, reference electrode. Image adopted with permission from [6]. . . . .	20
3.2	Principle of a GC/MS setup. . . . .	22
3.3	Sequence of electrode fabrication procedure featuring, a), tape cast precursor on both sides of Al current collector, b), scraped precursor and, c), punched electrodes with a set of current-collectors prepared for weighting . . . . .	23
3.4	Schematic of Coin cell assembly . . . . .	25
3.5	Schematic of Swagelock cell assembly . . . . .	25
3.6	Layout of pressure cell used for determining gas evolution from Na in contact with electrolyte. Based on illustration from [7]. . . . .	27
3.7	Experimental procedure used to compare degradation of binders by Na in EC:DMC- and diglyme-based electrolytes. . . . .	32

---

4.1	Pressure evolution at 25 ° C from Na metal stored, <b>A</b> ), in 1 M NaPF <sub>6</sub> in diglyme and , <b>B</b> ), in 1 M NaPF <sub>6</sub> in EC <sub>50</sub> :DMC <sub>50</sub> . At the left y-axis and at the right y-axis the total pressure and amount of gas related to the total number of moles of Na are shown, respectively. . . . .	34
4.2	Impedance spectra at different times for a symmetric Na Na Swagelok cell left at OCV for 90 hours. . . . .	35
4.3	A Na sphere stored with 1 M NaPF <sub>6</sub> in diglyme . . . . .	35
4.4	Walden plots for a NaPF <sub>6</sub> diglyme electrolyte at three different concentrations. 36	
4.5	Linear sweep voltammogram for 1 M NaPF <sub>6</sub> in diglyme (Blue) and 1 M NaPF <sub>6</sub> in EC <sub>50</sub> :DMC <sub>50</sub> (Orange), respectively. . . . .	37
4.6	Cyclic voltammograms showing 5 cycles from a half cell of NVPF using 1 M NaPF <sub>6</sub> in diglyme. Inset: Magnification at 3.4 V to visualise small features with related surface charge densities listed in figure header. . . . .	37
4.7	Linear voltammograms indicating reductive behaviour of diglyme and EC <sub>50</sub> :DMC <sub>50</sub> electrolytes with 1 M NaPF <sub>6</sub> on Cu-foil. Inset: magnified part of the curve. 38	
4.8	Typical cell profiles of half cells cycled in a diglyme 1 M NaPF <sub>6</sub> in diglyme 40	
4.9	Differential capacity curves of half cells cycled in a diglyme 1 M NaPF <sub>6</sub> in diglyme. . . . .	41
4.10	Typical cell profile in a cycled full cell using 1 M NaPF <sub>6</sub> in diglyme with corresponding differential capacities. Inset: visualisations of small features. The capacities are plotted in terms of the weight of cathode material, making comparison easier between half and full cells. . . . .	41
4.11	Capacity retention and coulombic efficiency per cycle of full cells, using 1 M NaPF <sub>6</sub> in diglyme ( <b>A</b> ) or 1 M NaPF <sub>6</sub> in EC <sub>50</sub> :DMC <sub>50</sub> ( <b>B</b> ) . . . . .	42
4.12	<b>A</b> ), total specific capacities and, <b>B</b> ), specific discharge capacities normalised by discharge capacity on first cycle for full and half cells of NVPF and HC. Setup using a 1 M NaPF <sub>6</sub> diglyme electrolyte. . . . .	43
4.13	Evolution of the two plateaus in the full cell with cycling. Inset: Legend to what parts of the full cell are denoted by upper plateau, lower plateau and full cell. . . . .	43
4.14	Actual and recombined efficiencies and accumulated irreversibilities for half and full cell. . . . .	44
4.15	Convention when naming the different voltage regions for a fully balanced system. Based on half cell profiles. . . . .	45
4.16	Specific capacity retention when exploring different regions of the electrode materials . . . . .	46
4.17	Specific capacity retention for a NVP NVP cell as compared to the NVPF HC full cell. . . . .	47
4.18	Gas chromatograms from experiment aiming to analyse soluble non-charged degradation products from cycled cell separators. . . . .	48
4.19	Reduction scheme based on the breaking of the C <sub>1</sub> -O <sub>1</sub> bond in the diglyme molecule. . . . .	49
4.20	Reduction scheme based on the breaking of the O <sub>1</sub> -C <sub>2</sub> bond in the diglyme molecule assuming that no environmental hydrogen is available. . . . .	50
4.21	Reduction scheme based on the breaking of the O <sub>1</sub> -C <sub>2</sub> bond in the diglyme molecule assuming that environmental hydrogen is available. Crossed out boxes relate to schemes deemed impossible according to the discussion in the text. . . . .	51

---

4.22	FTIR spectrum of a HC surface cycled 2 times compared to a pristine electrode soaked in electrolyte and dried for 12 hours. . . . .	51
4.23	SEM micrographs of pristine HC. Inset: Magnifications of one part of the pristine HC surface. . . . .	52
4.24	SEM - micrographs of a pristine HC electrode cycled in 1 M NaPF <sub>6</sub> in diglyme for 50 cycles. Upper and lower insets: Magnifications of lighter part and darker part of surface, respectively. . . . .	53
4.25	EDX spectrum acquired from a HC electrode cycled 1.5 times in full cell setup using a diglyme 1 M NaPF <sub>6</sub> electrolyte. . . . .	53
4.26	Photo taken of two electrodes cycled in full cell setups showing a bluish tone as compared to the pristine electrodes. . . . .	53
4.27	Pourbaix diagram for Vanadium species in aqueous solutions. Printed with permission from [8]. . . . .	54
4.28	Results from experiment studying binder degradation. PVDF binder experiences severe reaction in when exposed to Na in diglyme based electrolyte but seems to be stable in EC:DMC based counterpart. . . . .	55
4.29	Separator showing HC disintegration after cycling. . . . .	55
4.30	Different mechanisms occurring sequentially from right to left, top to bottom, that are contributing to system capacity fade. . . . .	56
B.1	Cyclic voltammogram from cycling an EC <sub>50</sub> :DMC <sub>50</sub> /NaPF <sub>6</sub> electrolyte beyond the third peak five times . . . . .	III
C.1	Capacity curves . . . . .	IV
D.1	Reduction scheme for PVDF binder. . . . .	V
E.1	Measured temperature dependence of Ionic conductivity and Viscosity for a G2 NaPF <sub>6</sub> electrolyte. In the case of ionic conductivity the 1 M electrolyte has only been measured once due to lack of availability. . . . .	VI
F.1	Different types of polymers used as insulation in Swagelok cells comprising NVPF and HC with a G2 1M NaPF <sub>6</sub> electrolyte. Films are recovered under glovebox conditions after cycling. . . . .	VII

# List of Tables

2.1	Characteristics of two NASICON-type materials, NVPF and NVP. . . . .	12
2.2	Chain length, common name, acronym, and physical properties of the first four glymes in the series. Data for EC and DMC are provided as a reference. Data adapted from [9] unless other reference explicitly stated. . . . .	16
2.3	Cost of diglyme per unit weight as compared to EC and DMC. . . . .	18
3.1	Electrode area, mean weight of current collector and standard deviation of current collector (C.C.) weight for two different sizes of electrodes used. . .	23
3.2	Cut-off voltages for cycling of materials in half-cells, using Na metal as counter electrode . . . . .	28
3.3	Cut-off voltages for cycling of materials in full cells . . . . .	29
3.4	Regions cycled and their approximate voltage intervals for the anode and cathode as approximated by half-cell reconstructions. masses are values used for one experiment. . . . .	29
3.5	Cycling scheme for symmetrical NVP/NVP cell . . . . .	30
3.6	Cut-off voltages and cycling scheme for further exploring possible vanadium extraction . . . . .	31
4.1	Reduction potentials and activation energies, $E_a$ , for diglyme at different levels of complexation with $\text{Na}^+$ . . . . .	39
4.2	Initial irreversibility ( $I_{initial}$ ) and coulombic efficiencies ( $\eta_c$ ) when cycling different regions of HC and NVPF in a 1 M $\text{NaPF}_6$ diglyme electrolyte using a full cell setup. The potential ranges have been estimated using half-cell reconstruction upon first charge. *: Not comparable since cell is not discharged fully. . . . .	47
A.1	Industrial uses of Mono- and diglyme. Directly adapted from [9] . . . . .	I
A.2	Industrial uses of glymes. Directly adapted from [9] . . . . .	II

## List of Abbreviations

Abbreviation	Explanation
<b>CV</b> Cyclic voltammetry	An electrochemical technique where the current response of a setup is recorded as the function of applied voltage.
<b>ESW</b> Electrochemical stability window	The range of potentials at which a substance can exist without oxidising or reducing.
<b>EIS</b> Electrical impedance spectroscopy	Technique where the frequency dependent ac-impedance of a system is investigated to monitor changes in bulk or surface morphology.
<b>C<sub>s</sub></b> Specific capacity	The capacity per unit mass of an electrode material. Measured in mAh g <sup>-1</sup> .
<b>E<sub>s</sub></b> Specific energy	The energy per unit mass of total electrode material or whole unit a complete cell or battery. Measured in Wh kg <sup>-1</sup> .
<b>GCPL</b> Galvanostatic cycling with potential limitation	Method for testing battery performance in which a constant current is drawn from the cell studied while the voltage is tracked.
<b>GC</b> Gas chromatography	An analytical technique used to separate gases with respect to their masses and tendency to flow through a gas column.
<b>LIB</b> Lithium-ion Battery	

Abbreviation	Explanation
<b>LSV</b> Linear sweep voltammetry	As cyclic voltammetry but only one voltage sweep is conducted either towards higher or towards lower potentials.
<b>MS</b> Mass spectrometry	An analytical technique where the ionised fragments of a substance are analysed. Coupled to GC it becomes a very sensitive analysis technique to precisely identify compounds in the analyte.
<b>NASICON</b> Na-ion super ionic conductor	A class of materials with good solid state ion conductive properties. Used as cathodes in SIBs.
<b>OCV</b> Open circuit voltage	The voltage between two battery terminal when no current is flowing.
<b>SHE</b> Standard hydrogen electrode	A measurement standard in electrochemistry, toward which different substances and processes are often referenced.
<b>SEI</b> Solid electrolyte interphase	The interphase formed upon degradation of electrolyte components on the negative electrode.
<b>SIB</b> Sodium-ion Battery	

# 1

## Introduction

Modern applied research is to a higher and higher degree focusing on solving the problems of a future sustainable energy system. Many efforts strive to find convenient, cheap ways of storing energy. Batteries surely belong to this category of solutions and has seriously been considered for use in larger scale applications since the advent of the Li-ion battery (LIB) during the 1990:s. Room temperature sodium-ion batteries (SIB), on the other hand, is a new category of systems that have recently appeared and been considered for future use. The thesis at hand investigates one type of SIB using a somewhat unconventional electrolyte. In this chapter a background to the research conducted is given along with the aim and limitations.

## 1.1 Importance of Stable SIBs for a Future Energy System

The signing of the climate treaty in Paris in 2015 was seen as a success from many perspectives. All members of the United Nations agreed upon collectively, but according to their ability, to reduce their greenhouse gas emissions, to keep global warming below 2 ° C. However, to still keep our current way of consuming energy, large structural reforms of each nation’s energy systems are needed. Batteries and their development may have a major role to play when it comes to such challenges. Not only are they a key element for storing energy in tomorrow’s fossil-free electric cars, but they are also candidates for load balancing in a power grid with more renewable, intermittent, sources of energy, such as wind and solar power [10].

The current state-of-the-art batteries for consumer use excelling in energy density at room temperature are all based on lithium-ion technology. However, stakeholders for Li are not limited to battery manufacturers. At the same time Li production and resources are limited and centred to a few certain regions (Figure 1.1). This means that both geopolitical and supply reasons, motivates finding an alternative to Li in battery technologies could prove to be crucial if a development and expansion in the sustainable energy sector is not to be halted [1, 11]. In recent years, Na has risen as a potential candidate to fill the shoes of its alkali metal cousin. A major reason is that Na is approximately three orders of magnitude more abundant in the earth’s crust and reserves are abundant nearly all over the globe [12]. If only considering the price and raw-material availability as the main attributes on how to judge a battery technology’s future viability, Na has a great advantage.

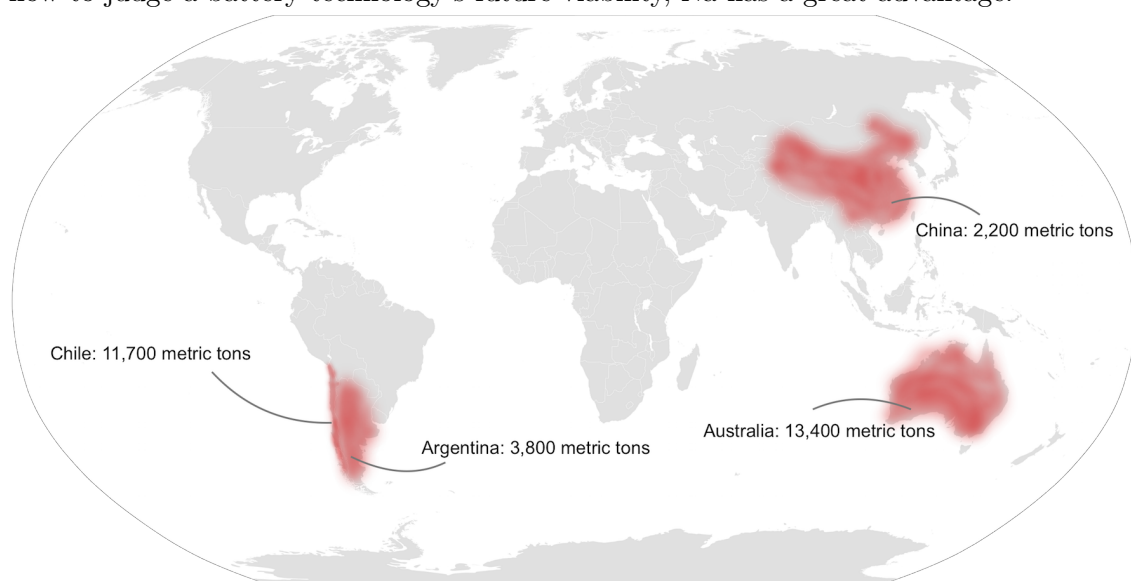


**Figure 1.1:** Map of world’s most Li producing countries and the total mining output during 2015 [1].

Even though theoretical energy density is lower for Na metal than for Li metal, pure metals are seldom used in real battery systems, due to safety reasons. This also gives SIBs a possibility of having a better performance than LIBs—if the SIB materials could be designed smart enough [13]. Such outlooks have spurred a revival of the SIB field, turning dormant after the commercialisation of LIB cells in the 1990:s. Many projects have started worldwide, connecting industry and academia to promote the development of commercially viable SIB solutions. One such endeavour is the “Naiades” consortium <sup>1</sup>,

<sup>1</sup><http://www.naiades.eu/>

funded by the EU Horizon 2020 programme.

As for now, a good candidate system for electrodes in a future commercial SIB consists of a cathode made of either the polyanionic framework  $\text{Na}_3\text{V}_2(\text{PO}_4)_2\text{F}_3$  (NVPF) or the polyanionic framework  $\text{Na}_3\text{V}_2(\text{PO}_4)_3$  (NVP), and an anode made of hard carbon (HC). Electrolytes for SIBs have so far not been studied as extensively as the different materials for anodes and cathodes but are also very important, since they often determine cycling stability and safety of a battery [14]. Such properties are equally important for commercialisation of any SIB system. Even though much know-how on is thought to be transferable from the LIB side, each electrolyte still has to be rigorously tested for use in these new systems. In the end it is the system which has to show good performance and not only the individual components.

The scene is thus open for improvements in electrolytes that stabilise prospective SIB systems. Any electrolyte living up to such criteria should be considered for use, since the correct choice might vary among different applications—a long term energy storage will not demand the same characteristics as a battery in a cell-phone or electric toothbrush. There is also a need to properly understand any capacity fade mechanism for a future SIB since it could help in the development of mitigation strategies.

Electrolytes based on diethylene glycol dimethyl ether, also known as diglyme or "G2", have been considered for use in batteries due to this solvent's good ionic conductivity, favourable viscosity, thermal stability and high donor number, having the ability to chelate small cations [15, 9]. Also, since diglyme is an ether and is already more reduced than any carbonate solvent, it is possibly more stable against further reduction at the anode. Despite this, no study has gone into detail of neither its electrochemical stability of diglyme based electrolytes, their performance in SIBs or evaluated their suitability in a prospective SIB systems.

### 1.2 Aim

This master's thesis project has aimed to evaluate the possibilities of using 1 M NaPF<sub>6</sub> in diglyme with future SIBs and to understand the electrolyte's stability and degradation mechanisms. Even though the main focus has been but on the electrolyte, the intricate nature of any battery system has required the work to also encompass studies of the interplay between all the system components. Apart from studying systems behaviour, the work has further aimed to evaluate the use of Na-metal electrodes as references using the mentioned electrolyte. The aim of the initial literature study has been for the reader to internalise knowledge of battery systems and to summaries the research relevant for anyone desiring to considering to use diglyme, also summarising such aspects as toxicity and cost.

### 1.3 Limitations

No focus has been put on changing the salt into other types than NaPF<sub>6</sub>, even though this might provide fruitful in terms of cell performance. Nor has any other solvent been tested. Instead previous data of the same system, using Ethylene Carbonate (EC) and Dimethyl Carbonate (DMC) in a 1:1 ratio as a solvent, has been used as a benchmark when considered necessary.

The cell setups have in these cases comprised the electrodes: NVPF, HC and NVP. No further studies of the electrodes used were done, even though there it is possible for such change being able to lead to capacity or stability improvement. The main task has been not to optimise all cell components, but to characterise the presumptive degradation and performance of the electrolyte at hand. Furthermore, the work has solely been a literature survey complemented by experimental work. Where modelling and computational methods have been needed, it has been provided by a third party. Even though, future commercialisation of SIBs would require an in-depth study of possible applications and a market analysis, no attempt has been made to do so here. Also for commercialisation, larger systems comprising many cell elements would have to be investigated to ensure proper performance. This, as well has not been considered and is left for future work.

# 2

## Batteries and SIBs

In the following sections, the theory relevant for this project is presented. First, the general concepts of batteries will be presented. Second, a section introducing the reader to electrolyte fundamentals is laid out. Third, comes a section presenting the background to electrolyte decomposition and the importance of formation of stable surface films. Fourth, a section explaining the SIB with its components, their challenges, and future prospects is presented. Finally comes a section featuring a short literature review of the glyme family of solvents—the category that diglyme belongs to. An attempt is made both to cover the electrochemistry relevant for batteries and the more practical aspects, such as cost and toxicity.

## 2.1 Batteries—Primary and Secondary Galvanic Cells

Galvanic cells are defined as devices able to store electrical energy as chemical energy. In daily life, we usually talk about "batteries" but strictly speaking a battery is a device comprising many galvanic cells. Since the main part of this thesis will not be dealing with such large systems, the words "battery", "galvanic cell", or simply "cell" will be used interchangeably, unless indicated otherwise. In the model battery, two electrodes of different electrochemical potential are kept apart by a separator, preventing the electrodes from touching each-other (Figure 2.1). The electrodes are often made up of an active material, a conductive matrix, such as carbon black, serving to improve electrical connection among active-material grains, and a binder that keeps everything together (Figure 2.2) [5]. The electrode is, further on, usually coated on top of a current collector made of metal providing mechanical stability and an evenly distributed surface current [16].

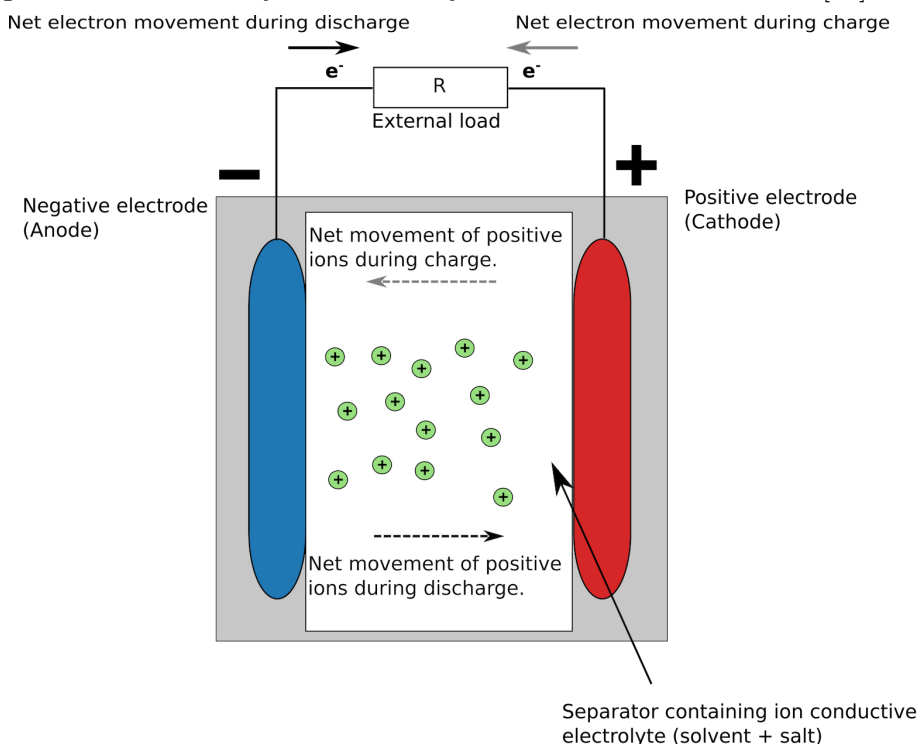


**Figure 2.1:** The fundamental principles of a galvanic cell.

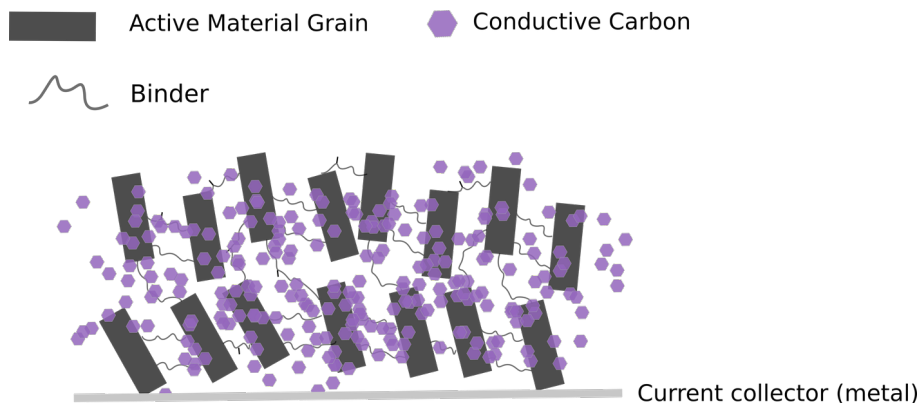


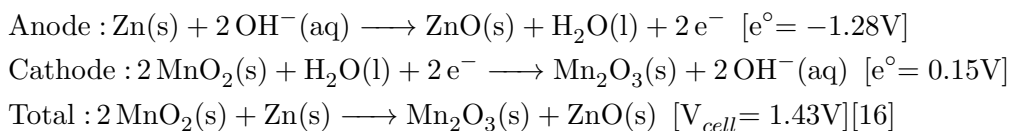
**Figure 2.2:** Conventional components of an electrode coated on a metal current collector.

Apart from preventing electrodes from touching each-other and short circuiting, the separator is responsible for hosting the electrolyte. Mostly consisting of a salt containing the ion of interest that is dissolved in an organic solvent, the purpose of the electrolyte is to conduct ions inside the cell [17]. Optimally the electrolyte should be stable at the redox potentials of the electrodes to not degrade and cause unwanted side-reactions.

When discharging a galvanic cell, the electrodes are connected by an external load. Because of a difference in redox potential associated with the anode and cathode, electrons will start flowing through the outer circuit [16]. At the same time ions will flow in the electrolyte to maintain charge neutrality. The flow of electrons and ions is sustained by a continuous oxidation of anode species, giving up electrons and ion, and a continuous reduction of cathode species, absorbing electrons and ions. A current supported by a change in oxidation state of participating species is denoted as a "Faradic current". In a battery, such a redox process gradually lowers the total internal energy of the system, the current being sustained until the full capacity of either of the active materials has been depleted. The discharge capacity is the the total number of redox conversions, providing a charge to the external circuit, that can occur reversibly, and is dependent on the type and amount of active material used. The potential at which extraction or insertion of ions and electrons takes place will instead be dependent on the material structure and instantaneous composition, making the fraction of inserted/extracted ionic charge carriers a factor determining the cell potential. When charging a galvanic cell, if that is possible, the opposite process takes place: Energy is supplied to the system and stored by reversing the flow of ions and electrons, causing the internal energy of the system to increase.

The separator and electrolyte can not be electrically conducting, since this would result in a self-discharge of the cell—i.e. electrons and ions would both propagate in the electrolyte, thermodynamically equilibrating the system. It is the energy of the flowing electrons in an *outer circuit* that can be harnessed by a battery-powered devices, such as a car or a laptop [18]. Features mentioned so far are common for all batteries. Making an initial distinction, galvanic cells can be divided into two main categories: primary and secondary cells.

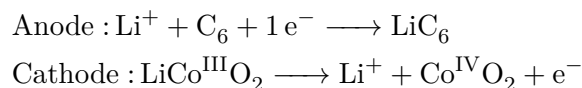
**Primary cells** are driven by chemical reactions that are irreversible, meaning that the cells cannot be recharged after the first cycle [16]. Cells are assembled in the charged state, discharge by the end consumer and then discarded—hopefully for material recycling. Thus, total energy density, cost and environmentally friendliness become important design parameters for primary cells. A common example of a primary cell is the alkaline batteries used by low demanding consumer electronics. The chemistry involved during discharge is given by:



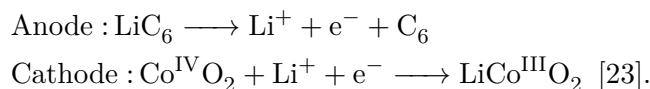
**Secondary cells**, on the other hand, are designed upon reactions that are reversible, yielding batteries that can be recharged [19]. With rechargeable cells other aspects of cell development than energy density and cost becomes important. A rechargeable battery must show good **cyclability** to not loose its capacity when charged and discharged. This is also referred to as showing a low **irreversibility**. Another requirement is that the amount of **polarisation** experienced during charge is low, polarisation meaning the

difference in cell voltage between charge and discharge at the same level of charge. Polarisation, thus, determines the energy efficiency <sup>1</sup> of storage in the battery. Furthermore, the systems must be **safe** with a margin to not risk to damage of persons or property, even if the batteries are slightly mishandled by the user. The **charge rate** is expected to be an increasingly important factor end-users of electrical vehicle [20] since people are expected to prefer rapid charge of their electrical vehicles.

In many cases secondary batteries are built upon intercalation electrode materials, where the ion responsible for shuttling the charge takes up a vacant space in the anode or cathode material matrix that keeps its structural integrity upon insertion and extraction [5]. Structures featuring these properties are often denoted "Topotactic materials" [21, p.9]. One of the most common chemistries employed in early high performance batteries showing reasonable performance in terms of both total capacity and cyclability, is the lithium ion rocking chair battery, commercialised by Sony in 1991 [22], which utilises a metal oxide cathode and a graphite anode. When charging, the half-cell reactions are given by:



and similarly upon discharge the reactions are given by



Upon charge (Co<sup>III</sup>) is oxidised. Li<sup>+</sup> ions will at the same time leave the LiCoO<sub>2</sub> to compensate for the lost electron's charge and intercalate inside the graphite. During intercalation Li<sup>+</sup> is recombined with the electron and reduced to its metallic state (Li). Upon discharge, the Li is instead oxidised to an ion (Li<sup>+</sup>) while the other specie (Co<sup>IV</sup>) is reduced. The ion is then incorporated into the lattice of the cathode material, to maintain charge neutrality [16].

The reason for using intercalation materials such as graphite for the anode, instead of pure lithium metal, which would yield a higher energy density, is that alkali metal electrodes have shown to experience unwanted dendrite formation. The dendrites are structures that successively grow upon cycling because of kinetic factors. They have the unwanted ability of penetrating the separator and finally short circuiting the battery. A short circuit, in turn, may cause dangerous overheating and explosion, which could endanger the end user [19].

---

<sup>1</sup>Not to be confused with coulombic efficiency, determining the ratio of charges shuttled at charge and discharge.

## 2.2 Electrolyte Fundamentals - Salts and Solvents

The most commonly used electrolytes reported for alkali metal ion batteries are made up of two components: a salt and an organic, non-aqueous, solvent. The salt is a source of the ions to be transported during charge and discharge and the solvent provides a matrix and a means of dissociating the salts. The ability of an electrolyte to conduct ions is called its ionic conductivity,  $\sigma$ , measured in  $\text{mS cm}^{-1}$ . Ionic conductivity is the ion analogue to conductivity (reciprocal resistivity) for electrons in an electrical circuit; it determines how much loss is associated with the process of moving ions back and forth in the electrolyte. Being related to a liquid behaviour, the ionic conductivity can be modelled by an empiric Vogel-Tamman-Fulcher expression [17, 24]:

$$\sigma = \sigma_0 e^{\frac{-B}{(T-T_0)}}, \quad (2.1)$$

where  $T$  is the absolute temperature,  $T_0$  is a temperature related to the glass transition temperature,  $B$  is an empiric parameter and  $\sigma_0$  is the ionic conductivity at  $T_0$ . Also, remembering that the viscosity,  $\eta$ , can be modelled using the similar functional relationship [24]:

$$\eta = \eta_0 e^{\frac{B}{(T-T_0)}}, \quad (2.2)$$

where  $\eta_0$  is the viscosity at  $T_0$ , we see that  $\sigma_0$  and  $\eta_0$  have a reciprocal relationship according to:

$$\eta\sigma = \text{constant}, \quad (2.3)$$

known as the "Walden rule" [25]. By plotting  $\frac{1}{\eta}$  against  $\sigma$ , experimentally it is possible to determine if the electrolyte conforms to equation (2.3) and a vehicular conduction mechanism of ions.

The ionic conductivity of an electrolyte is dependent on both the salt and solvent used. Figure 2.3 shows some common reported solvent molecules for both SIBs and LIBs [17]. Apart from providing a good conduction and electrochemical stability, which will be touched upon in Section 2.3, solvents have to fulfil other criteria [13]. The liquidus range of the electrolyte has to be broad; the electrolyte should neither freeze, nor boil, even if the ambient temperature drops or increases several tenths of degrees. Thermal stability (which is not the same as liquidus range) is also necessary to consider as it tells us how a solvent may respond to an unintended increase in temperature. In these cases the solvent should not degrade exothermally—causing thermal runaway; the final battery should be as unlikely to catch fire or even explode, as possible. Furthermore, viscosity of the electrolyte should be low enough to allow for proper soaking of the separator and electrodes [13]. Since no single solvent is usually able to meet all of the criteria above, practical electrolytes many times consist of mixtures of several solvents with one salt. One such composition, commonly used for Li ion batteries, is the LP 30 electrolyte—a 1:1 binary mixture of ethylene carbonate (EC) and dimethyl carbonate (DMC) with 1 M  $\text{LiPF}_6$  salt [13].

Salts have the same requirements as solvents when it comes to thermal stability [14]. Another important property is that the salt anion should not cause any unwanted side reaction with any part of the cell. Further characteristics of a good salt include easiness to remove residual waters, low cost, toxicity and a high degree of dissociation – i.e. to which degree the salt provides mobile charge carriers in the electrolyte [13]. The degree of dissociation is not only a salt dependent factor, but also depends on how strongly the specific solvents act to dissociate the salt – a property approximately proportional to the solvents dielectric constant. Salt dissociation is thus both a question of salt, solvent and how they match. One salt that has been shown to have good or decent performance with respect to these aspects for Li-ion batteries is  $\text{LiPF}_6$ —a component in the LP30 electrolyte.

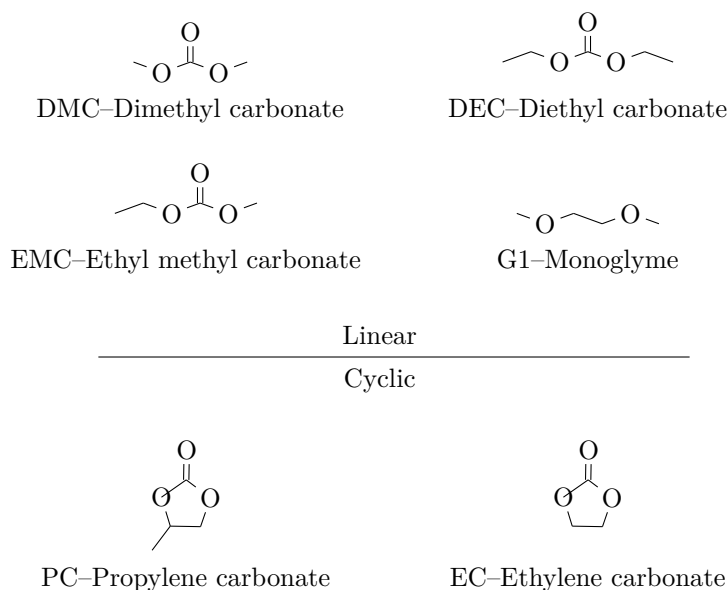


**Figure 2.3:** Molecular structure of some common solvents used in alkaline metal batteries.

## 2.3 Electrode-Electrolyte Interfaces and Interphases

Constructing stable, safe, alkali metal batteries with long cycling life does not only include developing efficient electrode materials. The interface between the electrolyte and the electrodes is also important. Many conventional solvents used in LIBs and SIBs have a too low reductive stability for the potentials reached at the cell anode, meaning that ionic charge carriers would get lost continuously if there was no balancing mechanism. The solution to the problem comes from the kinetics of electrolyte decomposition [17]. As predicted by reduction potentials, there is an initial solvent decomposition. However, instead of continuing the reaction, the decomposition products serve to render a film and passivate the surface. The film formed, commonly called the Solid Electrolyte Interphase (SEI), is formed during the first charge and then stabilised during subsequent cycles [17]. Petr Novák *et al.* have described properties of an ideal SEI, noting that it should be electrically insulating, leading to prevention of further electrolyte breakdown, but a good ion-conductor, leaving kinetic performance and polarisation of the cell unaffected [26]. Another quality would be that they are insoluble in the solvent used for the electrolyte, leaving a stable film.

Attempts to probe the SEI have been made in a number of studies for lithium ion batteries [26]. For SIBs results are scarce. Weadock *et al.* used colloidal probe microscopy on metal surfaces cycled against sodium metal in a 1 M NaPF<sub>6</sub> 1:1 ethylene carbonate and diethyl carbonate (EC:DEC) electrolyte [27]. By mapping out the Young's modulus of the surface at different cycles, he showed that the SEI seemed to consist of a bi-layered structure that had stabilised after the first cycles. The proposed structure corresponds to a model proposed by Doron Aurbach investigating SEI growth on Li metal anodes [28]. According to his study, the SEI in carbonate solutions forms a multi-layered structure relating to the difference in reduction potential of the possible species in the electrolyte solution; all components with a reduction potential higher than that of lithium will be reduced initially. Thereafter more selective growth of the films take place only featuring reduction products with the highest reduction potential.

In the same study the film formation on graphitic carbons was investigated. Since the carbons were cycled galvanostatically, the film growth is even more selective with only those components in solution that have a higher reduction potential reducing first. The films formed initially may thus be so resistive that solvent components with lower reduction potentials are never decomposed. Another feature of intercalation anode materials is that they show some degree of volume expansion when sodiated/lithiated. The expansion causes a cracking of the surface film and further decomposition of the electrolyte when the small cracks are healed. The cracking-healing is continued until a film with the right viscoelastic properties is formed [28].

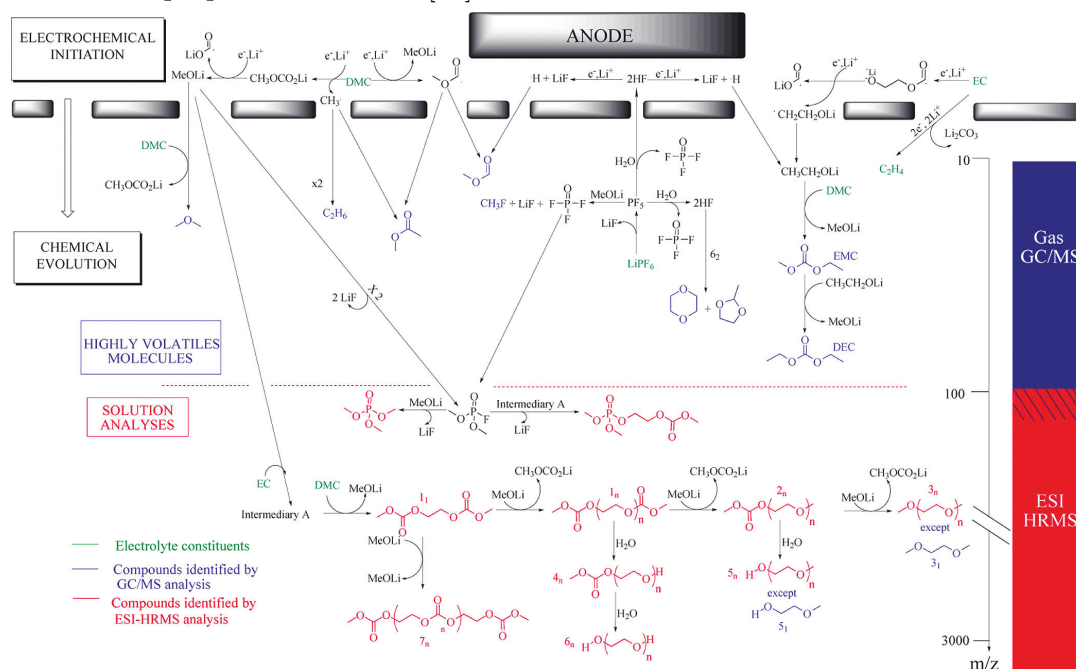


**Figure 2.4:** Decomposition scheme taking a range of different Li-ion battery processes into account when using carbonate electrolytes. Reprinted with permission from [2]. Copyright 2011 American Chemical Society.

Other studies have studied the chemical composition of the SEI. G. Gachot *et al.* used Gas Chromatography and Mass Spectrometry coupled to FTIR to investigate primary and secondary electrolyte decomposition products of LiPF<sub>6</sub> in cyclic and linear carbonates, such as EC-DMC (Figure 2.4) [2, 29]. When conducting a similar study for SIBs it was found that the higher redox potential of Na limited the rate of further reduction of decomposition products, such as diethylene carbonate. The lack of reduction indicates that the SEI would have a different character and different (worse) performance in terms of stability [30, 31].

## 2.4 Sodium-ion Batteries

The materials and concepts for possible future rechargeable SIBs are in many ways similar to the rocking chair lithium ion batteries described in Section 2.1. This is much because the chemistry of the two alkali metals are similar. Even though the research in room temperature SIBs is lagging behind its Li counterpart, the prospect of cheaper cells using a nearly unlimited sodium resource, has encouraged a revival of the field, as can be found in many recent reviews [23, 13, 5, 32, 33, 34]. In this section, a summary is given of the different materials and electrolytes currently used in SIBs.

### 2.4.1 SIB Anode Materials

In the case of sodium, as compared to lithium, graphite is not an optimal insertion material [21, p.9]. In graphite, the chemical potential for  $\text{Na}^+$  intercalation is higher than that for plating and thus the Na prefers to electroplate instead of intercalating [35]. Instead, hard carbon (HC), synthesised directly from pyrolysis of sugar, can be used, providing a specific capacity of more than  $300 \text{ mAhg}^{-1}$  [36, 37]. As elaborated upon by Stevens and Dahn, sodium inserts in two distinct ways into hard carbon resulting in two different insertion-voltage regions[35]: Nanoporous, turbostratic, graphite-like regions result in a sloping insertion-voltage region, which is followed by insertion into mesoporous regions, providing a steady voltage plateau at  $0.05 \text{ V vs. Na}^+/\text{Na}^\circ$ . The difference between intercalation in graphite-like regions and pure graphite is illustrated in Figure 2.5 [35]. Hard carbon is, thus, an attractive alternative as a future anode material. Unfortunately, it still shows a large initial irreversibility when cycled in conventional electrolytes. To tackle this it has been proposed to use extra sodium sources [31].

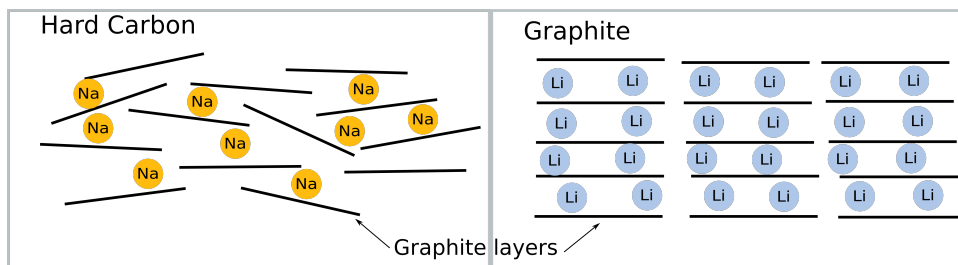


**Figure 2.5:** Intercalation of Na-atoms in turbostratic graphitic regions of HC and of Li-atoms between ordered layers of graphite

### 2.4.2 SIB Cathode Materials

The transition metal oxides used in lithium ion batteries have, in some cases, proved to be unsuitable as cathode materials due to large polarisation [38]. Also, the materials show less capacity than they theoretically could have [32, 5]. With this being said, the metal oxides could still very well prove to be usable. Instead of transition metal oxide a parallel class of polyanionic materials have been found to work [39]. One subclass of such compounds is called NASICONs (Na-ion super ionic conductors) and was initially used for solid electrolytes. These intercalation frameworks have been found to show good performance and specific capacities of up to  $128 \text{ mAh g}^{-1}$  [40]. Two NASICON type materials are  $\text{Na}_3\text{V}_2(\text{PO}_4)_3$  (NVP) [4, 40] and  $\text{Na}_3\text{V}_2(\text{PO}_4)_2\text{F}_3$  (NVPF) [41, 42]. Their general electrochemical properties are outlined in Table 2.1.

	Insertion potential vs $\text{Na}^+/\text{Na}^\circ$	Theoretical specific Capacity [ $\text{mAh g}^{-1}$ ]
NVPF	3.7, 4.1	128
NVP	1.6, 3.4	118

**Table 2.1:** Characteristics of two NASICON-type materials, NVPF and NVP.

For NVPF, each sodium atom is stored in a matrix of edge-sharing octahedra centred around  $\text{V}^{3+}$  species. Octahedral corners consists of either  $\text{PO}_4^{3-}$  anions or  $\text{F}^-$  anions. In the inter-layer spacing sodium ions are intercalated (Figure 2.6). The insertion and extraction of sodium from NVPF happens at four distinct voltages distributed over the two main plateaus (Table 2.1), elaborated upon by Park *et al.* [41]. Out of three adjacent sites for the alkali metal, two can be emptied without collapsing the NVPF structure.

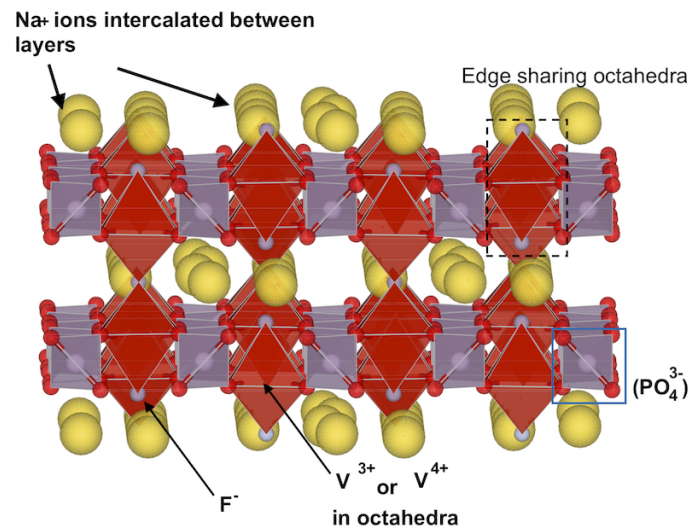
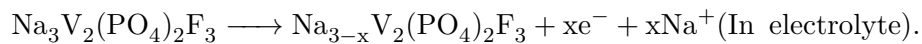


**Figure 2.6:** The polyanionic NVPF. Each vanadium atom is in the middle of an octahedra bonding  $\text{PO}_4^{3-}$  and  $\text{F}^-$  species. In the interlayer Na is intercalated. Rendered using VESTA [3].

Upon each extraction of a sodium-ion, a vanadium atom changes oxidation state from  $\text{V}_3^+$  to  $\text{V}_4^+$  according to:



Among the adjacent sites, the first sodium ion is easiest to extract as it leads to a metastable trans-configuration of the material, minimising the sodium ion-ion repulsion [41]. For both the first and second extraction of sodium from the lattice the associated potentials vs.  $\text{Na}^+/\text{Na}^\circ$  change (Figure 2.7).

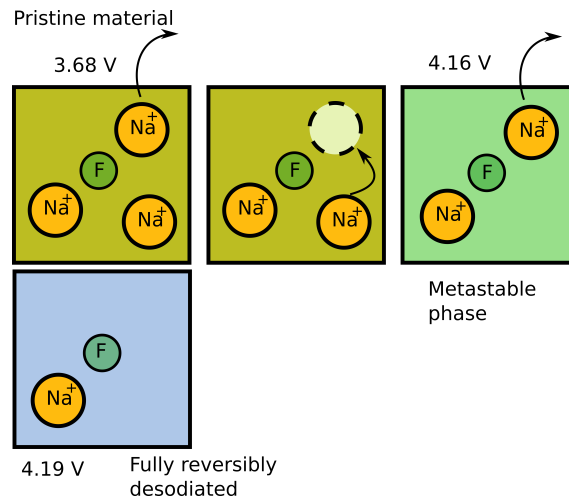


**Figure 2.7:** Schematic of the NVPF Na extraction mechanism looking down into the intercalation plane of Na : Showing 1) Extraction of the first sodium, 2) internal reorganisation into a 3) meta-stable phase and finally 4) extraction of the second reversible sodium. For each sodium extraction a vanadium changes oxidation state. Associated potentials of extraction are given vs.  $\text{Na}^+/\text{Na}^\circ$ . Based on [4].

NVP, on the other hand features two voltage plateaus of asymmetrical capacity ( $50 \text{ mAh g}^{-1}$ ,  $118 \text{ mAh g}^{-1}$ ) [4][40] but upon synthesis one intercalation site, at the lower potential of 1.6, is empty and one, at the upper potential of 3.4, is filled. This means that pristine NVP can be used both as a low capacity anode or as a high capacity cathode. The insertion potentials are, however, lower than for NVPF resulting in a lower specific energy [4]. Returning to the NVPF, the specific energy density of a system featuring a hard carbon anode and a NVPF cathode can be calculated. By assuming that the mean voltage of the slope and plateau of the hard carbon is  $0.25 \text{ V vs Na}^+/\text{Na}^\circ$  [43], the energy density of a perfectly balanced system becomes  $284 \text{ kWh kg}^{-1}$ . Such an energy density is comparable to the first generations of Li-ion batteries given that the assembled system, with electrolyte, has a good capacity retention.

### 2.4.3 SIB Binders and Current Collectors

Binders are often polymers serving to hold the active material of the electrodes together [5]. The molecular structure for some binders reported for SIB:s are shown in Figure 2.8. Among these, the fluorinated polymer PVDF, very similar in structure to Teflon®(PTFE), is the most commonly used in literature [5]. However, as reported in some recent studies, PVDF seems to suffer from gradual defluorination at low potentials when switching from a lithium to a sodium chemistry [5, 44, 45, 46]. Since the defluorination relies on the consumption of sodium, this is a process which inevitably contributes to capacity fade in the battery. Instead, carboxymethyl cellulose (CMC), has been suggested as a replacement [45]. This is an organic polymer sometimes found as a food additive [47]. When used as a binder for SIB applications the side-group, R, is chosen to be sodium. A third binder reported in literature is sodium alginate, a polymer extracted from brown algae [44]. Both CMC and sodium alginate have been reported to result in a slower capacity loss compared to PVDF when used as a anode material binder [44].

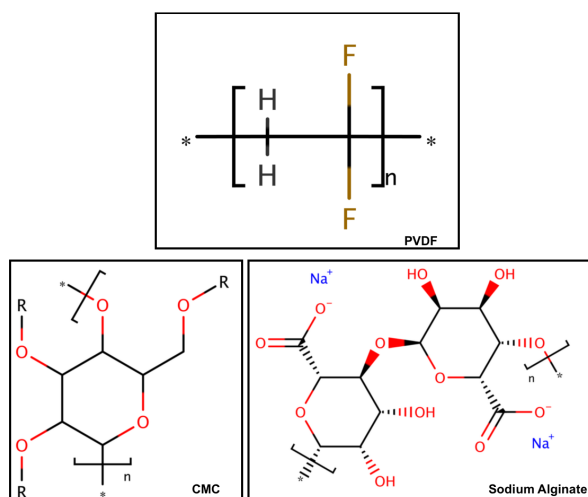


**Figure 2.8:** Molecular structure of binders used in SIB electrodes.

When it comes to current collectors, one of the major selling points when it comes to SIB-technology has been that cathodic current collectors can be switched from copper to aluminium since sodium does not alloy with the latter, while lithium does. The change of metals makes the cell setup both cheaper and lighter. As a figure of merit, the price for aluminium as of the end of March 2016 was 1 550 USD per ton while copper cost approximately 5000 USD per ton [48]. At the same time, the specific density of aluminium is  $2700 \text{ kg m}^{-3}$  while that of copper is  $8920 \text{ kg m}^{-3}$  [49]. The tensile strength of aluminium is about 60 % of that of copper, possibly forcing a manufacturer to use a current collector

with approximately the double thickness [50]. Judging from the physical characteristics, aluminium is still ca. 40 % lighter and 40 % cheaper than copper.

#### 2.4.4 SIB Electrolytes

For SIBs, the electrolyte is the one component that has received the least attention in literature (Figure 2.9). The reason is not necessarily that electrolytes deserve less attention but perhaps that many groups, during the time which the SIB concept boomed, have so far focused their efforts on developing those components setting the baseline for the capacity in SIBs. As described in the Section 2.3 electrolytes and their interplay with electrodes *are* very important in determining charge kinetics and stability of any battery.

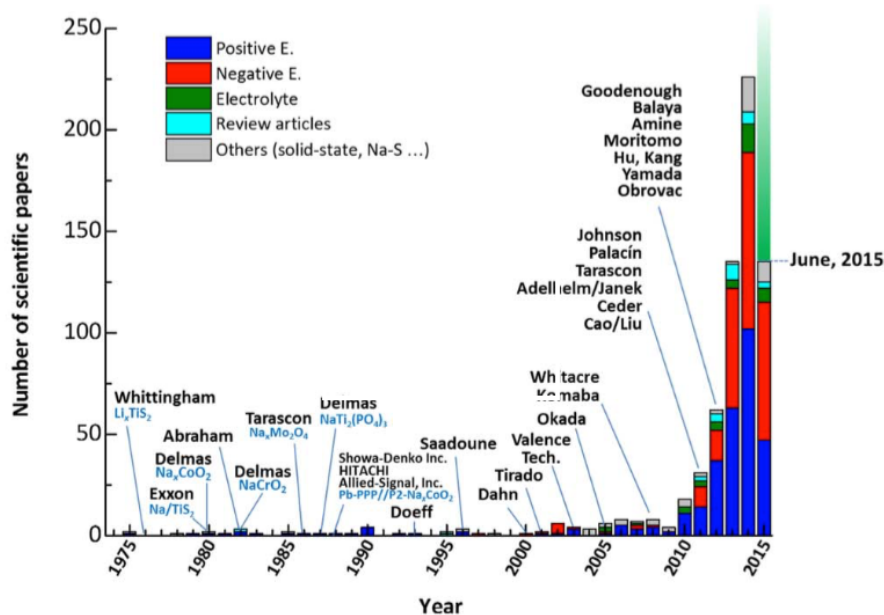
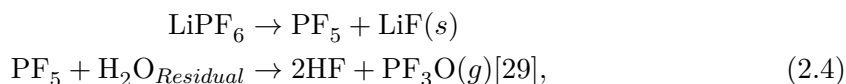


**Figure 2.9:** Number of publications until 2015 of the different parts of a SIB. Light green bar is projection for 2015. Reproduced under the CC-BY licence from [5].

Solvents reported for sodium-ion electrolytes are mainly those described in Section 2.2. Some common salts reported in literature for sodium-ion electrolytes can be seen in Figure 2.10. Eshetu *et al.* reported on the stability of these salts with respect to Al current-collectors [30]. They concluded that  $\text{NaPF}_6$  is the most stable candidate and attributed this stability to the formation of  $\text{AlF}_3$  species which protect the current collectors. The stability changes drastically if there is much residual water in the electrolyte, since  $\text{NaPF}_6$  risks breaking down according to the following mechanism:



producing HF, which in turn can serve to degrade other parts of the system. Taking the stability of  $\text{NaPF}_6$  into account, and assuming the amount of residual water is in the lower ppm range, many studies in SIBs have utilised the same LP 30 (1M  $\text{LiPF}_6$  in EC<sub>50</sub>:DMC<sub>50</sub>) electrolyte for investigations, only changing the ion from lithium to sodium [51].

Name of Na salt	Anion structure	Name of Na salt	Anion structure
NaPF <sub>6</sub>	$\left[ \begin{array}{c} \text{F} & \text{F} \\   &   \\ \text{F} & \text{P} & \text{F} \\   &   \\ \text{F} & \text{F} \end{array} \right]^{-}$	NaClO <sub>4</sub>	$\begin{array}{c} \text{O} \\    \\ \text{O}:\text{Cl}:\text{O} \\   \\ \text{O}^{-} \end{array}$
NaTFSI	$\begin{array}{c} \text{F} & \text{F} & \text{O} & \text{O} & \text{F} & \text{F} \\   &   &   &   &   &   \\ \text{F} & \text{S} & \text{N} & \text{S} & \text{F} & \text{F} \\   &   &   &   &   &   \\ \text{O} & & \text{O} & & \text{O} & \text{O} \end{array}$	NaFTFSI	$\begin{array}{c} \text{F} & \text{F} & \text{O} & \text{O} & \text{F} & \text{F} \\   &   &   &   &   &   \\ \text{F} & \text{S} & \text{N} & \text{S} & \text{F} & \text{F} \\   &   &   &   &   &   \\ \text{O} & & \text{O} & & \text{O} & \text{O} \end{array}$
NaFSI	$\begin{array}{c} \text{O} & \text{O} \\    &    \\ \text{F} & \text{S} & \text{N} & \text{S} & \text{F} \\   &   &   &   \\ \text{O} & & \text{O} & \end{array}$		

**Figure 2.10:** Molecular structure of some salts used in SIBs.

## 2.5 The Glyme Family of Solvents

Another set of organic molecules, than those described in Section 2.2, that have been considered for use in SIB electrolytes is the glyme family of solvents (Figure 2.11) [52]. For the sake of brevity only those members with  $n$ :s ranging from 1 to 4 and featuring  $R = \text{CH}_3$  will be reviewed here. The glymes are also abbreviated as "G( $n$ )"—G1 being monoglyme, G2 being diglyme, and so on. The names of the compounds studied are presented in Table 2.2, together with physical properties relevant for battery research. All the members of the glyme family are stable, amphiphilic, solvents, meaning that they to some degree show mixing both in polar and non-polar liquids. Another common feature of the glymes is that many of them are able to complex with metal ions to some degree, a property also denoted as "Chelation" in literature [53].

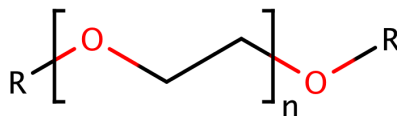


**Figure 2.11:** General structure of glymes. "n" denotes chain length.

n	Common name	Acronym	Density at 25 °C (g cm <sup>-3</sup> )	Melting point (°C)	Boiling point (°C)	Dielectric constant, $\epsilon$ at 25 °C
-	Ethylene Carbonate	EC	1.321 [54]	36 [54]	248 [54]	89.8 [17]
-	Dimethyl Carbonate	DMC	1.064 [54]	5.0 [54]	90 [54]	3.1 [17]
1	Monoglyme	G1	0.859-0.864	-69	84.5-85.2	7.3 [55]
2	Diglyme	G2	0.938-0.939	(-70)-(-64)	162	7.2 [55]
3	Triglyme	G3	0.980-0.986	(-45)-(-40)	216-220	7.5 [56]
4	Tetraglyme	G4	0.861-0.868	(-30)-(-29)	275	7.7 [56]

**Table 2.2:** Chain length, common name, acronym, and physical properties of the first four glymes in the series. Data for EC and DMC are provided as a reference. Data adapted from [9] unless other reference explicitly stated.

The glymes have, partly because of their stable solvent properties and their ability of chelation, been found useful in a range of different applications, both in industry and academia, as summarised by Tang and Zhao [9]. Main fields in academia include electrochemistry, organic synthesis, bio-catalysis, in material synthesis and for use in chromatography and NMR-techniques. Industrial applications involve uses as solvents in inks, components of refrigeration fluids, production of Active Pharmaceutical Ingredients (API). A number of industrial uses of G1-G4 are listed in Table A.2 in Appendix A. One noteworthy application to highlight is the use of glymes in products dedicated towards etching of fluorinated polymers—relevant to the implications of using fluorinated binders in an electrode of a battery featuring a glyme-based electrolyte.

In the subsections below, first the metal complexing properties of the glymes will be presented. Then, the main areas of usage of glymes in electrochemistry in battery research will be given a brief treatment. Finally, the findings of recent years', regarding the toxicity of glymes will be highlighted to point out possible difficulty and moral implications of using glymes in commercial application.

### 2.5.1 Metal Complexing Properties of Glymes

The G1 to G4 glymes all have ether oxygens interconnected by flexible alkoxy chains. Solvation of cations can thus occur by pairing the polar oxygens to the ion, rendering effective complexing agents [9]. For example, the coordination number diglyme with lithium is two, while the total coordination number of lithium is four, meaning that two of the oxygens of two molecules will coordinate with the cation [9]. In the case of diglyme, Jache *et al.* suggested that the same was true for sodium and that two diglyme molecules tightly embrace the Na-ions within the solvent [52]. Computational studies have indicated that the chelation mechanisms lead to a large amount of free ions in the solution, lowering the amount of ion pairing [9]. One explanation provided for the effective complex formation was that the loss in entropy associated with forming a glyme-ion complex is small [9]. Other *ab-initio* calculations have indicated that the high chain flexibility of the glymes allows many metastable structures for the metal-glyme complex featuring different geometries [57].

### 2.5.2 Electrochemistry of Glymes

The glymes' complexing properties have lead them to be used in a range of electrochemistry applications. Xia *et al.* showed the importance of the phase transfer catalysis role of the glymes when used in Na-Air battery concepts [58]. Here, the glymes play both the role of ion conduction and of facilitating NaO<sub>2</sub> super-oxide growth because of their phase-transfer properties. For conventional battery chemistries, Aurbach and Granot pointed out how glyme-based solvents were unsuitable for use with Li-metal anodes. This was because of the growth of a rough morphology, resembling dendrite formation, occurring during dissolution-deposition. They also suggested an anodic electrochemical instability [59]. The resulting anodic decomposition was mainly observed for ethyl glyme (R = CH<sub>2</sub>CH<sub>3</sub>, n=1) and it was concluded that in spite of decomposition, the stability was much better for the glymes than for comparable cyclic ethers, esters or carbonates.

Cui *et al.* conducted a smaller study where the authors claimed to observe anodic ether reduction products in XPS-spectra of cycled surfaces. The reduction was proposed to yield a very thin layer of ROCH<sub>2</sub>-Na species on top of a layer of inorganic NaF and NaO<sub>2</sub> species. They furthermore demonstrated how a diglyme-based electrolyte leads to a very efficient plating-stripping behaviour which they attributed to the stability and mechanical properties of the aforementioned film [60]. In two subsequent studies Jache *et al.* showed how graphite could be activated as an anode material when used in electrolytes based on

mono-, di- and tetraglyme [61, 52]. They attributed this to the co-intercalation, readily supported by XRD data. The co-intercalation seems to allow the Na to form so-called ternary graphite-intercalation compounds (t-GIC) featuring a site in the active material, a sodium atom and a solvent molecule supporting the intercalation. Comparing the results to similar experiments carried out with tetraglyme, they did not see any co-intercalation, suggesting that the coordination of triglyme with Na ions was unsuitable for t-GICs to form. Furthermore, the study showed how the t-GIC were supposedly very stable and associated with a high coulombic efficiency and good capacity retention.

Common for all of the studies using diglyme, is that they ascribe stable reductive behaviour to the solvent molecules or the films the solvents form upon reduction. No studies found in this literature review have focused solely on determining the oxidative and reductive limits of the G1-G4 molecules when used as a components in electrochemical systems. However, the general belief seems to be that they are stable against reduction when used with alkali metals or at least with sodium, either because a good SEI is formed or because no reduction takes place at all.

### 2.5.3 Toxicity and Cost of Glymes

The reason for deciding if a specific electrolyte is suitable for use in a future battery systems should not rely solely in its electrochemical performance. Two other notable factors are cost and toxicity. In Table 2.3 the costs of diglyme, EC and DMC are presented. The costs are based on the vendor price for purchasing solvent at 99.5 % purity in the largest possible volume [62]. Where volume based prices have been converted to weight based ones, the lowest value for density tabulated in 2.2 has been used.

Chemical name	Cost (EUR kg <sup>-1</sup> )
EC	51.5
DMC	104
Diglyme (G2)	303

**Table 2.3:** Cost of diglyme per unit weight as compared to EC and DMC.

Regarding the toxicity, a few studies have been conducted on the glymes—much due to the rise of the solvents’ use during the advent of semi-conductor and IT-industries [9]. With its base in animal trials on rats the toxicity of some members of the glyme family have been evaluated and concluded to show a "moderate *acute toxicity*" [9]. The  $LD_{50}$  dose for all the glymes listed in Table 2.2 is more than 2900 mg kg<sup>-1</sup>, with diglyme showing a  $LD_{50}$  dose of 3779 mg kg<sup>-1</sup>. Concerns regarding glymes have instead been directed towards the long-term reproductive effects. McGregor *et al.* reported the increase in sperm abnormalities detected in rats exposed to 250 - 1000 ppm concentrations of diglyme. Furthermore, doses of 684 mg kg<sup>-1</sup> suggested a pathological change in the testicles of exposed rats.

In 2011, the U.S Environmental protection agency announced that three glymes pose a high concern to the public because of these indications of reproductive toxicity [9]. In relation to this, the safety data sheet of the glymes in Table 2.2, carry the phrases "May impair fertility" and "May harm the unborn child". When it comes to impact on the natural environment, the same substances are mentioned as benign, with low bio-accumulation factors [9]. Searching for the Mono-Tetraglymes in the European REACH database, screening tests indicates inherent biodegradability in water for di-, tri- and tetraglyme, but not for monoglyme [63].

# 3

## Description of Experiments

Battery research spans a whole ensemble of measurement techniques and instruments. This project has focused on a few of those methods, for which the underlying theory is described in the first section of this chapter. The second section presents some general considerations and methodology used and also motivates the choice of electrode materials used. The third section presents experimental methods carried out to investigate the suitability of Na metal as a reference electrode in a diglyme-based electrolyte. Section four presents the techniques used for viscosity and ionic conductivity measurements. This is followed by section five, where experiments for stability of a future SIB using diglyme are presented. The sixth and final section presents experiments targeting identification of possible degradation mechanisms.

### 3.1 Theory of Main Methods Employed

The battery field, being multidisciplinary features the use of many different techniques. Only for studying SEI properties Pallavi Verma *et al.* listed no less than 22 different techniques [26]. In this section, the theory behind the methods mainly used in this project are elaborated on. Other techniques not used to a large extent or not being the main techniques for myself, are not treated herein. Some examples of such techniques with data nevertheless reported in this thesis are:

- Rolling ball viscosimetry to obtain electrolyte viscosity.
- SEM to study surface microstructure of electrodes.
- EDX to analyse elemental composition of cycled electrode surfaces.
- EIS to measure electrolyte ionic conductivity.

#### 3.1.1 Galvanostatic Cycling with Potential Limitation-GCPL

One common method to test electrode materials and cell setups is through galvanostatic cycling. By connecting the cells to a potentiostat that can track and regulate the current and voltage applied to the cell very precisely, arbitrary working conditions for a cell can be simulated.

Experiments are often run in either three or two electrode setups. In the prior case, two of the electrodes—denoted the counter- and working electrode—are constantly referenced towards a third, reference electrode (Figure 3.1). With such a setup, the electrochemical processes taking place at the anode and cathode in a battery setup can be properly separated. In a two electrode setup, one of the electrodes will instead serve as both reference and counter electrode. In this case, the proper working electrode voltage can only be controlled if the electrochemical potential is constant at the counter/reference electrode, which is sometimes the case when using alkali metal counter electrodes.

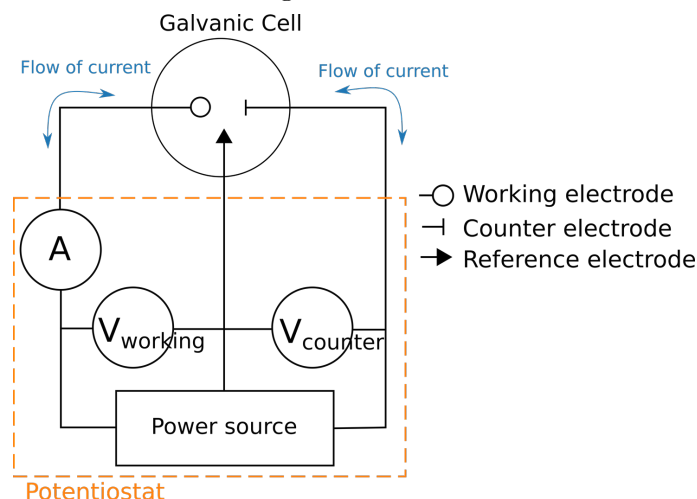


**Figure 3.1:** Principle of a three electrode setup. A current is measured between the counter and working electrodes. Voltages are, instead measured against a third, reference electrode. Image adopted with permission from [6].

In galvanostatic cycling, the current is set to some finite constant value by the user. Mostly, a potential limit is also set for both charge and discharge of the cell. The setup tested can

then be cycled between the upper and lower voltage cut-off limit for any number of times at the programmed current, while the total charge that can be harnessed upon charge and discharge is tracked along with the voltage at accumulated value of charge extracted per charge/discharge cycle.

It is common practice to define the amount of current drawn in terms of C-rates, expressing the number of times the theoretical capacity of the active material is passed in one hour. For example, a rate of C/10 equals a current that will extract/insert the complete theoretical capacity from the electrode material in 10 hours. A rate of 10C instead indicates that all theoretical charge is extracted/inserted 10 times in one tenth of an hour. Since the C rate is dependent on the total amount of theoretical charge available, the current drawn during an experiment will vary with both the type and amount of active material used.

### 3.1.2 Cyclic Voltammetry–CV

In cyclic voltammetry (CV), the voltage applied to the cell, instead of the current, is controlled and the current is recorded. When interpreting cyclic voltammetry data, the current,  $I$ , detected at each voltage,  $V$ , is plotted in a so called voltammogram. Each peak in the voltammogram will correspond to a specific electrochemical process taking place [17].

### 3.1.3 Electrical Impedance spectroscopy–EIS

The different mechanisms and regions that are present in any electrochemical system can be modelled as an equivalent circuit featuring a set of resistive and capacitive elements. As with every equivalent circuit featuring a network of passive components, it can be reduced to a single, frequency dependent, equivalent impedance. For example, the multilayered structure of the SEI described in Section 2.3 will contribute with a certain phase shift and damping of any time dependent electrical signal. So will the transfer of ions in the bulk of the electrolyte and the transfer of electron in the bulk of the electrode.

By applying a small amplitude sinusoidal voltage at varying frequencies and tracking the current response, the equivalent impedance of a system can be probed at different frequencies and plotted on a Bode or Nyquist form. From the shape of the Nyquist curve, it is later possible to extract parameters for previously designed models, giving information about system kinetics and charge transfer [64]. However, it is also possible to use the techniques to simply detect any change taking place in the SEI structure or bulk of the electrode, as this would change the EIS spectrum.

### 3.1.4 Gas Chromatography, Mass spectrometry–GC/MS

The principle of coupled gas chromatography/mass spectrometry setup is illustrated in Figure 3.2. For the gas chromatography (GC) part, an analyte in gas phase is injected into the column where a steady stream of inert gas is flowing. The gas flow then separates the different components of the analyte based on their tendency to be retained inside the column. Retention will in turn depend on the amount of interaction the component experiences with the column walls, which are often coated with some kind of polymer to improve separation. In case the analyte was a liquid, it would first have to be heated for evaporation, thus limiting the detection to that of substances able to evaporate.

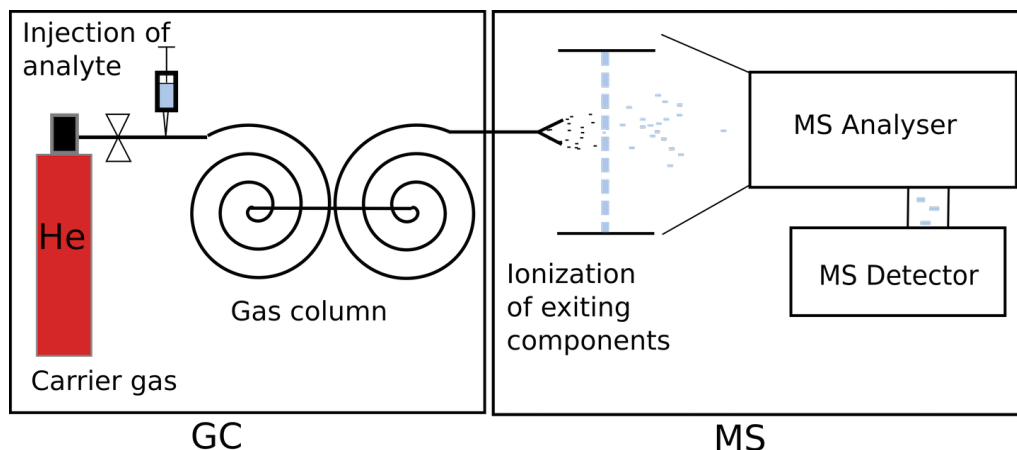


**Figure 3.2:** Principle of a GC/MS setup.

After the GC-column, the components separated will reach a mass spectrometer (MS) at different times. The mass spectrometer works by first ionising the analyte component and then separating the resulting fragments by their mass/charge ratio in the analyser. Each substance emerging from the gas column produces a cascade of ionised fragments serving as a fingerprint for the substance. In this way the contents of the analyte can be determined one-by-one [65, 66].

### 3.1.5 FTIR Spectroscopy

Fourier Transform Infrared Spectroscopy (FTIR) involves illuminating a sample with broadband infrared radiation and recording reflected or scattered light. Because some frequencies of the incoming IR-radiation will match vibrational transitions in the sample, the response will be a modulated signal containing information about the frequencies that were absorbed. Illuminating a sample at an angle and taking advantage of the IR radiation being heavily absorbed in the bulk of the material sample studied, the technique can be used to probe surface layers. SEIs from cycled surfaces in batteries could thus be analysed if they remain intact [67].

## 3.2 Experimental Techniques—General Considerations

Laying the foundation for the description of the further experiments described in this chapter, the following section aims to summarise all those methods that were employed repeatedly throughout the project. Such experimental considerations include the choice of electrode materials, the way electrodes were fabricated, how electrolytes were prepared and how cells were assembled. If not noted otherwise, the methods and choices of materials outlined here will be assumed in the following sections.

### 3.2.1 Choice of Electrode Materials

Even though the main focus has been to study degradation mechanism and performance of employing diglyme as an electrolyte solvent, it is impossible to overlook the role of the electrodes in any battery system. A future SIB could comprise many different electrode materials. However not all are as well documented and practical for use in large batches, as is desired when testing electrolytes. Furthermore, not all electrodes are stable and undergo irreversible phase transformations upon cycling. One SIB candidate can be built using a NVPF cathode and a HC anode. These materials have shown stable cycling behaviour and high specific capacities. Combining the electrodes the theoretical energy density becomes

284 Wh kg<sup>-1</sup>, when only considering the active materials. Another stable material that could be used is NVP, which can act as both an anode and a cathode. NVPF, NVP and HC were chosen for this work, because they have a previously documented stable cycling performance. Also they have well documented capacity/voltage profiles, with major parts of the profiles being distinct voltage plateaus, mitigating identification of anomalies in a system. A third reason for using NVPF and HC, was that the materials were accessible as large batches of tape cast products—improving reproducibility in experiments.

### 3.2.2 Tape-Cast Electrodes

Electrodes of HC and NVPF were manufactured using a pre-fabricated, tape cast product (CEA, Grenoble), on two sides of a aluminium current-collector. To make electrodes, one side of the collector tape was scraped using small amounts of ethanol and a scalpel (Figure 3.3).

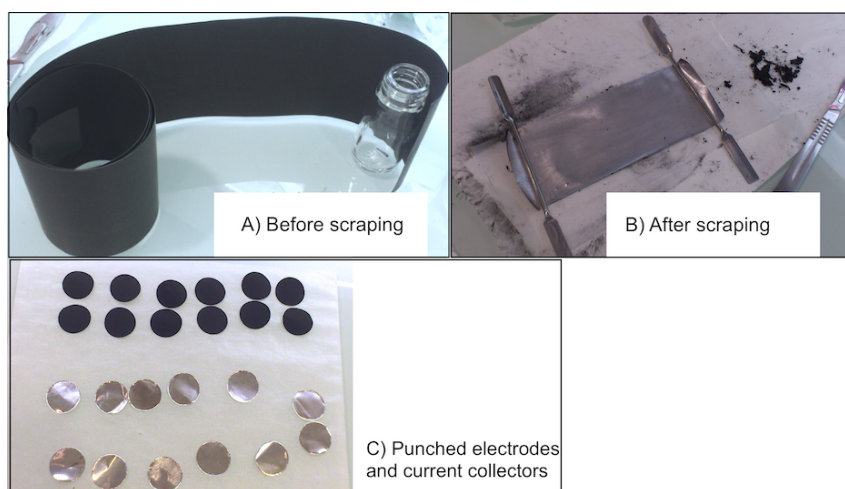


**Figure 3.3:** Sequence of electrode fabrication procedure featuring, a), tape cast precursor on both sides of Al current collector, b), scraped precursor and, c), punched electrodes with a set of current-collectors prepared for weighting

The scraped tape was left to dry over night in room temperature. After drying, electrodes of desired size were punched from the electrode tape using a punching-tool. Also, 10 pieces of aluminium foil of the same thickness, size and composition as that used for the tape electrode were punched using the same size of punching-tool. Foil pieces were produced to be able to estimate the average weight of a electrode current-collector and make an estimate of the error associated with spread in the weight distribution of the current collectors. The resulting characteristics of two sizes of electrodes used are shown in Table 3.1. After punching, each electrode was weighed and labelled, and then dried in a Büchi-oven for 24 hours at 80 ° C and brought into the glovebox, while remaining under vacuum in the Büchi tube.

Electrode area [cm <sup>2</sup> ]	Mean weight of Al-current collector [mg]	C.C. weight standard deviation [mg]
0.62	3.57	0.073
0.95	5.19	0.040

**Table 3.1:** Electrode area, mean weight of current collector and standard deviation of current collector (C.C.) weight for two different sizes of electrodes used.

#### 3.2.3 Powdered Electrodes

In a handful of measurements it was not practically possible to use the tape cast electrodes. Here the experiments had to fall back on powdered electrodes of either NVPF or NVP. For the powders, the pristine active material was ball milled for 15 minutes with Super Carbon to form a 80:20 mixture by weight. This was done to ensure proper mixing and good conduction among the different active material grains. An important feature of powdered electrodes is that they do not contain any binder, making the system less complex in terms of components, but also less stable in terms of mechanical rigidity. Less rigidity makes them more susceptible to disconnection of active material grains.

#### 3.2.4 Electrolyte Preparation

The main component investigated – the 1 M NaPF<sub>6</sub> in diglyme electrolyte– for use in a future full cell system was prepared by mixing diglyme (Sigma-Aldrich, Anhydrous, 99.5 % purity) and NaPF<sub>6</sub> salt (Stella-Chemifa). Solutions were prepared with molarities of 1 M, 0.75 M or 0.5M, removing any residual water using molecular sieves. Water content was verified to be less than 20 ppm using Karl-Fischer titration. After half of the project the Karl-Fischer apparatus broke down. Subsequent preparations of electrolytes were instead left to dry according to previous know how, drying for at least 7 days with the molecular sieves before usage, to be completely sure the water content was low. In experiments where other solvents were used for bench-marking, the same procedure as outlined above was employed.

#### 3.2.5 Cell Assembly

For the experiments where performance and degradation of systems using a diglyme based electrolyte was studied, cells were built according to two layouts - coin cells and Swagelok cells. Because of the air-sensitive nature of the SIB-system and salt, all cells were assembled in a inert Ar-atmosphere inside a glovebox (MBRAUN MB200-MOD) with the surrounding oxygen and water content being less than 10 ppm. In this section follows the assembly description for the two types of cells used.

#### 3.2.6 Coin Cells

Coin cells made out of stainless steel were assembled according to Figure 3.4. Electrodes were placed on both sides of a boro-silicate glass-fiber separator (Whatman GF/D). Electrode size was varied due to the specific balancing required for each setup. In case of a NVPF positive electrode, a piece of Al-foil was cut and placed to completely cover the the cathode part of the casing to avoid corrosion of the stainless steel, which had been indicated by earlier tests. In the case of a Na-metal anode, the stainless steel disk in the anode side was coated with a thin layer of Na that was rolled out with a test-tube that was separated from the Na by a Mylar®, ensuring that the metal covered the whole electrode and that the surface was as flat as possible. Surface flatness was desired to not introduce any roughness-related effects in the system that would not be reproducible.

After putting the electrodes and foil in place, 14 drops of the desired electrolyte were added to the separator using a Pasteur pipette to ensure proper soaking of the separator. The cell was sealed through clamping and then brought to testing within 30 minutes after assembly.

#### 3.2.7 Swagelok Cells

Swagelok cells were assembled according to the illustration 3.5. All cell components, apart from electrodes and separator, were first washed and scrubbed with a Scotchbrite sponge, water and dish-washing liquid. Then the plungers were polished with a grade 1000

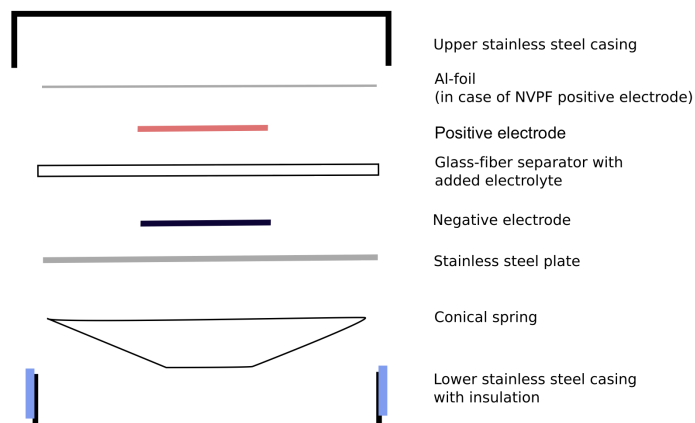


**Figure 3.4:** Schematic of Coin cell assembly

sandpaper to remove any surface roughness and surface contaminants (such as surface oxides). Finally the components were sonicated in ethanol and then in acetone for 15 minutes each. After sonication the components were dried in a oven at 55 ° C for at least 3 hours. The cell components were then pre-assembled as far as was possible for the cell type to be built. In the case of EC-DMC being used as electrolyte a PTFE tape was used to insulate the plungers from the cell body. In case of diglyme being used as an electrolyte solvent, instead a Mylar® foil was used and cut to precisely cover the inner part of the cell body. Mylar was used because of earlier experiments indicating that PTFE was degraded upon cycling in Swagelok cells.

When it turned out that the Mylar® foil might suffer from a similar problem, two other insulation materials were tested. One was Kapton® film. The other was a Poly-amide 6,12 laminate, commonly employed in food-packaging industry, which was provided by AlfaPac AB, Sweden. These materials were tested to finally fall back to the coin-cell concept when cycling cells. The resulting polymer films after cycling experiments in Swagelok cells are presented in Appendix F.

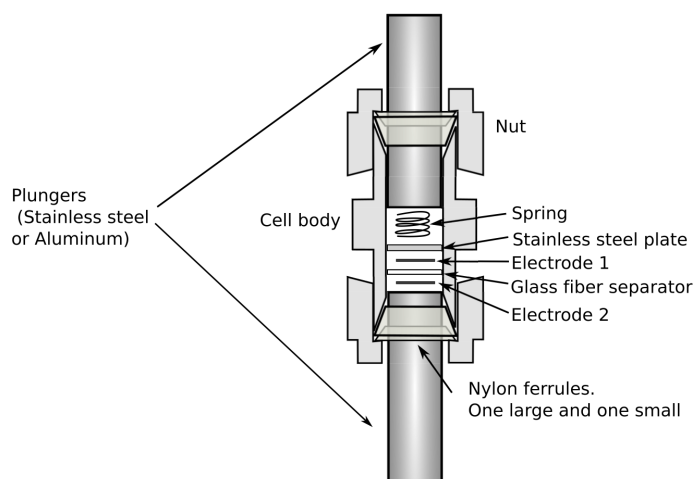


**Figure 3.5:** Schematic of Swagelok cell assembly

### 3.3 Electrolyte Stability with Na-metal

To be able to proceed with any further testing of full cell systems employing 1 M NaPF<sub>6</sub> in diglyme, the initial part of the project focused on determining the stability of pure Na electrodes. Earlier test in EC:DMC based electrolytes [68] had shown that stability of the alkali metal electrodes is not necessarily the case and that continuous reduction of the electrolyte seems to be occurring at a Na metal electrode. Since such a process would interfere with further measurements, reactivity of Na electrodes was determined by studying gas evolution, visual inspection and by impedance spectroscopy of symmetric Na|Na cells.

#### 3.3.1 Investigating Film Growth on Na Surfaces

To judge whether a presumed electrolyte decomposition resulted in a growing resistive SEI on the Na, an EIS study was made in Swagelok cell using symmetric Na|Na electrodes and Mylar film for insulation. The spectroscopy measurement was performed using BIO-logic VMP-3 potentiostat recording the impedance each 6 hour for 96 hours applying a 10 mV sinusoidal voltage at frequencies ranging from 0.02 Hz to 200 kHz with 10 points sampled per frequency decade. In each 6-hour interval the cell was left at OCV to let the growth of any SEI continue.

#### 3.3.2 Investigating Gas Release from Electrolyte Decomposition

To study if a possible decomposition of diglyme electrolyte on Na metal surfaces resulted in any continuous gas release, a pressure-cell featuring a Swagelok body, a column and a pressure sensor was assembled according to Figure 3.6. On the bottom part of the cell a 5.52 mg disk with radius 4 mm of Na metal was coated. 250  $\mu$ L of 1 M NaPF<sub>6</sub> in diglyme electrolyte was added to the cell, whereupon the cell was sealed directly. The pressure evolution in the cell was tracked for more than 9 days.

#### 3.3.3 Storage Experiment

A final experiment was carried out to detect any film formation arising from reduction of diglyme on a Na metal surface. This was done by submerging a sphere of Na metal in a vial of the 1 M NaPF<sub>6</sub> diglyme electrolyte. The colour change of the disk was then recorded over 30 days.

### 3.4 Ionic Conductivity and Viscosity

An electrolyte suitable for a future industry application needs to have a high ionic conductivity, since this property impacts the potential charging rate of a battery. Furthermore, the temperature dependence of such a property would also be important as a future battery would be assumed to operate at a range of different temperatures without losing too much performance. Aiming to further characterise if the diglyme electrolyte had practical use in a future SIB, the ionic conductivity was measured at different concentrations of NaPF<sub>6</sub>. A further reason to do so was to understand if the special, chelating, properties of the solvent could have any immediate impact on the ionic conduction in the electrolyte and if the Walden rule was obeyed.

The ionic conductivity was tested for 0.5M, 0.75M and 1 M solutions of NaPF<sub>6</sub> using a Biologic, MCS 10 temperature controlled frequency response analyser at temperatures between 10°C and 80° C, sampling at steps of 5 ° C. For the 0.75M and 0.5M concentrations, two simultaneous measurements were carried out. For the 1 M solution the amount of electrolyte prepared was not enough, leading to only one measurement being possible for

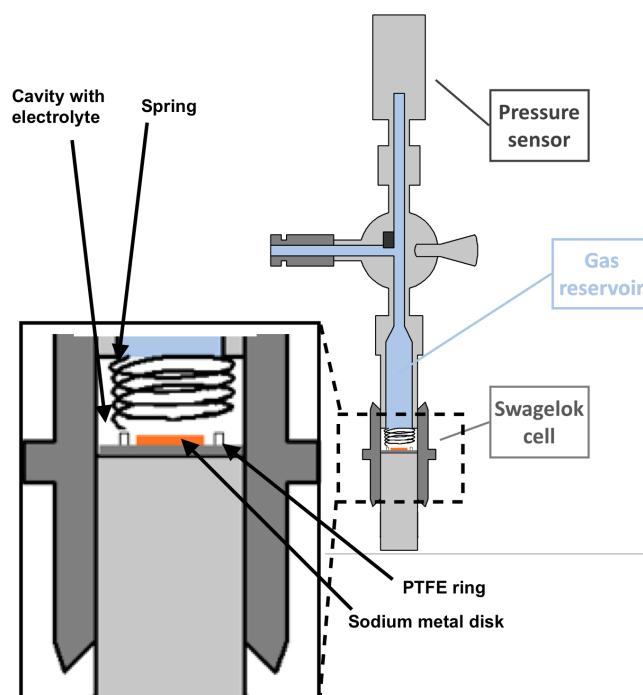


**Figure 3.6:** Layout of pressure cell used for determining gas evolution from Na in contact with electrolyte. Based on illustration from [7].

the conductivity measurement. Viscosity was measured for the same set of concentrations using a Anton Paar, Lovis 2000 M/ME rolling-ball microviscosimeter with a capillary tube featuring a 1.59 mm diameter. Temperatures were sampled at 5 ° C steps between 10°C and 60°C.

### 3.5 Electrolyte Stability Window

Guided by the indication of being able to use Na as a stable reference and realising that ionic conductivity was satisfactory, further work was carried out to characterise the oxidative and reductive stability of the electrolyte 1 M NaPF<sub>6</sub> in diglyme, thus determining the electrochemical stability window. The oxidative potential was studied using linear sweep and cyclic voltammetry in Na Swagelok half-cells using working electrode of NVPF to maintain the cathode present in future full cells. The cell was then cycled between 3 and 5 V vs Na<sup>+</sup>/Na<sup>0</sup> at a rate of 0.1 mVs<sup>-1</sup> using a BIO-logic VMP3 potentiostat. As an electrolyte, both 1 M NaPF<sub>6</sub> in diglyme and a 1 M NaPF<sub>6</sub> in EC<sub>50</sub>DMC<sub>50</sub> were tested – the EC<sub>50</sub>DMC<sub>50</sub> being used as a reference to detect any solvent-independent electrochemical processes. The the onset potential was defined to occur when the current density of the cell reached 50 μ A cm<sup>-1</sup>, the area of the electrode being 0.95 cm<sup>2</sup>. Such a condition was consistent with previous work on electrocatalysis [69]. After determining the oxidation potential at the NVPF electrode, an equal setup was constructed to cycle a NVPF half-cell 5 times below the oxidative stability limit. The cycling was done to further study the insertion/extraction characteristics of the electrode at hand.

Reductive stability for diglyme electrolyte at the anode could not be tested with the same demand for realistic condition, since hard carbon shows insertion of Na starting for

relatively high potentials continuing almost to 0V vs  $\text{Na}^+/\text{Na}^\circ$ , thus masking any reduction of the electrolyte. Instead, the reductive potential was studied using a Cu-foil working electrode, since previous studies had indicated excellent plating/stripping efficiencies on such foils when using diglyme as a solvent [60]. The foil had previously been roughened with a grade 300 sandpaper, to increase the available surface area. The cells were cycled to 0V vs  $\text{Na}^+/\text{Na}^\circ$  at a rate of  $0.1 \text{ mVs}^{-1}$  using a BIO-logic VMP3 potentiostat and any reductive peaks were recorded in the voltammogram. The same measurement was later repeated using a EC<sub>50</sub>:DMC<sub>50</sub> 1 M NaPF<sub>6</sub> electrolyte for comparison. The results acquired from the reduction experiment were later compared to calculations of reduction potential made by Piotr Jankowski at Chalmers University of Technology. Here density functional theory calculations were used, including an implicit solvation by C-PCM for diglyme in solution at different levels of complexation with an  $\text{Na}^+$  cation.

### 3.6 Galvanostatic Cycling Experiments

Noting that Na-metal electrodes seemed stable in the electrolyte and that the ESW of the 1 M NaPF<sub>6</sub> in diglyme electrolyte seemed broad, further steps were taken to characterise how individual HC, NVPF and NVP electrodes performed in full and half cells. The reason doing so was that any electrolyte for future commercial cells, a stable cycling behaviour must first be verified. In this section, various cycling experiments conducted to characterise the considered electrolyte are presented. All capacity/voltage profiles for the described experiments were acquired at C/10 using a BIO-Logic VMP3 potentiostat at room temperature. The C rate was calculated based on the extraction of 2 Na from NVPF, making rates consistent between half cells and full cells. For NVP, instead, the C rate was based on the mass of anode.

#### 3.6.1 Half-cell Capacity Tests of Diglyme Electrolytes

To study capacity fading and performance of the two different electrodes in a diglyme electrolyte, half-cell galvanostatic cycling was performed in coin cells using Na-metal as an anode. The cells were cycled 15 times using the cut-off potentials given in table 3.2 and then stopped based on the stable capacity retention seen. Based on the results from the half-cell, a full cell reconstruction was done by subtracting the half-cell voltages corresponding to when the electrodes at each level of extraction/insertion of ionic charge carriers.

Working electrode	Lower cut-off potential (V vs $\text{Na}^+/\text{Na}^\circ$ )	Upper cut-off potential (V vs $\text{Na}^+/\text{Na}^\circ$ )
HC	0	2
NVPF	2	4.3

**Table 3.2:** Cut-off voltages for cycling of materials in half-cells, using Na metal as counter electrode

When doing the reconstructions, further presented in appendix C, irreversibility was not accounted for, passing from one cycle to the next, with the purpose of saving time. Instead the reconstructions from only the first cycle were used to approximate the potential vs. Na of each electrode in a full cell.

#### 3.6.2 Full Cell Capacity Tests of Diglyme Electrolyte - Galvanostatic Cycling

Recording a good cycling behaviour in half-cells, the focus was shifted towards full cells of HC/NVPF—the type of setup which would have a chance of being commercialised.

Cycling was done as in using 1 M NaPF<sub>6</sub> in diglyme in coin cell, using one HC anode and one NVPF cathode and employing the cut-off scheme in table 3.3. In the full cells, the electrodes were not completely balanced in capacity because of difficulties doing so with tape cast electrodes. Instead, the capacity ratio between carbon and NVPF was approximately NVPF:HC 1.0:1.1 based on charge capacity of the first charge in half-cells. Since HC capacity was in excess, the mass of active NVPF was used to set the C-rate.

Electrode setup	Lower cut-off potential ( $V_{cell}$ )	Upper cut-off potential ( $V_{cell}$ )
NVPF/HC	2	4.3

**Table 3.3:** Cut-off voltages for cycling of materials in full cells

Swagelok cells were also built to test full cell behaviour, but because of problems with stability and reproducibility, this concept was abandoned for the more stable coin-cell setup.

### 3.6.3 Cycling Different Voltage-regions of the Active Materials

Wanting to understand the voltage dependence of the capacity fade observed in full cells the different potential-regions of the electrode materials were explored by changing the balancing of the electrodes and cycling them in coin-cells. The different schemes employed are listed in 3.4. Here, also the regular full cell is included as a reference. The electrode masses listed are typical for one repetition of the experiment. Were the experiments to be repeated, the exact mass of one electrode would most likely be different, forcing the mass of the other electrode to be changed in order to maintain the balancing.

Region cycled	Lower cut-off voltage [ $V_{cell}$ ]	Upper cut-off voltage [ $V_{cell}$ ]	Cathode active material mass [mg]	Anode active material mass [mg]	Comment
NVPF plateaus, HC slope and plateau	2.0	4.3	9.50	4.89	-
Upper plateau of NVPF only, HC Slope and Plateau	3.8	4.3	9.64	4.68	Mostly HC plateau is used, NVPF completely discharged on first cycle to reach second plateau
Lower plateau of NVPF only, HC slope and plateau	2	3.8	12.85	3.28	-
Both NVPF plateaus, HC slope only	2.0	4.3	6.259	4.74	-
Both NVPF plateaus, HC slope only	2.0	4.0	6.259	4.74	Upper cut-off voltage in previous scheme was lowered after 16 cycles

**Table 3.4:** Regions cycled and their approximate voltage intervals for the anode and cathode as approximated by half-cell reconstructions. masses are values used for one experiment.

### 3.6.4 Cycling of NVP/NVP Cells

Further investigating the potential dependence of the capacity loss seen in full cells, a NVP/NVP coin cell was assembled using NVP powder electrodes as both anode and cathode. The reason for doing so was to be able to explore plateaus featuring yet another set of voltage plateaus to decide whether the diglyme 1 M NaPF<sub>6</sub> was stable at those,

well-defined, potentials. The cycling was performed in coin-cells with a scheme that can be seen in Table 3.5. Worth noting is that the upper cut-off was lowered after 10 cycles because it was feared that some of the conductive carbon sp was also used to intercalate Na at the end of charge, when the anode reaches its lowest potential. By lowering the cut-off the risk of doing so could be mitigated.

Region cycled	Lower cut-off voltage [V <sub>cell</sub> ]	Upper cut-off voltage [V <sub>cell</sub> ]	Cathode active material mass [mg]	Anode active material mass [mg]	Comment
NVP upper plateau, NVP lower plateau	0.0	2.8	3.23	7.81 mg	Capacity for the two plateaus of NVP are not symmetrical
NVP upper plateau, NVP lower plateau	0.0	2.0	3.23	7.81 mg	Same setup as previous row, upper cutoff lowered after 10 cycles.

**Table 3.5:** Cycling scheme for symmetrical NVP/NVP cell

### 3.7 Physico-chemical Characterisation of Capacity Fade

The final part of the project aimed towards characterising cycled cell components and to further investigate the capacity fade seen in full and half cells. In this section methods used in trying to do so are presented. The techniques employed vary from quite complicated (GC/MS) to simple storage experiments to detect colour changes.

#### 3.7.1 GC/MS of Cycled Cell Separators

Observing a large initial irreversibility from hard carbon half-cells, an attempt was made to identify possible decomposition products using coupled liquid injection-GC/MS and the chromatograms to reduction schemes of the electrolyte. The separators from full cells that had been cycled 50 times and half-cells that had been cycled 10 times were recovered and soaked in 1 mL of dry acetonitrile ( $H_2O < 0.001\%$ ). The separators were then removed from the soaking liquid and discarded. The remaining blend of acetonitrile and soluble compounds from the separator was diluted 100 times before being injected into the GS/MS setup, consisting of a trace 1300 series GC ultra-gas chromatograph coupled to an ISQ mass spectrometer. The chromatographic separation was performed by using a “BPX70” cyanopropylpolysilene-siloxane- based capillary column (30 m 0.25 mm i.d., 0.25 mm) from SGE.

#### 3.7.2 SEM and EDX Analysis of Cycled Anodes

Complementing the GS/MS analysis to detect any solid degradation products in HC half cells using 1 M in  $NaPF_6$  diglyme, SEM micrographs of cycled cells were recorded using a Hitachi S-3400N Microscope. Before imaging, HC anodes from full cells had been cycled 1.5, 2 and 50 times in 1 M  $NaPF_6$  diglyme electrolyte using the same cut-off voltages as in Section 3.6.2. Because of limitations in the movement of the stage of the microscope, the samples had to be transferred in air before being mounted inside the microscope.

While inside the microscope, an EDX analysis was carried out on the samples to identify any elemental contamination. After detecting vanadium in the EDX spectra it was decided to investigate if the metal came from soluble species forming at the cathode and if it was only deposited during the first cycle. This was done by cycling a NVPF cathode in

half cell and HC anode in half cell according to the scheme in table 3.6. The half cells were then disassembled and the electrodes recovered. The NVPF was then washed in fresh electrolyte, with the purpose of removing any soluble species. The washed NVPF electrode and the extracted HC electrode were then used to assemble a new coin cell which was cycled 10 times according to the scheme on the third line of table 3.6. After cycling the full cell was disassembled and the anode analysed using EDX.

Electrode setup	Lower cut-off potential	Upper cut-off potential	Cycles	Comment
NVPF/Na	3.5 V vs Na <sup>+</sup> /Na <sup>°</sup>	4.3 V vs Na <sup>+</sup> /Na <sup>°</sup>	1	
HC/Na	0 V vs Na <sup>+</sup> /Na <sup>°</sup>	1.4 V vs Na <sup>+</sup> /Na <sup>°</sup>	1	
NVPF/HC	2 (V <sub>cell</sub> )	4.3 (V <sub>cell</sub> )	10	Assembled using the active materials from previous 2 rows after washing the NVPF.

**Table 3.6:** Cut-off voltages and cycling scheme for further exploring possible vanadium extraction

### 3.7.3 FTIR-Spectroscopy of Cycled Cells

To further determine if there was any SEI film formation on the surface of cycled hard carbon anode, FTIR was used to study electrodes cycled 2 and 1.5 times in full cells using the same cut-off voltages as in Section 3.6.2. The reason for not examining electrodes cycled more times was that any film formation was thought to happen mainly at the first and second cycles, since these cycles were associated with the largest irreversibilities. For the FTIR analysis, cycled coin cells were disassembled under argon glove-box conditions and the carbon anodes allowed to dry in the glove-box atmosphere for more than 24 hours. The electrodes were then transported in sealed coffee-bags to a nitrogen-filled glove-box, standing in the same clean-room as the IR spectrometer. The cycled anodes were mounted in a praying mantis diffuse reflectance accessory (HARRICK) to allow for airtight transfer to the spectrometer. IR measurements were carried out in diffuse reflectance mode using a Vertex 70 FT-IR spectrometer, sampling 16 times after having flushed the sample chamber with nitrogen gas for 5 minutes. To remove any contributions from the bulk hard carbon, a background of a pristine HC-electrode was initially recorded. Also a spectrum was recorded for a hard carbon electrode that had been soaked in the diglyme 1 M NaPF<sub>6</sub> electrolyte for 20 minutes and then allowed to dry for 2 hours in glove-box conditions. The soaked and dried electrode was made as a comparison, to record any effects arising solely from the electrolyte penetrating the electrode or evaporating, leaving a crystalline surface film behind.

### 3.7.4 Binder Stability

The half-cell capacity fade in hard carbon was thought to come partly from the reaction with binder material. Evaluating the hypothesis, PVDF binder was dissolved in acetone and coated on one side of two stainless steel, reference, disks. The disks were dried at 55 ° C for 24 hours and then brought into the argon filled glove-box. Thereafter, one disk was submerged in a vial containing 1 M NaPF<sub>6</sub> in diglyme electrolyte and the other in a vial containing 1 M NaPF<sub>6</sub> in EC<sub>50</sub>:DMC<sub>50</sub> electrolyte. Change of colour of the liquid and PVDF film was then monitored for 5 days (right part in Figure 3.7). In the next stage, the same experiment was repeated, now coating the other side (the one not coated with PVDF) of the steel disk with Na metal. The purpose of this was to bring the binder and metal into electrical contact without physical contact. For the Na/binder system the change of colour of the liquid was also monitored for 5 days (left part in Figure 3.7).

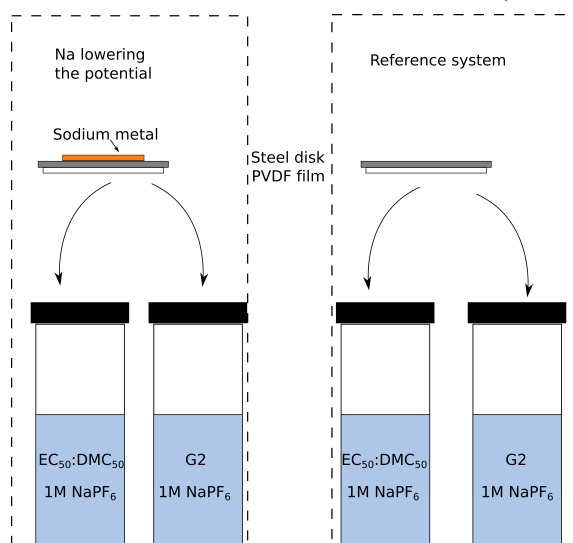


**Figure 3.7:** Experimental procedure used to compare degradation of binders by Na in EC:DMC- and diglyme-based electrolytes.

# 4

## Results and Discussion

In this chapter the results from the project are presented. The first section elaborates on the stability of Na electrodes in G2 NaPF<sub>6</sub> electrolyte. This lays the foundation for further work with Na as a stable reference electrode. The second section presents another perspective of the solvent studied, focusing on its ion conducting characteristics. In the third section the electrochemical stability window of the solvent is investigated using a series of voltammetry experiments. The fourth section moves on to the study of full and half cells comprising active materials that are considered for future commercial SIBs: HC, NVPF and NVP. The fifth and final section presents results pointing towards the reasons for the loss observed in HC electrodes and full cells.

## 4.1 Stability of Na Electrodes

Aiming to evaluate 1 M NaPF<sub>6</sub> in diglyme as an electrolyte for future SIBs the stability of the mixture at Na metal electrodes was initially tested. Below results are presented from experiments studying the gas evolution from Na surface that are in contact with the electrolyte considered. Furthermore, results from impedance spectroscopy and storage experiments of Na with the electrolyte are elaborated on.

### 4.1.1 Gas Evolution from Na Surfaces

As a first check for the reductive stability of the 1 M NaPF<sub>6</sub> in diglyme, gas evolution was studied from storing Na metal at open circuit conditions. The pressure as a function of time shows that an equilibrium of ca. 1.050 bar is reached (Fig. 4.1 A), which corresponds to  $5 \times 10^{-3}$  moles of gas per mole of available Na.

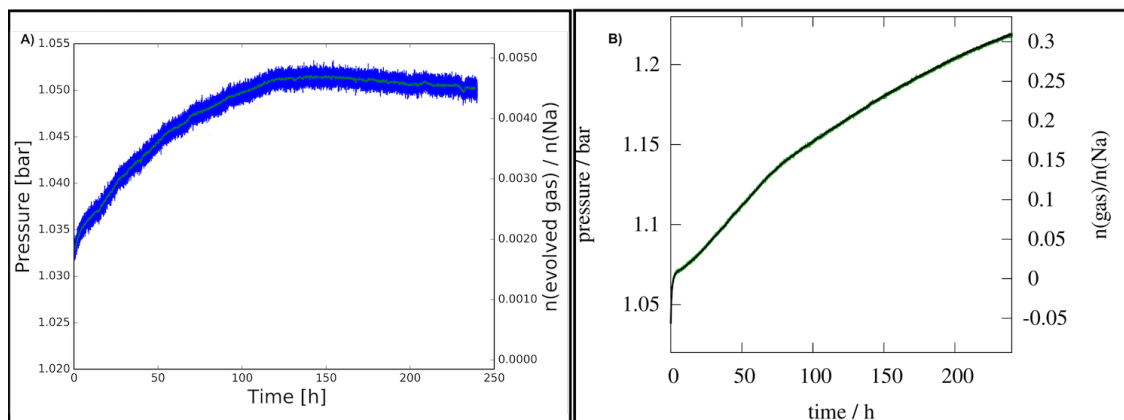


**Figure 4.1:** Pressure evolution at 25 ° C from Na metal stored, **A**), in 1 M NaPF<sub>6</sub> in diglyme and **B**), in 1 M NaPF<sub>6</sub> in EC<sub>50</sub>:DMC<sub>50</sub>. At the left y-axis and at the right y-axis the total pressure and amount of gas related to the total number of moles of Na are shown, respectively.

Putting the pressure into perspective, 1 M NaPF<sub>6</sub> in EC<sub>50</sub>:DMC<sub>50</sub> experiences a continuous gas evolution reaching fractional values well above 0.3: 2 orders of magnitude higher than the diglyme-based electrolyte<sup>1</sup>. Using diglyme as a solvent thus clearly prevents any pronounced gas evolution upon contact with metallic Na. The lack of continuous gas evolution could be due either to the decomposition product(s) forming a passivating SEI on the Na surface and/or only being solid/soluble species and not gases. A third option is that the electrolyte is completely stable. Since a PTFE ring and insulation is used, the small gas evolution might come from the degradation of this ring.

### 4.1.2 Impedance Evolution of Na Electrodes diglyme electrolyte

For a further indication of any potential SEI formation leading to the formation of solid surface species, EIS was employed on symmetrical Na|Na cells. The main feature recorded was an impedance profile shrinking and stabilising as time progresses (Figure 4.2). After 36 hours the impedance spectra of the circuit is almost not changing.

<sup>1</sup>Data provided by Romain Dugas, Collège de France.

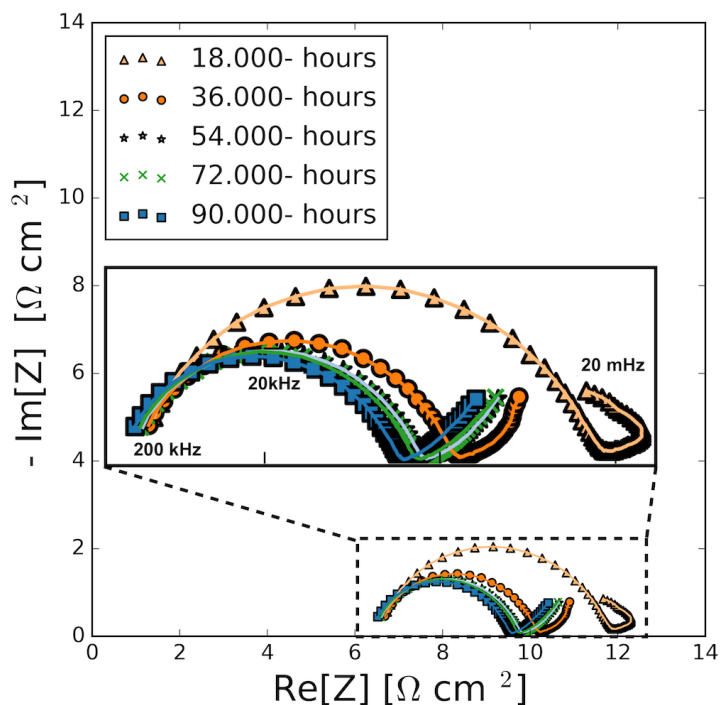


**Figure 4.2:** Impedance spectra at different times for a symmetric Na|Na Swagelok cell left at OCV for 90 hours.

A decreasing total impedance would not be expected with the growth of a film on the Na-disks, which instead would show a growing impedance (as is reported in [51]). The reason for the observed stability could either be due to the formation of very thin electrically insulating surface film, giving rise to only a small total impedance, or a continuous reduction of the electrolyte giving rise to only soluble reduction products. A final reason could be that there is no film formation at all. In either case, the impedance measurement highlights one important feature: the Na electrode is a stable reference for other systems, since the voltage drop from the Na metal will not grow as a result of continued exposure to the electrolyte.

#### 4.1.3 Storing Na Metal in Electrolyte

As a simple final test of reactivity between a 1 M  $\text{NaPF}_6$  in diglyme electrolyte and Na, a Na sphere was stored in electrolyte for 30 days. The lack of colouration seen in Figure 4.3 further indicates a lack of such reactivity.



**Figure 4.3:** A Na sphere stored with 1 M  $\text{NaPF}_6$  in diglyme

## 4.2 Ionic Conductivity of Diglyme-based Electrolyte

A future electrolyte for any type of battery must show a high  $\sigma$ , allowing for low energy loss ion transport, even when charge or discharge rates are moderately high. Also  $\eta$  of the electrolyte should be low to allow for proper soaking. The relation between  $\sigma$ , and  $\eta$  is usually expected to follow a Walden behaviour. The ionic conductivity for the 1 M, 0.75M and 0.5M NaPF<sub>6</sub> in diglyme does not conform to a Walden behaviour with slopes less than one for all concentrations (Figure 4.4). The lower the concentrations gets, the more the behaviour deviates. However, at room temperature, the conductivity for 1 M NaPF<sub>6</sub> is  $\approx 7 \text{ mS cm}^{-1}$ , which is comparable to other, more conventional, electrolytes [13].

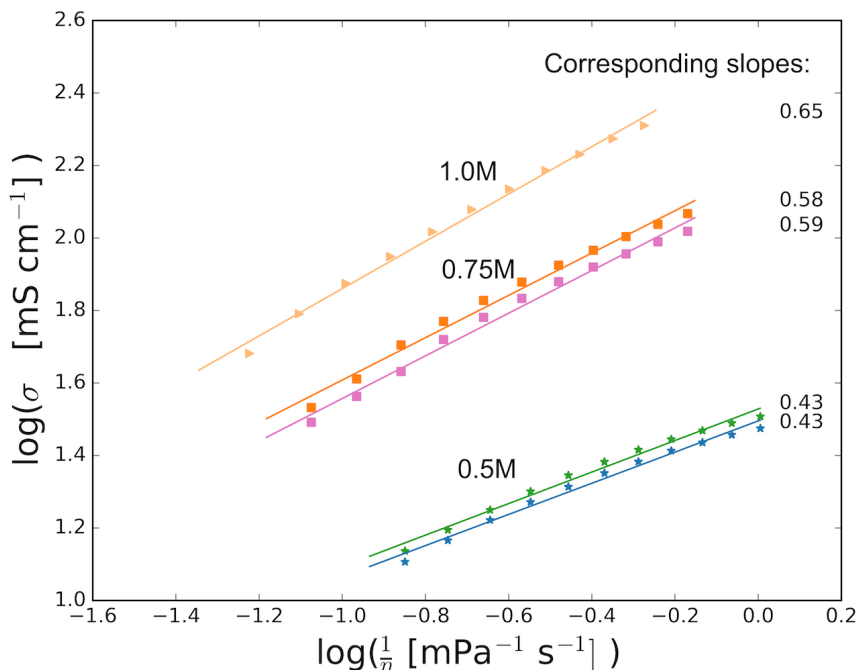


**Figure 4.4:** Walden plots for a NaPF<sub>6</sub> diglyme electrolyte at three different concentrations.

The measured temperature/viscosity/conductivity data can be found in Appendix E. That the tested electrolytes do not conform to a Walden behaviour could indicate a non-vehicular transport mechanism. With only three concentrations of NaPF<sub>6</sub> investigated, it becomes difficult to evaluate any specific concentration dependence of such a behaviour. Future studies should extend the range of concentrations to further investigate this behaviour.

## 4.3 ESW of the Diglyme-based Electrolyte

After confirming good ionic conductivity of the considered electrolyte, the electrochemical stability window of 1 M NaPF<sub>6</sub> in diglyme was further investigated; for use in a SIB, a good electrolyte will show a satisfactory electrochemical stability, without pronounced oxidation or reduction. Experiments performed to evaluate the ESW of the electrolyte are presented below.

### 4.3.1 Oxidative Stability of Diglyme-based Electrolyte

During a linear voltage sweep, using Na as a reference electrode, the two major extraction peaks of NVPF, appear for 1 M  $\text{NaPF}_6$  in both  $\text{EC}_{50}:\text{DMC}_{50}$  and in diglyme (Figure 4.5). The peaks are followed by an onset of oxidative decomposition for the diglyme-based electrolyte at 4.47 V, indicated by the intersection between the dashed green and solid orange line at  $50 \mu\text{Acm}^{-1}$ . That the shoulder appearing is related to oxidative decomposition is indicated both by a high current, that no other Faradic process can provide, and by a appreciable gas-release when opening the cell.

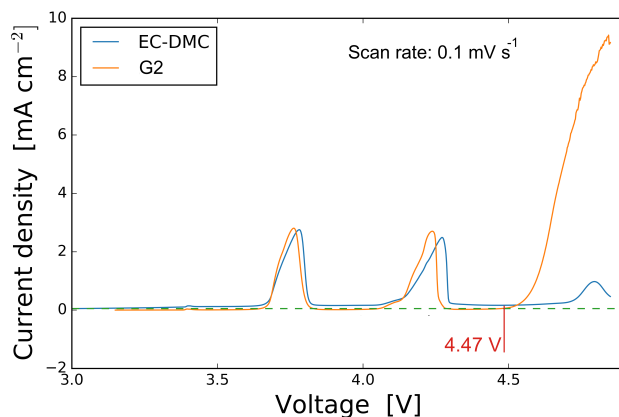


**Figure 4.5:** Linear sweep voltammogram for 1 M  $\text{NaPF}_6$  in diglyme (Blue) and 1 M  $\text{NaPF}_6$  in  $\text{EC}_{50}:\text{DMC}_{50}$  (Orange), respectively.

For 1 M  $\text{NaPF}_6$  in  $\text{EC}_{50}:\text{DMC}_{50}$  there is no appreciable oxidation in the voltage window explored. The peak at the end of the scan is related to the start of the extraction of the final Na from the NVPF, beginning at  $\approx 4.6$  V—further explained in appendix B. That the oxidation potential for diglyme is higher than the extraction potentials of the NVPF is important for a stable cycling behaviour when assembling half and full cells using NVPF as an active material. Comparing the electrolytes it is obvious that the diglyme-based electrolyte is less stable against oxidation than the  $\text{EC}_{50}:\text{DMC}_{50}$ -based one. However, a too high oxidative stability is redundant since it in many cases would be related to a poorer reductive stability.

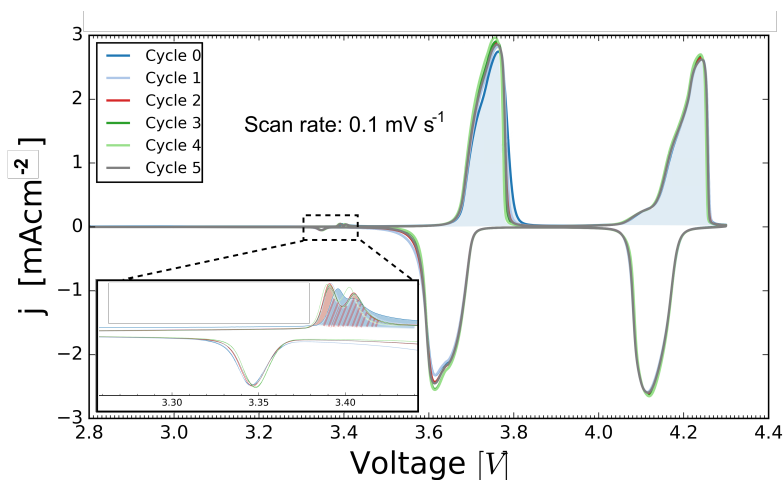


**Figure 4.6:** Cyclic voltammograms showing 5 cycles from a half cell of NVPF using 1 M  $\text{NaPF}_6$  in diglyme. Inset: Magnification at 3.4 V to visualise small features with related surface charge densities listed in figure header.

Returning to Figure 4.5, a tiny peak appears at 3.4 V vs.  $\text{Na}^+/\text{Na}^\circ$ . To analyse and to further understand the insertion/extraction behaviour of the cathode, a CV was recorded cycling NVPF 5 times below the oxidative stability limit. The total surface charge density that was available from the major extraction peaks amounts to  $3708 \text{ mC cm}^{-2}$  (Shaded blue region of large peaks in Figure 4.6). The minor featured, is a peak appearing at 3.4 V (Figure 4.6 inset). The shaded blue and red regions in the inset demonstrate the charge per unit surface area extracted during the first ( $120 \text{ mC cm}^{-2}$ ) and second discharge ( $17 \text{ mC cm}^{-2}$ ), respectively—the mixed colour region representing their overlap. The peak area is larger during the first cycle than for subsequent cycles while it, after the first charge, seems very reversible. A partly reversible peak at 3.4 V is indicative of a NVP contamination inside the NVPF, NVP having exactly this insertion potential. During the first charge the small peak corresponds to 3 % of the total charge available (including the two main extraction peaks). This number decrease decreases to 0.5 % upon subsequent charges. This could indicate that any contamination is lost or transformed. Future studies should aim towards confirming that the contamination is really NVP and its evolution upon charging, for example, by recording a XRD spectra of the electrode.

#### 4.3.2 Reductive Stability of Diglyme Electrolyte

Comparing to oxidation, reduction current densities are low when investigating reduction of 1 M  $\text{NaPF}_6$  in diglyme and in  $\text{EC}_{50}:\text{DMC}_{50}$  on Cu-foils (linear sweep voltammograms in Figure 4.7). Both densities, however, are non-negligible and well above the error of the potentiostat. The first sharp decrease for the case of  $\text{EC}_{50}:\text{DMC}_{50}$  comes from the potentiostat applying a initially defined voltage. For  $\text{EC}_{50}:\text{DMC}_{50}$  the initial voltage did not match the open circuit voltage, resulting in a voltage step leading to a capacitive effect.

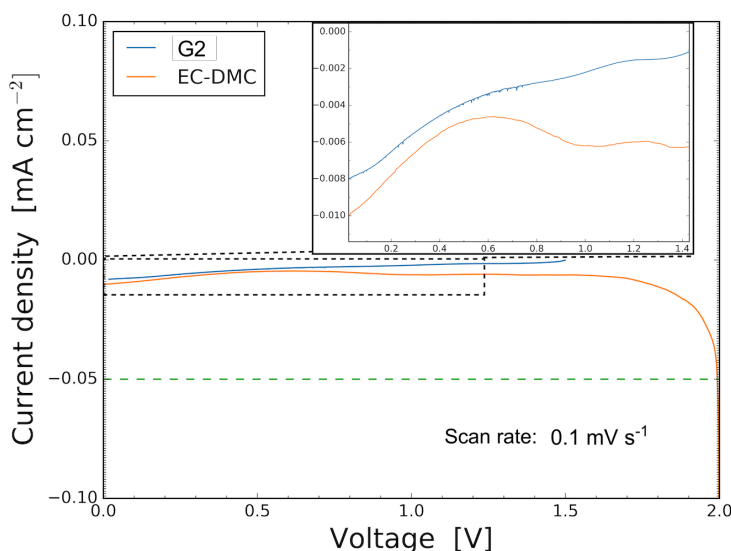


**Figure 4.7:** Linear voltammograms indicating reductive behaviour of diglyme and  $\text{EC}_{50}:\text{DMC}_{50}$  electrolytes with 1 M  $\text{NaPF}_6$  on Cu-foil. Inset: magnified part of the curve.

The remaining current after capacitive charging could indicate a reduction of the solvents. Such a reduction is obviously not associated with any fast kinetics, which would lead to much larger current densities in the voltammogram. Instead the current could arise due to the formation of stable reduction products slowly leaving the surface, exposing it to new solvent. Speaking against such an interpretation is the miss-match between the data

and previous work in literature presenting cycling experiments with both EC<sub>50</sub>:DMC<sub>50</sub> and diglyme as a solvent. Such work has been concluded that EC<sub>50</sub>:DMC<sub>50</sub> forms a rather stable SEI [51, 30], preventing further reduction. SEI formation has also been linked to the reversible plating/stripping of Na on Cu-foils [60]. A clear SEI-formation should be associated with a distinct increase of the current density followed by a distinct decrease arising from the passivation of the electrode. An SEI formation resulting from EC reduction could be attributed to the tiny peak appearing for EC<sub>50</sub>:DMC<sub>50</sub> at 1V vs Na<sup>+</sup>/Na<sup>°</sup>, preceding a slight decrease in current density. However, even after accounting for a SEI-formation, the current density is still non-zero and matches that of the diglyme cell. The reductive effect thus seems independent of the solvent used.

Following previous literature and assuming a formed SEI should, at least locally in the voltammogram, decrease the current, the observed reduction must instead arise due to something else than the degradation of the electrolyte. The current could be related to reduction of organic species left at the surface of the Cu foil, contaminations, slowly reaching the cathode or perhaps a small intercalation of Na species in any impurity of silicon or lead. Future experiments should aim to use Cu-foil with a higher purity than the one used here. The lack of clear evidence for reduction of the diglyme should be compared to the calculated reduction potentials of the same substance, at various degrees of complexation with Na<sup>+</sup><sup>2</sup>. All potentials are below 0V vs. Na<sup>+</sup>/Na<sup>°</sup>, featuring high to moderate activation energies ( Table 4.1), indicating that reduction of diglyme complexes in solution are not thermodynamically favourable. The calculated potentials further point towards the reduction currents observed coming from other processes.

Type of complexation	Bond	Red. potential vs. Na <sup>+</sup> /Na <sup>°</sup> (V)	E <sub>a</sub> (eV)
G2	C <sub>1</sub> -O <sub>1</sub>	-1.14	0.767
	O <sub>1</sub> -C <sub>2</sub>	-1.21	0.774
	C <sub>3</sub> -O <sub>2</sub>	-1.12	0.728
[NaG2] <sup>+</sup>	C <sub>1</sub> -O <sub>1</sub>	-0.07	1.02
	O <sub>1</sub> -C <sub>2</sub>	-0.21	0.847
	C <sub>3</sub> -O <sub>2</sub>	-0.11	0.841
[Na(G2) <sub>2</sub> ] <sup>+</sup>	C <sub>1</sub> -O <sub>1</sub>	-0.21	0.392
	O <sub>1</sub> -C <sub>2</sub>	-0.32	0.667
	C <sub>3</sub> -O <sub>2</sub>	-0.29	0.672

**Table 4.1:** Reduction potentials and activation energies, E<sub>a</sub>, for diglyme at different levels of complexation with Na<sup>+</sup>.

## 4.4 Characterising Loss and Performance

The indications of a good match between the ESW of 1 M NaPF<sub>6</sub> in diglyme with the redox potentials of HC and NVPF, motivated using the electrolyte in prototype cells with NVPF and HC. The electrode pair is a candidate for a future SIB since it renders a relatively high energy density. In this section, cycling experiments of full and half cells assembled using 1 M NaPF<sub>6</sub> in diglyme, with NVPF as a cathode material and HC as an anode material, are presented.

<sup>2</sup>*ab-initio* calculations made by Piotr Jankowski at Chalmers University of Technology.

#### 4.4.1 Half Cell Capacity/Voltage Profiles

For HC, the slope and plateau regions are clearly distinguishable, while the NVPF shows two clear plateaus, when cycled in half cells using 1 M NaPF<sub>6</sub> in diglyme and Na reference electrode (Figure 4.8). It can further be observed that both materials suffer from an initial irreversibility. For the NVPF, the initial irreversibility of 3%, related to the loss of the 3% (by charge) NVP contamination that was described in Section 4.3.1. For the HC, it is much larger (23 %) and should be attributed to some initial parasitic process, perhaps an SEI formation, consuming Na. It could also be related to an initial loss of active material.

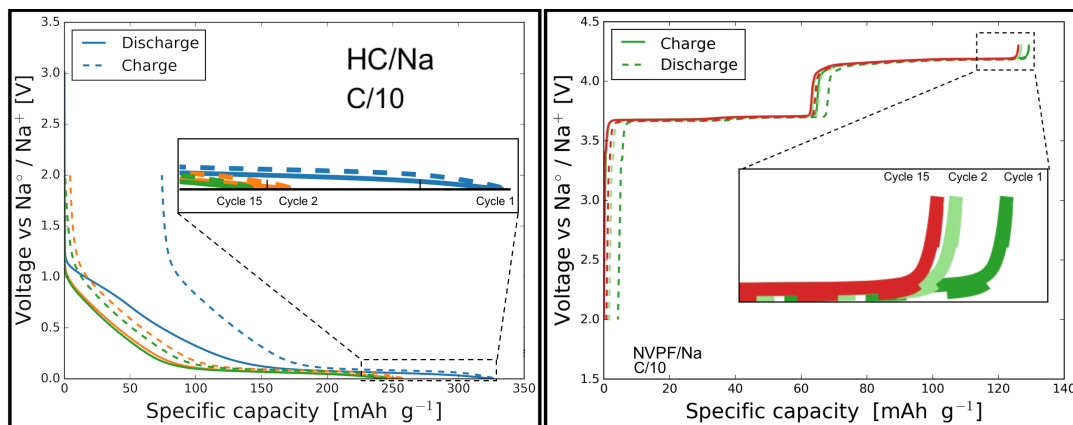


**Figure 4.8:** Typical cell profiles of half cells cycled in a diglyme 1 M NaPF<sub>6</sub> in diglyme

Differential capacities helps with further interpretation of the data. In the case of NVPF, there is little difference among cycles, and three clear peaks are shown—the first two relating to the two first sub-plateaus of the material and the third one relating to the second main plateau (Figure 4.9).

HC instead shows an initial sloping region in the differential capacity curve, relating to the slope seen in the charge profile. Then comes a sharp peak relating to the insertion plateau of Na into the carbon. Worth noting is that during the first charge, there is a small peak appearing at around 1.02 V. A conventional attribution of the peak would be to the formation of an SEI coming from the reduction of the electrolyte during the first cycle, but since there is already a doubt that there is any reduction of the electrolyte, such an interpretation is not necessarily correct. Other electrochemical reactions or an initial phase transformation of the HC may also contribute. Any future work should try to confirm if the size of the peak observed is consistent when changing solvent so as to determine if it is a solvent non-specific process.

#### 4.4.2 Full Cell Capacity/Voltage Profiles

Full cells of NVPF and HC could prove to make up tomorrow's SIBs. However, for commercialisation and use in a sustainable energy system, an electrolyte offering stable cycling performance is needed. In this section the cycling behaviour of full NVPF|HC cells is presented and compared to the half-cell behaviour. From full cell profiles recorded at first, second and 41<sup>st</sup> cycle in a galvanostatic cycling experiment show how the corresponding half cells contribute to the different regions seen (Figure 4.10 **A**). A sloping region in the beginning arises because of the sloping part of the HC. Then comes a sharp rise associated with change of NVPF plateau, the plateau also appearing in the differential capacity curve as a small peak at 3.4 V during the first charge (inset in Figure 4.10 **B**). The sharp rise is followed by an almost flat plateau associated with the matching of the upper NVPF plateau and the lower HC plateau.

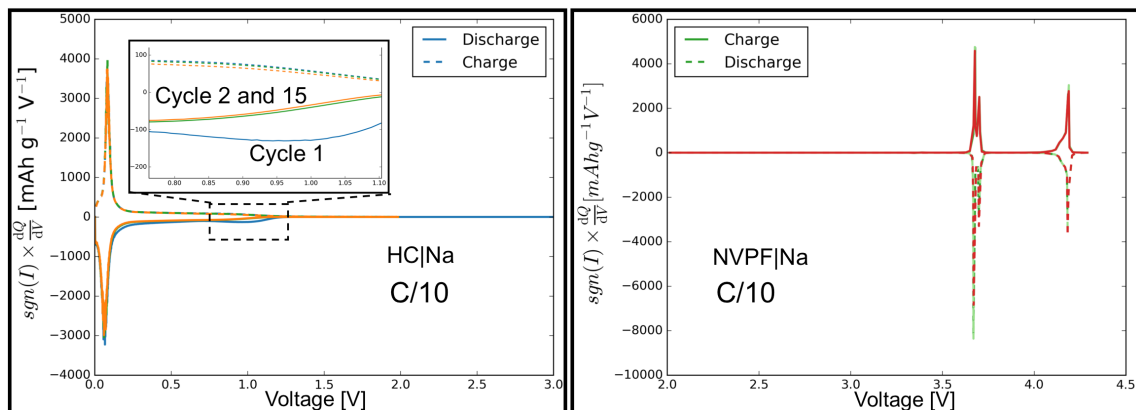


**Figure 4.9:** Differential capacity curves of half cells cycled in a diglyme 1 M  $\text{NaPF}_6$  in diglyme.

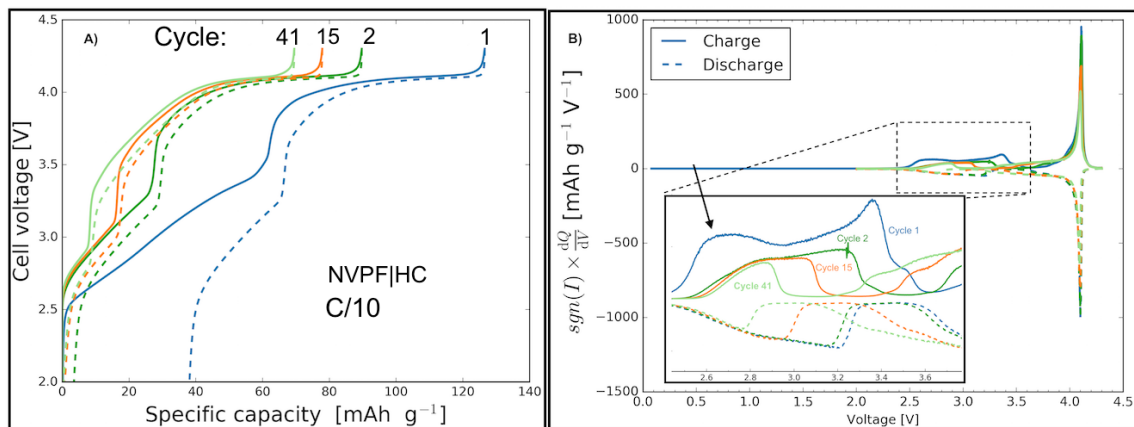


**Figure 4.10:** Typical cell profile in a cycled full cell using 1 M  $\text{NaPF}_6$  in diglyme with corresponding differential capacities. Inset: visualisations of small features. The capacities are plotted in terms of the weight of cathode material, making comparison easier between half and full cells.

Returning to the differential capacity curve, there is a peak appearing at a cell voltage of around 2.6 V during the first charge (arrow in Figure 4.10). The peak is not related to the initial intercalation into the HC plateau since it does not appear during subsequent cycles. It is thus associated with the initial irreversibility, amounting to  $\approx 37 \text{ mAh g}^{-1}$  in the full cell. Remembering that a similar feature was present in HC half cell at around 1V vs  $\text{Na}^+/\text{Na}^\circ$ , a reconstruction of half cell profiles was utilised to find the approximate cathode and anode half cell potentials when the full cell voltage was 2.6 V. The cell reconstruction confirmed that the anode should have a potential of  $\approx 1.06\text{V}$  vs.  $\text{Na}^+/\text{Na}^\circ$ , thus relating very well to the initial irreversibility seen in HC.

Any extra capacity arising from the 3 % NVP present in the cathode could also have been responsible for a part of the initial full cell peak. However, the cell reconstruction indicated that the cathode voltage was already 3.68 V vs.  $\text{Na}^+/\text{Na}^\circ$  for the peak in the full cell differential capacity curve. The NVP-related peak appearing at 3.4 V vs.  $\text{Na}^+/\text{Na}^\circ$  in the CV-measurement could thus only contribute at even lower full cell voltages.

### 4.4.3 Comparing Full and Half Cell Capacity Retention

Capacity retention is one of the most important factors that will deem if a future NVPF|HC cell using diglyme as an electrolyte solvent will be commercially viable. For the diglyme-based cell,  $\approx 30\%$  of the capacity is lost during the first cycle, which is followed by a continuous specific capacity fade of  $\approx 0.45 \text{ mAh g}^{-1}$  per cycle (Figure 4.11 **A**). The same figures for a setup using EC<sub>50</sub>:DMC<sub>50</sub> as a solvent are  $\approx 19\%$  and  $\approx 0.15 \text{ mAh g}^{-1}$  per cycle, respectively (Figure 4.11 **B**)<sup>3</sup>. 1 M NaPF<sub>6</sub> in diglyme both has a worse initial irreversibility and a worse long term capacity retention when compared to Na LP30 equivalent.

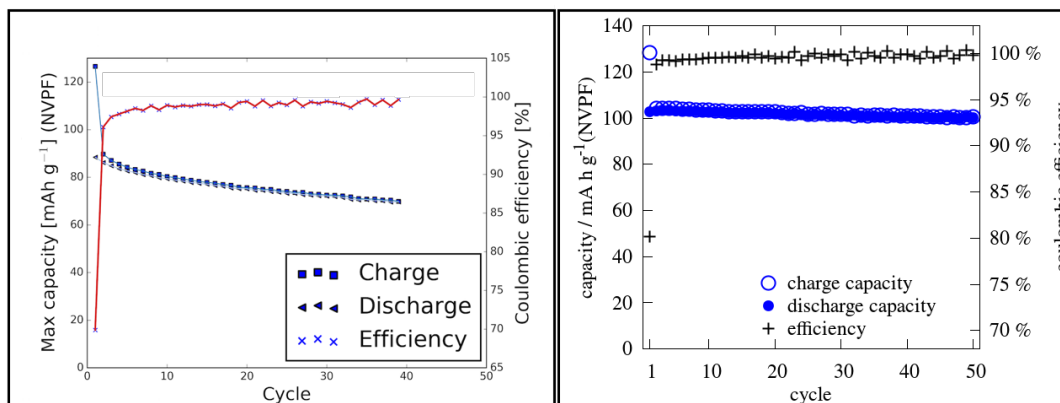


**Figure 4.11:** Capacity retention and coulombic efficiency per cycle of full cells, using 1 M NaPF<sub>6</sub> in diglyme (**A**) or 1 M NaPF<sub>6</sub> in EC<sub>50</sub>:DMC<sub>50</sub> (**B**).

Comparing the capacity fade per cycle in full and half cells using 1 M NaPF<sub>6</sub> in diglyme, full cells degrade much faster than any of the half cell setups (Figure 4.12), seen both from the total specific capacities (**A**) and the discharge capacities normalised to the first discharge (**B**). The capacity fade difference between full and half cells is not strange on its own; half cells have a practically unlimited supply of Na from the Na metal anode. Any discharge capacity loss in half cells must instead relate to a loss of active material, decreasing the number of intercalation sites. Such a loss could be both due to a disconnection of the material or because of irreversible phase transitions of the active material. From the relative capacity fade plots (Figure 4.12 **B**) we note that approximately 30 % of the total discharge capacity fade in the full cell could be accounted for by the loss of HC active sites. However, the capacity fade is not entirely transferable, since if there were other parasitic processes of comparable magnitude, a loss of intercalation sites in the HC could be unimportant if the amount of available Na was always less than the number of available sites. In any case, the half cell capacity establishes an upper limit for capacity retention of full cells.

Loss of NVPF material, does not seem to contribute anything to the continuous capacity fade in full cells, judging from its very stable half-cell cycle performance. A lack of NVPF-loss is also indicated by the asymmetric loss between the characteristic lower/upper NVPF plateaus in full cells (Figure 4.13). A symmetrical loss of the plateaus would indicate cathode material loss. Here, however, only the lower plateau is lost, indicating that it is the anode material or any chemical processes which is consuming Na.

<sup>3</sup>Data provided by Romain Dugas, CdF.

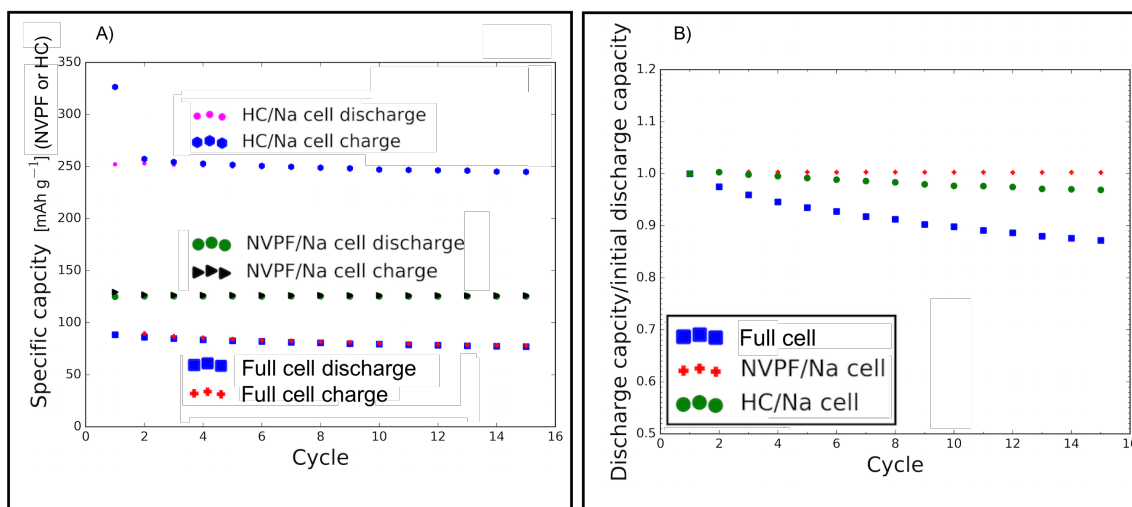


**Figure 4.12:** A), total specific capacities and, B), specific discharge capacities normalised by discharge capacity on first cycle for full and half cells of NVPF and HC. Setup using a 1 M  $\text{NaPF}_6$  diglyme electrolyte.

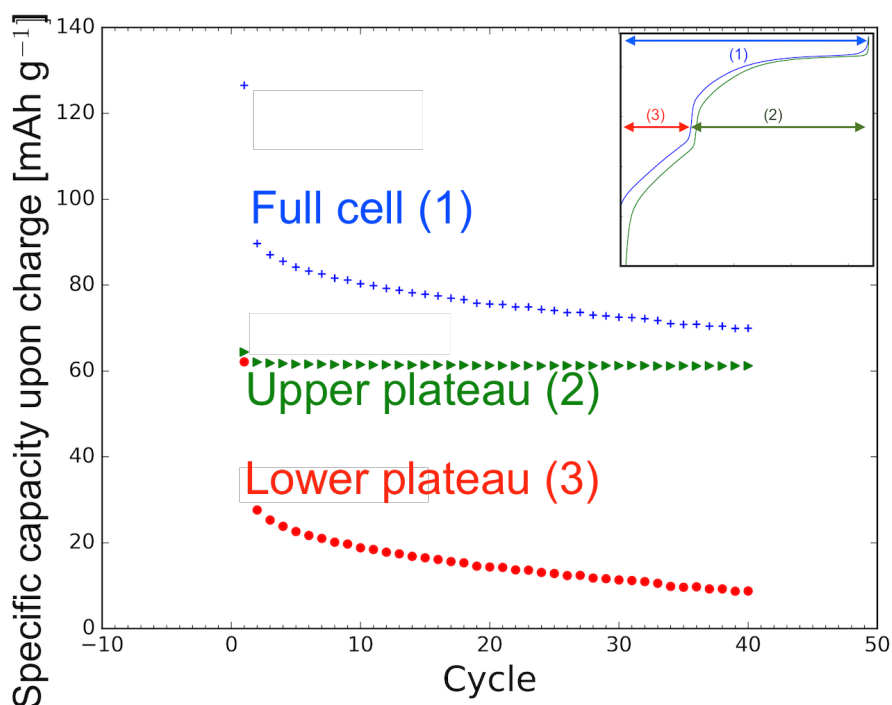


**Figure 4.13:** Evolution of the two plateaus in the full cell with cycling. Inset: Legend to what parts of the full cell are denoted by upper plateau, lower plateau and full cell.

#### 4.4.4 Comparing Efficiency and Irreversibility of Full and Half Cells

It is apparent that half cell capacity, because of the nearly unlimited Na supply, can not tell the full story about what is causing the capacity fade in full cells, using diglyme as an electrolyte solvent. What could provide more details are the cycle coulombic efficiencies, which relate to how much charge is lost between charge and discharge. Efficiencies of HC half cells using 1 M NaPF<sub>6</sub> in diglyme have a higher efficiency than corresponding NVPF cells, which, in turn, are higher than full cell efficiencies (Figure 4.14 A). The recombined full cell efficiency<sup>4</sup>,  $\eta_f$ , lays between that of HC and NVPF in half cells. The difference in efficiencies indicate that any parasitic processes happening at HC are less pronounced than their NVPF counterparts. The lower half-cell efficiency of NVPF is not necessarily equivalent to the NVPF contributing more to the full cell capacity fade, since it could also relate to other overcharging processes that are occurring, such as oxidation of the salt anion, which would not remove any Na-ions.

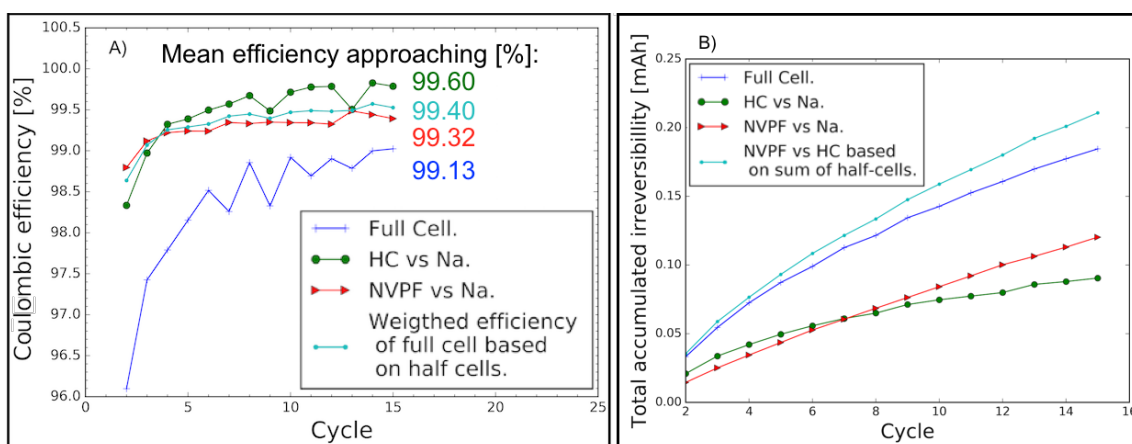


**Figure 4.14:** Actual and recombined efficiencies and accumulated irreversibilities for half and full cell.

If instead the accumulated irreversibilities of half and full cells are compared, using the full cell electrode masses, there is a trend suggesting that full cell capacity loss is related to the irreversibility in NVPF at each cycle (Figure 4.14 B). If not taking the NVPF into account, the total irreversibility of the full cell can not be fully accounted for. If the NVPF irreversibility is instead added, there is a very good match between the full cell accumulated irreversibility at the first cycles. Then, however, the measured and reconstructed full cell data sets separate. Worth noting in the plot is that the first cycle is excluded to avoid taking the initial large irreversibility of carbon, that only serves to shifts the HC line (green) upwards, making comparison less straightforward.

Why the recombined data in figures 4.14 A) and 4.14 B) predict different behaviour the full cells—in one case better and in one case worse than the real cell—can be related to the kind of processes they take into account. When calculating the efficiency it is assumed that all irreversibility is equally divided across the whole voltage range. A half cell measurement where the initial part of the intercalation is associated with more irreversibility than the

<sup>4</sup>Calculated as

$$\eta_f = \frac{m_{HC}^{full} \eta_{HC}^{half} + m_{NVPF}^{full} \eta_{NVPF}^{half}}{m_{HC}^{full} + m_{NVPF}^{full}}$$

, where  $m$  denotes the mass of active material,  $\eta$  denotes the coulombic efficiency, and the subscripts and superscripts indicate electrode type and cell setup (half or full), respectively.

the final intercalation stages will penalise the final efficiency exactly as much as a cell where irreversibility is the same per unit of differential voltage change.

If there was an uneven distribution of loss in the HC used, the combination of half cell coulombic efficiencies would constantly overpredict the full cell coulombic efficiency. Since in the full cells, there is a surplus capacity available at the anode due to non-perfect balancing between electrodes, the initial voltage/capacity region of HC would be given a higher importance than the later region, thus decreasing the apparent coulombic efficiency if the initial region was associated with more loss. For the accumulated irreversible capacity the opposite would be true: the added irreversibilities would constantly under-predict the full cell value. The reason for under-prediction is that, even if the efficiency for a HC electrode in half cells was high, the total amount of irreversibility would be greater in the half cells than in the full cells, since more Na was intercalated in the material. More intercalated species would in turn lead to more species potentially contributing to parasitic processes. The comparatively higher irreversibilities would add up and lead to the diverging measured and added full cell irreversibilities seen in Figure 4.14 **B**). Since the difference between recombined efficiency and accumulated irreversibility is observed, it is suggested that the slightly unbalanced HC anode is responsible for capacity fade. Since NVPF should not contribute directly to capacity fade (no Na is consumed here) it is also possible that some systems effects exists in full cells—contributing to lowering the efficiency at each cycle.

#### 4.4.5 Performance at Different Voltage Regions of the Cathode and Anode

As was argued Section 4.4.4, a loss at the electrodes not being spread evenly across the voltage range would lead to a difference between full and half cells, especially when having a slightly unbalanced full cell system. Aiming to gain further insight into the potential dependence of the capacity fade in NVPF|HC cells using 1 M NaPF<sub>6</sub> in diglyme, the different voltage regions of the active materials here explored. The naming convention for these regions are found in Figure 4.15.

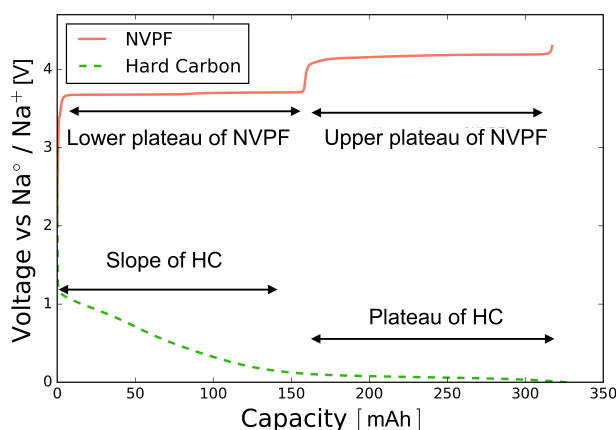


**Figure 4.15:** Convention when naming the different voltage regions for a fully balanced system. Based on half cell profiles.

Judging from total specific capacities (Figure 4.16 **A**)) and normalised capacities ( Figure 4.16 **B**)), no cycling scheme manages to fully stabilise the system (Table 4.2) and no scheme is more stable than 1 M NaPF<sub>6</sub> in EC<sub>50</sub>:DMC<sub>50</sub>, plotted as a reference. Cycling of of the upper plateau of NVPF, after initially charging past the lower plateau, leads to a much lower coulombic efficiency than the regular setup. Also the associated capacity fade

is faster. For cycling the lower plateau the opposite behaviour is true: The efficiency is higher than for the symmetric electrode balancing and associated capacity fade is lower.

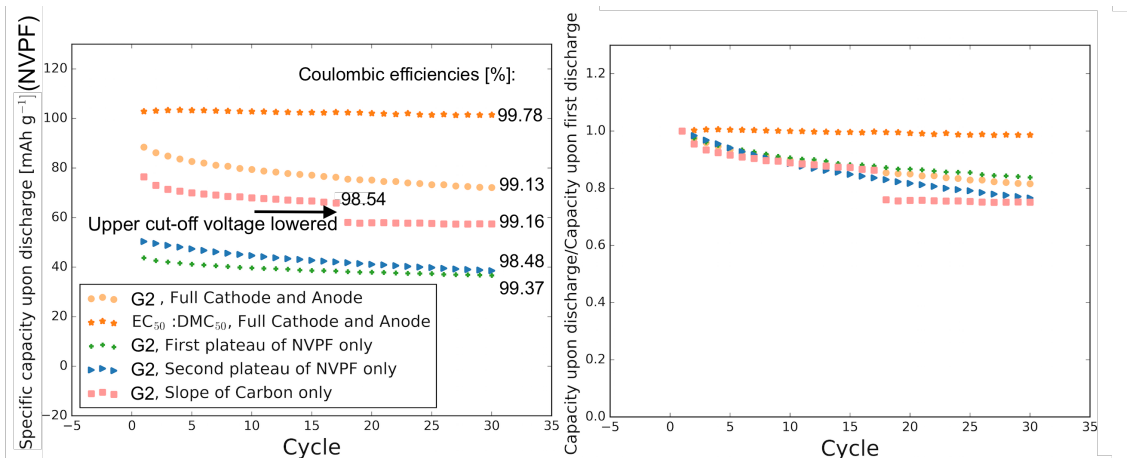


**Figure 4.16:** Specific capacity retention when exploring different regions of the electrode materials

The reason for the coulombic efficiency,  $\eta_c$ , being low in the case of cycling the upper plateau of NVPF is probably related to the overcharging phenomena experienced in half cells. By cycling the lower plateau of NVPF only, overcharging is avoided, making the coulombic efficiency higher. The oxidative stability of the electrolyte is thereby brought into new light; oxidation of the solvent, not appreciable in cyclic voltammetry measurements (Section 4.3.1) may be taking place even at lower potentials than those previously found. By lowering the cathode potential the oxidation effect is minimised, thus increasing  $\eta_c$ . A lower degree of oxidation might also be responsible for the cycling performance of the HC slope and the increase in coulombic efficiency experienced when lowering the cell cut-off voltage. A lowered cell cut-off voltage both increases the final potential of the HC, and lowers the final potential of the NVPF. With a lower potential of the NVPF, the oxidative effect on the cathode seems to be partly avoided, thus increasing the efficiency.

Before lowering the cut-off, the capacity retention and initial irreversibility of using the HC slope in a full cell are the worst so far measured, indicating that any parasitic process occurring at the anode is active already in the sloping region. If the irreversibility would have been related only to the plateau region, it would instead have been avoided by just cycling the slope. These results are consistent with the discussion in Section 4.4.4 and adds to the picture of the slope of the HC being worse than the plateau of the same material, partly explaining why actual full cell efficiencies are worse than reconstructed ones.

#### 4.4.6 Another voltage range—NVP|NVP-cells

As a measure to explore yet another potential range, a NVP|NVP cell was tested using 1 M NaPF<sub>6</sub> in diglyme. The result is a very low capacity loss with a high coulombic efficiency (Figure 4.17 and lower part of Table 4.2). Since the type of electrode has been changed for this setup, it is hard to say if the stability arises due to a change in structure/composition of the electrode or if it comes from only the higher anode potentials/lower cathode potentials. However, the NVP|NVP cell shows that it is possible to build stable systems using a diglyme-based electrolyte. Also it tells us that the electrolyte is at least stable in the potential range of NVP, either used as a cathode or as an anode.

Electrode system	Region cycled	Estimated potential range Cathode / Anode [V vs $Na^+/Na^\circ$ ]	$\eta_c$ [%]	$I_{initial}$ [%]	Comment
NVPF HC	NVPF plateaus, HC slope and plateau	[2-4.35]/[0.05 - 2]	99.13	29	-
NVPF HC	NVPF plateaus, HC slope and plateau	[2-4.35]/[0.05 - 2]	99.78	19	<b>EC:DMC-</b> based electrolyte
NVPF HC	Upper plateau of NVPF only, HC Slope and Plateau	[3.8-4.3]/[0.05 - 0.2]	98.42	- *	Mostly HC plateau is used, NVPF completely discharged on first cycle to reach second plateau
NVPF HC	Lower plateau of NVPF only, HC slope and plateau	[2-3.8]/[0.0 - 2.0]	99.37	31	-
NVPF HC	Both NVPF plateaus, HC slope only	[2-4.3]/[0.06 - 1.95]	98.48	40	-
NVPF HC	Both NVPF plateaus, HC slope only	[0.2-4.2]/[0.1 - 2.0]	99.17	-	Upper cut-off voltage of scheme above lowered after 16 cycles
NVP NVP	Full cathode and anode mode	[2-3.4]/[1.6-2]	99.91	8.7	One NVP is used as anode and one as cathode. Polarisation of 232 mV.

**Table 4.2:** Initial irreversibility ( $I_{initial}$ ) and coulombic efficiencies ( $\eta_c$ ) when cycling different regions of HC and NVPF in a 1 M  $NaPF_6$  diglyme electrolyte using a full cell setup. The potential ranges have been estimated using half-cell reconstruction upon first charge.

\*: Not comparable since cell is not discharged fully.

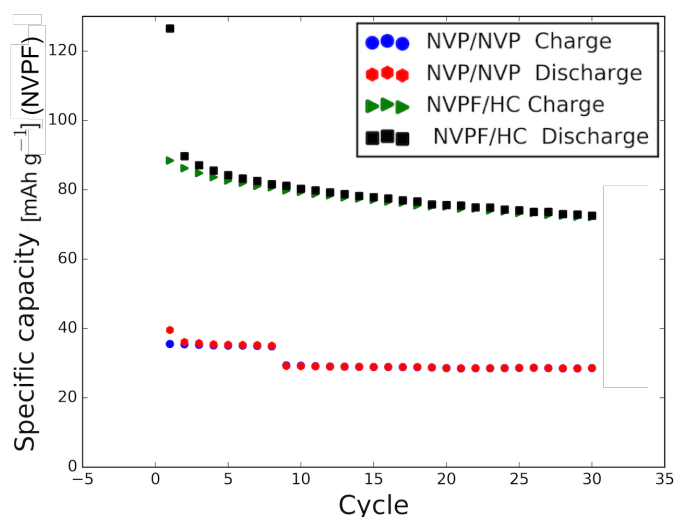


**Figure 4.17:** Specific capacity retention for a NVP|NVP cell as compared to the NVPF|HC full cell.

## 4.5 Investigating Degradation Mechanisms

Realising there was capacity loss in full cells assembled using a diglyme 1 M NaPF<sub>6</sub> electrolyte, seeming especially related to the anode, the individual capacity fade, of the HC electrode was investigated. Arguably, any source of capacity fade that should be understood, and improved upon, since it would increase the total performance of full cells. Furthermore, the more parasitic reactions that could be eliminated, the easier it would be to find the remaining ones—hopefully allowing us to fully stabilise a full-cell systems.

### 4.5.1 GC/MS Analysis of Degradation Products in Cycled Cells

An important feature to understand was the large initial irreversibility, amounting to 30% in full cells. Explanation models for other electrolytes have attributed such a loss to the initial formation of an SEI, growing through reduction of the electrolyte. Any reduction, forming an SEI or not, could possibly also be coupled to a formation of soluble decomposition products. Investigating such decomposition products, cycled separators from full and half cells were analysed using a GC/MS setup.

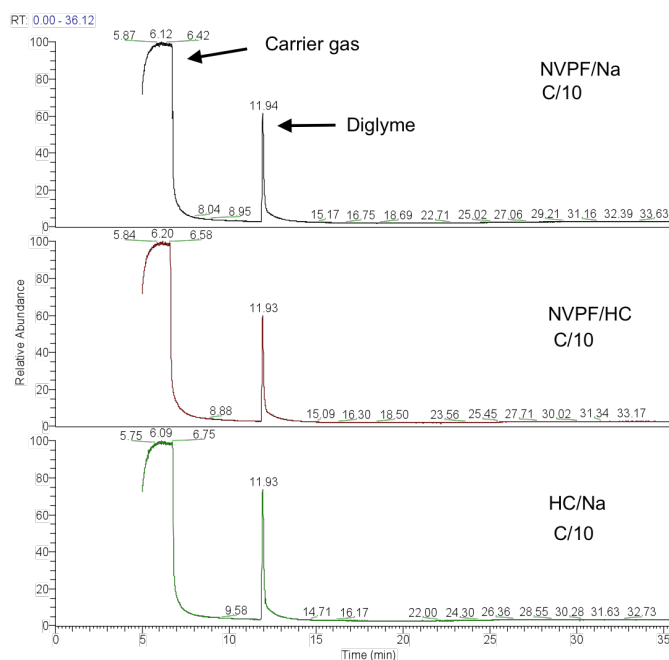


**Figure 4.18:** Gas chromatograms from experiment aiming to analyse soluble non-charged degradation products from cycled cell separators.

The resulting chromatograms indicated no soluble light, non-charged, reduction products—the only peak appearing being those from the carrier gases and that from diglyme (Figure 4.18). A lack of peaks is not definitive evidence for a lack of electrolyte reduction. Reduction products could be salts, either meaning that they would not be dissolved, or that they would not be gasified at the injection point of the GC. Also the reduction products could be radicals, polymerising to form large oligomers that would lay beyond the detection range of the GC/MS setup. The analysis does, however, indicate which reduction pathways are still possible. Together with DFT calculations (Section 4.3.2) and the realisation that there is no continuous gas release from Na-contacted electrolyte (Section 4.1.1), one can suggest possible remaining reduction pathways. Mapping out available pathways could further help in investigating if the initial irreversibility arises because of solvent reduction and an associated SEI formation.

### 4.5.2 Reduction Schemes for Diglyme

Even if the DFT calculation, presented in Section 4.3.2, did not indicate any reduction of diglyme in solution at the potential of Na metal or sodiated HC, reduction schemes were drawn to gain further insight into which reduction products that are possible. Before going deeper into any decomposition mechanism, one detail has to be clarified: all reduction steps for a certain type of molecule will be considered to be mutually exclusive; if the breaking of one bond is the most energetically favourable, it is this bond and no other that will be considered broken.

For reductive scissioning of the C<sub>1</sub>-O<sub>1</sub> bond—the weakest according to DFT calculations—the reduction scheme predicts a methyl radical and a Na-salt (Figure 4.19). The methyl radical can further pick up environmental hydrogen to form methane (<1> in Figure 4.19) or react with another methyl radical to form ethane (<2>), both entering the gas phase. That we can only have gas phase species should be related to the gas evolution experiments in the Section 4.1.1.

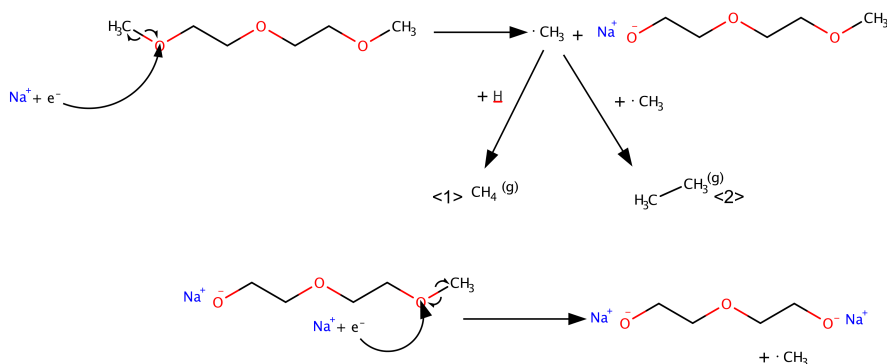


**Figure 4.19:** Reduction scheme based on the breaking of the C<sub>1</sub>-O<sub>1</sub> bond in the diglyme molecule.

Assuming reduction of the solvent takes place and it propagates through the mechanism in Figure 4.19, there would be a gas release. The reasons that could be responsible for only seeing a tiny, or possibly no, continuous gas release from the Na surfaces could then be the following:

- The salts predicted result in a very stable SEI preventing further gas release.
- There is no reduction of the diglyme solvent.

If instead assuming that reduction progresses by scissioning of the O<sub>1</sub>-C<sub>2</sub>-bond, a more diverse chemistry is possible. To make a further distinction for the sake of clarity, we can divide the reduction into two cases: one where we assume there is environmental hydrogen available and one where there is not. If there is no available hydrogen, the reduction scheme (Figure 4.20) predicts the formation of Na methoxide, a salt probably soluble in diglyme—the solvent being amphiphilic and the salt being soluble in polar solvents such as ethanol or methanol. The methoxide anion, being a nucleophile, could attack the ends of the diglyme molecule, yielding dimethyl ether (<3>) or it might just reform diglyme molecule. The radical formed during the first reduction could, react with other similar radicals of the same sort. By reducing the end groups successively there could be the formation of the oligomers (<4>) seen in the lower right part of Figure 4.20. The salts and oligomers formed might, furthermore, be insoluble, rendering a stable SEI, or they could

be soluble. In either case none of the experimental techniques used so far could indicate their existence. However, if there was evolution of dimethyl ether, the salt rendered would have to be insoluble and passivate the surface, otherwise the continuous gas release would be detected.

Continuing with the case of available environmental hydrogen, the chemistry is even richer and some more assumptions will have to be made to reduce complexity. Apart from any reduction only breaking one type of bond, it is assumed that all  $C\cdot$ -type radicals will pick up a hydrogen directly further reduction. If a specie is a gas at room temperature, then it will be assumed to leave its environment and not react any further. It is also assumed that Na methoxide and Na ethoxide are soluble. In the associated reduction scheme species that are likely to be soluble because of their short chain length and/or similarity to diglyme are denoted by "(sol)" (Figure 4.21). Based on the properties discussed, all pathways that lead to continuous gas evolution (detected as pressure increase) or as soluble species (detectable by the GC/MS) have been crossed out. The resulting pathways are those that can possibly exist in an SEI with a possible small initial gas release, or in the solution if related with no gas release.

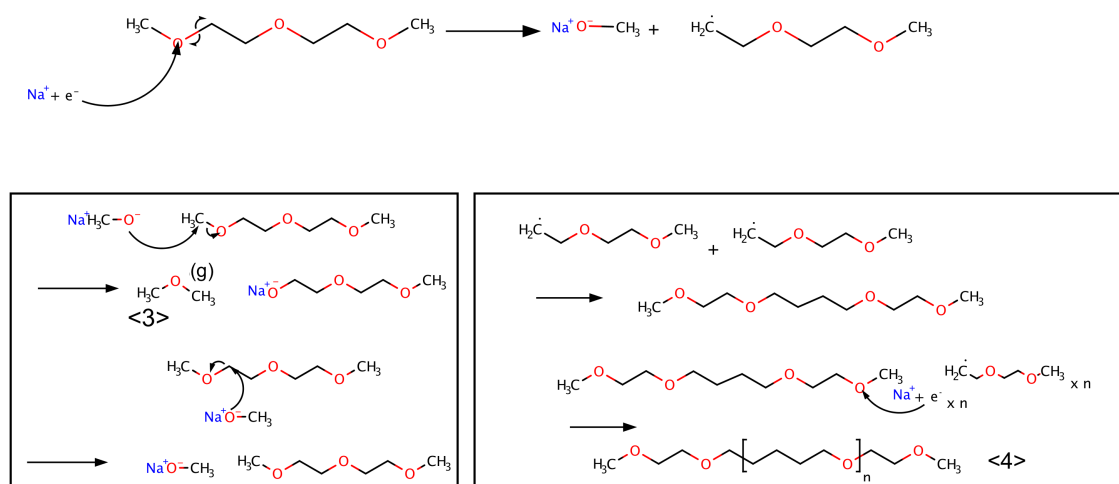


**Figure 4.20:** Reduction scheme based on the breaking of the  $\text{O}_1-\text{C}_2$  bond in the diglyme molecule assuming that no environmental hydrogen is available.

To further narrow down the reduction scheme, future work should aim to test the solubility in diglyme of those Na salts that, in the process of their formation, also yield gases. If a salt was soluble, the corresponding processes could be eliminated from the scheme. To be completely certain that the assumptions made are correct, also solubility of Na ethoxide and Na methoxide in diglyme should be evaluated. An attempt could also be made to apply a complementary technique, such as NMR or EPR, in solution, for detecting possibly remaining reduction products.

#### 4.5.3 FTIR of Cycled HC Anodes

Realising that there still were some candidates that could be associated with a SEI formation because of diglyme degradation, FTIR spectroscopy was employed to study of HC surfaces that had been cycled 2 times with the hope of detecting any change in surface chemistry during cycling. In the resulting spectra there is very little difference between cycled electrodes and those that have been soaked in electrolyte and left to dry (Figure 4.22).



Some peaks are disappearing in the band between  $1000\text{ cm}^{-1}$  and  $1100\text{ cm}^{-1}$  when going from a soaked electrode to a cycled electrode. The peaks could arise due to the longer time allowed for the cycled electrodes to dry, causing more solvent evaporation, thus removing corresponding peaks from the spectrum. An attempt was made to pair the seen peaks in both spectra to the NIST database [70] entry of diglyme. However, none of the peaks had a direct match. One explanation could be that what is left on the surface after excess solvent evaporation are diglyme/Na complexes and that such complex tends to shift the IR spectra of the diglyme molecules. Either it is only such complexes left on the surface or they cover the signal from any SEI. It can, however, be concluded that solely based on the spectra in Figure 4.22 there seems to be no indication of an appreciable SEI forming during the two first cycles. With longer cycling, a supposedly weak interface signal could improve, in spite of cycling experiments suggesting that it is the first two cycles that are associated with the most SEI formation, if any. Also in a future experiment it could be tried to wash the surfaces in excess diglyme solvent before recording the spectra, so as to remove any residual salt/glyme complexes.

#### 4.5.4 Surface Structure of Pristine and Cycled HC

Trying to visually confirm any SEI formation relating to the initial irreversibility of HC, SEM micrographs of pristine and cycled electrodes were recorded. Micrographs of pristine HC clearly image both the grains of HC (green contour in Figure 4.23), distributed evenly across the surface, and, smaller particles of conductive carbon (red contour). In the less magnified part of the figure also some binder is possibly seen to have formed a film on the surface. However, most of the binder will be distributed among the grains, keeping the structure together.

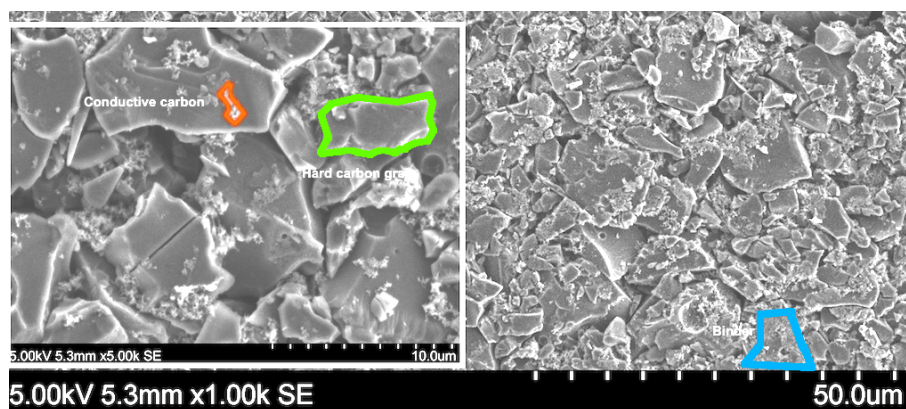


**Figure 4.23:** SEM micrographs of pristine HC. Inset: Magnifications of one part of the pristine HC surface.

Corresponding micrographs of HC after cycling 50 times in full cells appear show a lighter and a darker part of the electrode, (Figure 4.24). Upon further magnification, the lighter region (upper inset) appears to have a film formed on the surface, looking very different from the pristine electrodes. The darker area (lower inset), on the other hand, looks similar to the pristine electrode.

Because the electrode was exposed to air during transfer to the microscope, the film shown in the lighter area might relate to an inhomogeneous growth occurring during transfer. It is also possible that the film was formed during cycling and that one part was torn away when the separator was removed. For better understanding, the experiments should be repeated using a argon filled transfer chamber when mounting the electrodes in the microscope.

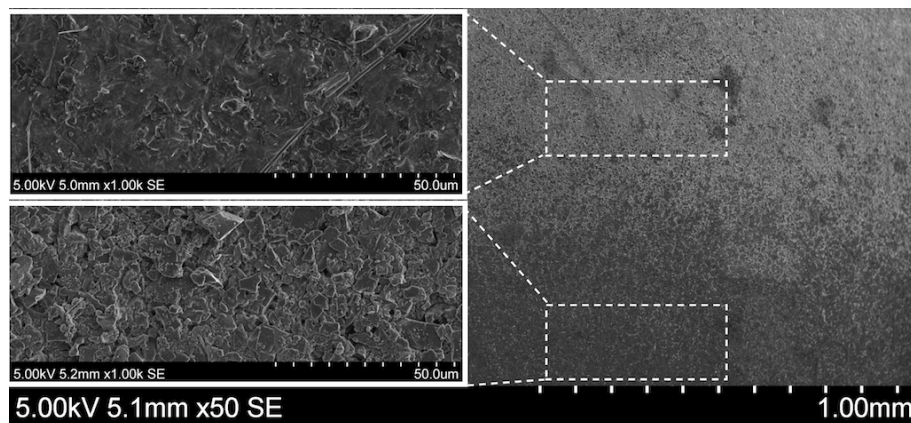


**Figure 4.24:** SEM - micrographs of a pristine HC electrode cycled in 1 M  $\text{NaPF}_6$  in diglyme for 50 cycles. Upper and lower insets: Magnifications of lighter part and darker part of surface, respectively.

#### 4.5.5 EDX of Anodes from cycled Full Cells

An EDX analysis of surface elemental composition of the cycled electrodes was also carried out. The EDX spectrum revealed unexpected vanadium present at the anodes from several cycled full cells (Figure 4.25). The spectrum can be correlated to a bluish tone observed on cycled electrode surfaces at two different occasions (Figure 4.26). Since vanadium(IV)-species often appears in bluish compounds [71], the visual inspection and SEM analysis seems to correlate well.

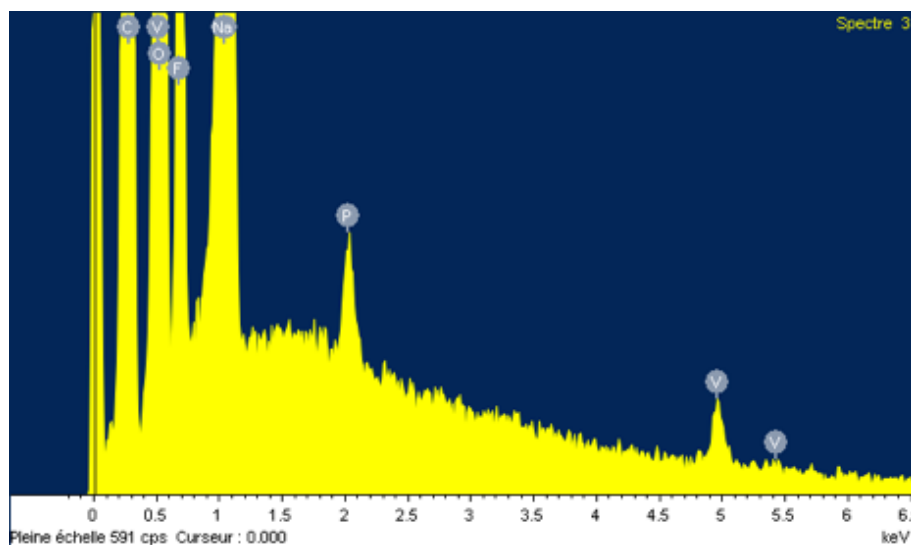


**Figure 4.25:** EDX spectrum acquired from a HC electrode cycled 1.5 times in full cell setup using a diglyme 1 M  $\text{NaPF}_6$  electrolyte.



**Figure 4.26:** Photo taken of two electrodes cycled in full cell setups showing a bluish tone as compared to the pristine electrodes.



## 4.6 Test of Binder Defluorination

Realising that the HC seemed to yield a high initial irreversibility even though there were still doubts about any reduction of the electrolyte, it was thought the binder material (PVDF) might be responsible for parts of the capacity fade, as had been proposed in earlier work [5]. Reference disks with only binder coated on a stainless steel submerged in electrolyte showed no sign of discolouration as compared to the disks with Na on one side and PVDF on the other side, stored in diglyme-based electrolyte (Figure 4.28). It can clearly be seen how the binder in the later case gives the solution a brownish hue as compared to the uncoloured EC<sub>50</sub>:DMC<sub>50</sub>-based solution. The colour is thought to arise due to a binder defluorination in the diglyme-based electrolyte. Such a chemistry would probably be similar to the kind of Na etching reported for PTFE in glyme-based solvents, also proposed in earlier works [72]. In appendix D a drawn reduction scheme for PVDF based on such etching processes.

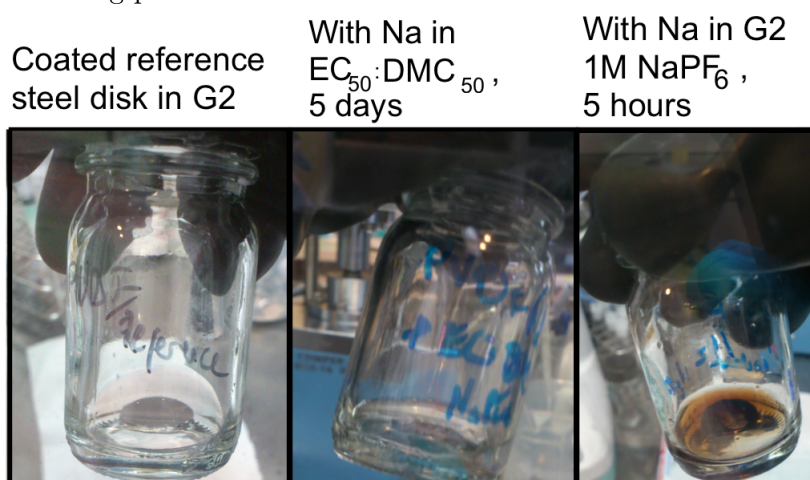


**Figure 4.28:** Results from experiment studying binder degradation. PVDF binder experiences severe reaction in when exposed to Na in diglyme based electrolyte but seems to be stable in EC:DMC based counterpart.



**Figure 4.29:** Separator showing HC disintegration after cycling.

Upon inspecting cycled separators (Figure 4.29), a similar brownish hue could be detected. Also grains of HC are seen to be stuck in the separator. The grains indicate a loss of mechanical rigidity of the electrode and is what would be expected if the binder was degraded. The reason why the same decomposition is not seen in the the EC<sub>50</sub>:DMC<sub>50</sub>-based solution could be due to this electrolyte forming a protective film at the interface between the binder and the steel disk. Another reason could be that the diglyme could be better at dissolving any reduction products (i.e. NaF), thus continuously exposing new bonds for defluorination. Even if the binder in EC<sub>50</sub>:DMC<sub>50</sub>-based electrolyte doesn't show any apparent degradation, the results should lead to a general questioning of using PVDF binder in SIB systems. PVDF binder degradation might also provide another explanation to why cycling tests with NVP|NVP cells were stable: here the electrodes were powders and contained no binder.

Binder reduction could be directly and indirectly responsible for the initial and partial irreversibilities seen in HC half cells and NVPF|HC cells. The direct effect can be evaluated assuming that the binder makes up 4 % of the anode, weighting 4.9 mg and that active material makes up 90% of the cathode, weighting 9.6 mg. The resulting ratio between F-C bonds and available Na is approximately 1:6 ((C-F):Na)). Even though this figure does not match a 30 % initial irreversibility in full cells and half cells, the indirect effect of having a weakened binder should be considered as well. A weakened binder would probably lead to some disconnection of the active material, also contributing to the initial irreversibility.

## 4.7 Visual Summary of Degradation Mechanisms

In Figure 4.30 the proposed degradation mechanisms for a NVPF|HC cell using 1 M NaPF<sub>6</sub> in diglyme are summarised: A), charging, Na starts to intercalate in HC. B), Na defluorinates the PVDF binder, promoted by diglyme, forming NaF, and an SEI is formed. Both mechanisms may contribute to the large initial irreversibility observed at 1 V vs. Na<sup>+</sup>/Na<sup>0</sup>. Furthermore, V<sup>4+</sup> ions are dissolved, either due to NVP contamination (more probable) or directly from the NVPF (less probable), possibly promoted by diglyme. C), if no SEI is formed, NaF is possibly dissolved. If an SEI is formed it does not prevent further defluorination. In any case binder is lost, weakening the structural integrity of the electrode, leading to, D), active material disconnecting from the electrode. Vanadium ions reaching the anode starts to reduce intercalated Na.

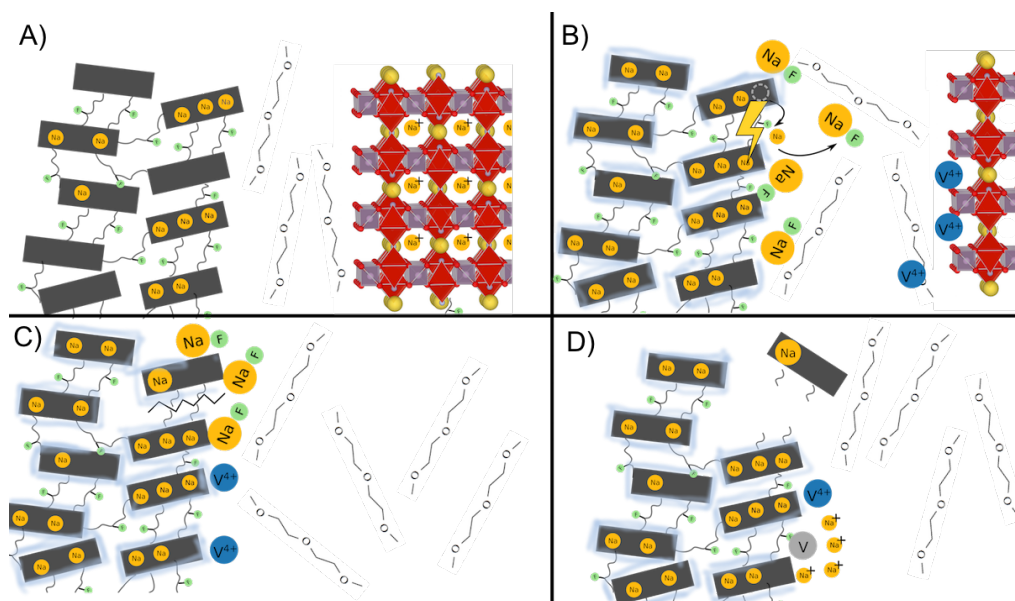


**Figure 4.30:** Different mechanisms occurring sequentially from right to left, top to bottom, that are contributing to system capacity fade.

# 5

## Conclusions and Outlook

The SIB field is still young, with many challenges left to solve to optimise commercial cells. In this thesis the use of diglyme as an electrolyte solvent with 1 M NaPF<sub>6</sub> has been evaluated for performance and redox stability with materials platforms of a NVPF or NVP cathode and a NVP or HC anode. All of these materials are currently being seriously considered for SIBs. This study has shown that:

- Na metal electrodes can be used as stable reference electrodes, when using 1 M NaPF<sub>6</sub> in diglyme, important for future work on SIBs within academia.
- NVPF|HC cells using 1 M NaPF<sub>6</sub> in diglyme experiences a larger initial irreversibility (30%) than cells employing EC<sub>50</sub>:DMC<sub>50</sub> (19%). This irreversibility originates from the HC side and occurs at a potential of 1.06 V vs Na<sup>+</sup>/Na<sup>0</sup>. For continued cycling, diglyme results in higher capacity fade ( $\approx 0.45$  mAh g<sup>-1</sup> per cycle) than for EC<sub>50</sub>:DMC<sub>50</sub> ( $\approx 0.15$  mAh g<sup>-1</sup> per cycle).
- NVP|NVP cells using 1 M NaPF<sub>6</sub> in diglyme experiences small initial irreversibility (8%) and almost no continued capacity fade. Coulombic efficiency for these cells were  $\approx 99.91\%$ .
- The ionic conductivity three differently concentrated diglyme-based electrolytes of NaPF<sub>6</sub> was satisfactory for SIBs. The conductivity did not conform to a regular Walden behaviour.
- The reductive stability of 1 M NaPF<sub>6</sub> in diglyme was high according to DFT calculations. LSV, testing reductive stability on Cu-foils indicated a reduction process, but lacking any distinct SEI-formation, it should come from parasitic processes.
- There are no clear indications of an SEI being formed based on data from both IR spectroscopy of cycled anode surfaces and from GS/MS analysis of cycled separators.
- The oxidative stability of 1 M NaPF<sub>6</sub> in diglyme appears high from LSV, when using NVPF as a working electrode. However, for full cells, cycling of the upper NVPF plateau yielded large irreversibilities.
- About 3% of the available capacity in the NVPF electrodes, initially comes from a process occurring at 3.4 V vs Na<sup>+</sup>/Na<sup>0</sup>, likely from a NVP present.
- By exploring different potential-regions of the active materials, a larger part of the irreversible capacity upon cycling comes from the slope of the HC.
- There exists a cross-talk mechanism, where vanadium ions deposit on the anode, as detected by a colour change and through EDX analysis. The vanadium ions arise due to an initial phase transformation of the NVP impurity in the NVPF.

- The PVDF binder reacts with Na when using diglyme as an electrolyte solvent but not when using EC<sub>50</sub>:DMC<sub>50</sub>. This points towards diglyme promoting binder defluorination and thus, even if the initial irreversibility in HC half cells occurring at 1.06 V could be attributed to SEI formation, binder defluorination may explain a large a large part of both the initial and subsequent irreversibility.

These results directs future research involving diglyme towards:

- Determining possible degradation products, to conclude if there the solvent reduces. This could for example be done by NMR or EPR analysis.
- Construct NVP|HC and NVPF|NVP cells with 1 M NaPF<sub>6</sub> in diglyme to further evaluate if NVPF|HC cells experience problems with anodic or cathodic stability.
- Further investigating the oxidative stability. This could be done by further LSV experiments, using other working electrodes than NVPF.
- Using different binders to avoid defluorination.
- Further investigating the conduction mechanisms concentration dependence of ionic conductivity/viscosity and coupling this to spectroscopic studies of ion-pairing in solution.
- Further understanding and confirming any vanadium dissolution mechanism. This should be done by studying the high voltage behaviour of pure NVP.
- Use 1M NaPF<sub>6</sub> in diglyme and cycle only the plateau of the HC to see if the mesoporous region of HC is related to less irreversibility than the graphitic/nanoporous regions.

Based on the work at hand it is still to early to say if diglyme will be a component in tomorrows SIBs. By removing parasitic processes mentioned above, it might still be possible to build a high performing SIB system using diglyme as a solvent. If this can be confirmed, practical aspects such as toxicity and cost will also have to be evaluated more thoroughly and weighed towards any potential gains that could be acquired from using the solvent studied.

# Bibliography

- [1] B. W. Jaskula. Lithium Statistics and Information, 2016. <http://minerals.usgs.gov/minerals/pubs/commodity/lithium/mcs-2016-lithi.pdf>, Accessed 2016-05-20.
- [2] Gachot *et al.* Gas chromatography/mass spectrometry as a suitable tool for the li-ion battery electrolyte degradation mechanisms study. *Anal. Chem.*, 83(2):478, 2011.
- [3] K Momma and F Izumi. *VESTA 3* for three-dimensional visualization of crystal, volumetric and morphology data. *J. Appl. Crystallogr.*, 44(6):1272–1276, 2011.
- [4] Saravanan *et al.* The First Report on Excellent Cycling Stability and Superior Rate Capability of  $\text{Na}_3\text{V}_2(\text{PO}_4)_3$  for Sodium Ion Batteries. *Adv. Energy Mater.*, 3(4):444–450, 2013.
- [5] K. Kubota and S. Komaba. Review—Practical Issues and Future Perspective for Na-Ion Batteries. *J. Electrochem. Soc.*, 162(14):A2538–A2550, 2015.
- [6] Yudanov M., Palm C., Ögren L., and Chalmers University of Technology Westman K., Bachelor Thesis. Catalysts for a more efficient splitting of water, 2014.
- [7] Lepoivre *et al.* Long-Time and Reliable Gas Monitoring in Li-O<sub>2</sub> Batteries via a Swagelok Derived Electrochemical Cell. *J. Electrochem. Soc.*, 163(6):A923–A929, 2016.
- [8] Ecolé Polytechnique de Montréal. One-metal eh vs ph pourbaix diagram, 2016. [www.crct.polymtl.ca/ephweb.php](http://www.crct.polymtl.ca/ephweb.php), Retrieved 10 May 2015.
- [9] S. Tang and H. Zhao. Glymes as versatile solvents for chemical reactions and processes: from the laboratory to industry. *RSC Adv.*, 4(22):11251, 2014.
- [10] Tesla Motors. Powerwall | The Tesla Home Battery. [https://www.teslamotors.com/sv\\_SE/powerwall](https://www.teslamotors.com/sv_SE/powerwall), Accessed 2016-05-27.
- [11] Grosjean *et al.* Assessment of world lithium resources and consequences of their geographic distribution on the expected development of the electric vehicle industry. *Renewable and Sustainable Energy Reviews*, 16(3):1735–1744, 2012.
- [12] Peter H. Stauffer and James W. Hendley II. Rare Earth Elements, Critical Resources for High Technology | USGS Fact Sheet 087-02. <http://pubs.usgs.gov/fs/2002/fs087-02/>, accessed 2016-05-20.
- [13] Ponrouch *et al.* Non-aqueous electrolytes for sodium-ion batteries. *J. Mater. Chem. A*, 3(1):22–42, 2015.

- [14] Ponrouch *et al.* In search of an optimized electrolyte for na-ion batteries. *Energy Environ. Sci.*, 5(9):8572–8583, 2012.
- [15] Geoffroy. *et al.* Electrolytic characteristics of ethylene carbonate–diglyme-based electrolytes for lithium batteries. *Electrochim. Acta.*, 45(13):2019–2027, 2000.
- [16] K. Nishio and N. Furukawa. Practical Batteries. In *Handbook of Battery Materials, Second Edition*, pages 27–85. Wiley-VCH Verlag GmbH & Co. KGaA, 2011.
- [17] Damien Monti, Chalmers University of Technology, Chalmers tekniska högskola, Condensed Matter Physics (Chalmers) Department of Physics, and Kondenserade materiens fysik (Chalmers) Institutionen för fysik. Innovative electrolytes for safer sodium-ion batteries, 2016. Doctoral thesis.
- [18] Ma. Winter and R. J. Brodd. What Are Batteries, Fuel Cells, and Supercapacitors? *Chem. rev.*, 104(10):4245–4270, 2004.
- [19] M. Armand and J.M. Tarascon. Issues and challenges facing rechargeable lithium batteries. *Nature*, 414(6861):359–367, 2001.
- [20] Rajagopalan *et al.* Fast charging: An in-depth look at market penetration, charging characteristics, and advanced technologies. In *Electric Vehicle Symposium and Exhibition (EVS27), 2013 World*, pages 1–11. IEEE, 2013.
- [21] R. A. Huggins. *Advanced Batteries*. Springer US, Boston, MA, 2009.
- [22] Sony Corporation. Sony Global - Sony History Chapter13 Recognized as an International Standard. <http://www.sony.net/SonyInfo/CorporateInfo/History/SonyHistory/2-13.html#block3>, accessed 2016-03-30.
- [23] M. R. Palacin. Recent advances in rechargeable battery materials: a chemist’s perspective. *Chem. Soc. Rev.*, 38:2565–2575, 2009.
- [24] Gordon S. Fulcher. Analysis of recent measurements of the viscosity of glasses. *J. Am. Ceram. Soc.*, 8(6):339–355, 1925.
- [25] Sun *et al.* Effect of Structure on Transport Properties (Viscosity, Ionic Conductivity, and Self-Diffusion Coefficient) of Aprotic Heterocyclic Anion (AHA) Room-Temperature Ionic Liquids. 1. Variation of Anionic Species. *J. Phys. Chem. B*, 119(48):15030–15039, 2015.
- [26] Pallavi Verma, Pascal Maire, and Petr Novák. A review of the features and analyses of the solid electrolyte interphase in li-ion batteries. *Electrochim. Acta.*, 55(22):6332–6341, 2010.
- [27] Weadock *et al.* Determination of mechanical properties of the SEI in sodium ion batteries via colloidal probe microscopy. *Nano Energy*, 2(5):713–719, 2013.
- [28] D. Aurbach. Review of selected electrode–solution interactions which determine the performance of Li and Li ion batteries. *J. Power Sources*, 89(2):206–218, 2000.
- [29] Gachot *et al.* Gas chromatography/fourier transform infrared/mass spectrometry coupling: a tool for li-ion battery safety field investigation. *Anal. Methods*, 2014.
- [30] Eshetu *et al.* Comprehensive Insights into the Reactivity of Electrolytes Based on Sodium Ions. *ChemSusChem*, 2016.

- 
- [31] Dugaset *et al.* Optimization of Na-Ion Battery Systems Based on Polyanionic or Layered Positive Electrodes and Carbon Anodes. *J. Electrochem. Soc.*, 163(6):A867–A874, 2016.
- [32] Hong *et al.* Charge carriers in rechargeable batteries: Na ions vs. li ions. *Energy Environ. Sci.*, 6(7):267–281, 2013.
- [33] Palomares *et al.* Update on na-based battery materials. a growing research path. *Energy Environ. Sci.*, 6:2312–2337, 2013.
- [34] Yabuuchi *et al.* Research development on sodium-ion batteries. *Chem. rev.*, 114(23):11636, 2014.
- [35] D. A. Stevens and J. R. Dahn. The mechanisms of lithium and sodium insertion in carbon materials. *J. Electrochem. Soc.*, 148(8):A803, 2001.
- [36] A. Ponrouch, A.R. Goñi, and M. R. Palacín. High capacity hard carbon anodes for sodium ion batteries in additive free electrolyte. *Electrochem. Commun.*, 27:85–88, 2013.
- [37] D. A. Stevens and J. R. Dahn. High Capacity Anode Materials for Rechargeable Sodium-Ion Batteries. *J. Electrochem. Soc.*, 147(4):1271–1273, 2000.
- [38] Han *et al.* A comprehensive review of sodium layered oxides: powerful cathodes for na-ion batteries. *Energy Environ. Sci.*, 8:81–102, 2015.
- [39] C. Masquelier and L. Croguennec. Polyanionic (Phosphates, Silicates, Sulfates) Frameworks as Electrode Materials for Rechargeable Li (or Na) Batteries. *Chem. rev.*, 113(8):6552–6591, 2013.
- [40] Palomares *et al.* Na-ion batteries, recent advances and present challenges to become low cost energy storage systems. *Energy Environ. Sci.*, 5:5884–5901, 2012.
- [41] Park *et al.* A Family of High-Performance Cathode Materials for Na-ion Batteries,  $\text{Na}_3(\text{VO}_{1-x}\text{PO}_4)_2\text{F}_{1+2x}$  ( $0 < x < 1$ ): Combined First-Principles and Experimental Study. *Adv. Funct. Mater.*, 24(29):4603–4614, 2014.
- [42] Zhang *et al.* Insertion compounds and composites made by ball milling for advanced sodium-ion batteries. *Nat. Commun.*, 7:10308, 2016.
- [43] Dahbiet *al.* Negative electrodes for na-ion batteries. *Phys. Chem. Chem. Phys.*, 16(29):15007, 2014.
- [44] Chou *et al.* Small things make a big difference: binder effects on the performance of Li and Na batteries. *Phys. Chem. Chem. Phys.*, 16(38):20347–20359, 2014.
- [45] Dahbi *et al.* Sodium carboxymethyl cellulose as a potential binder for hard-carbon negative electrodes in sodium-ion batteries. *Electrochem. Commun.*, 44:66–69, 2014.
- [46] Muñoz-Márquez *et al.* Composition and Evolution of the Solid-Electrolyte Interphase in  $\text{Na}_2\text{Ti}_3\text{O}_7$  Electrodes for Na-Ion Batteries: XPS and Auger Parameter Analysis. *ACS Appl. Mat. Inter.*, 7(14):7801–7808, 2015.
- [47] Tanja Wuestenberg. *Cellulose and Cellulose Derivatives in the Food Industry: Fundamentals and Applications*. Wiley-VCH, DE, 1 edition, 2015;2014;.

- [48] Lars Norlin. Metallpriser i mars [metall prices in march], 2016. <http://www.sgu.se/om-sgu/nyheter/2016/januari/metallpriserna-under-2015/>, Accessed 2016-05-15.
- [49] Mark Winter. WebElements, 2016. <https://www.webelements.com/>, Accessed 2016-05-15.
- [50] Young’s modulus, 2016. [https://en.wikipedia.org/w/index.php?title=Young%27s\\_modulus&oldid=721000447](https://en.wikipedia.org/w/index.php?title=Young%27s_modulus&oldid=721000447), accessed 2016-05-20, Page Version ID: 721000447.
- [51] Iermakova *et al.* On the Comparative Stability of Li and Na Metal Anode Interfaces in Conventional Alkyl Carbonate Electrolytes. *J. Electrochem. Soc.*, 162(13):A7060–A7066, 2015.
- [52] Jache *et al.* A comparative study on the impact of different glymes and its derivatives as electrolyte solvents for graphite co-intercalation electrodes in lithium-ion and sodium-ion batteries. *Phys. Chem. Chem. Phys.*, 2016.
- [53] Diglyme, 2015. Wikipedia, the free encyclopedia, Page Version ID: 688587904, <https://en.wikipedia.org/w/index.php?title=Diglyme&oldid=688587904>, Accessed 2016-02-26.
- [54] Kim *et al.* PubChem Substance and Compound databases. *Nucleic Acids Res.*, 44(D1):D1202–D1213, 2016.
- [55] American Chemical Society. Common Organic Solvents: Table of Properties. [https://www.organicdivision.org/orig/organic\\_solvents.html](https://www.organicdivision.org/orig/organic_solvents.html), accessed 2016-05-05.
- [56] O. Madelung, editor. *Static Dielectric Constants of Pure Liquids and Binary Liquid Mixtures*, volume 6 of *Landolt-Börnstein - Group IV Physical Chemistry*. Springer-Verlag, Berlin/Heidelberg, 1991.
- [57] Johansson *et al.* Local coordination and conformation in polyether electrolytes: Geometries of M-triglyme complexes (M = Li, Na, K, Mg and Ca) from ab-initio molecular orbital calculations. *Solid State Ion.*, 86-88:297–302, 1996.
- [58] Xia *et al.* The critical role of phase-transfer catalysis in aprotic sodium oxygen batteries. *Nat. Chem.*, 7(6):496–501, 2015.
- [59] D. Aurbach and E. Granot. The study of electrolyte solutions based on solvents from the “glyme” family (linear polyethers) for secondary Li battery systems. *Electrochim. Acta.*, 42(4):697–718, 1997.
- [60] Seh *et al.* A Highly Reversible Room-Temperature Sodium Metal Anode. *ACS Cent. Sci.*, 1(8):449–455, 2015.
- [61] B. Jache and P. Adelhelm. Use of Graphite as a Highly Reversible Electrode with Superior Cycle Life for Sodium-Ion Batteries by Making Use of Co-Intercalation Phenomena. *Angew. Chem. Int. Ed.*, 53(38):10169–10173, 2014.
- [62] Sigma-Aldrich. Sigma-Aldrich product search. <http://www.sigmaaldrich.com/france.html>, Accessed 2016-05-16.
- [63] European Chemicals Agency. Registered substances - ECHA. <http://echa.europa.eu/information-on-chemicals/registered-substances>, Accessed 2016-05-11.

- 
- [64] E. Barsoukov and J. R. Macdonald, editors. *Impedance spectroscopy: theory, experiment, and applications*. Wiley-Interscience, Hoboken, NJ, 2. ed edition, 2005.
- [65] J. B. M. Libarondi. Comparing the Capabilities of Time-of-Flight and Quadrupole Mass Spectrometers. <http://www.chromatographyonline.com/comparing-capabilities-time-flight-and-quadrupole-mass-spectrometers-0>, accessed 2016-05-16.
- [66] Linde Group. Gas chromatography. [http://hiq.linde-gas.com/en/analytical\\_methods/gas\\_chromatography/index.html](http://hiq.linde-gas.com/en/analytical_methods/gas_chromatography/index.html), accessed 2016-05-16.
- [67] Fourier transform infrared spectroscopy, 2016. [https://en.wikipedia.org/w/index.php?title=Fourier\\_transform\\_infrared\\_spectroscopy&oldid=719558915](https://en.wikipedia.org/w/index.php?title=Fourier_transform_infrared_spectroscopy&oldid=719558915), accessed 2016-05-16, Page Version ID: 719558915.
- [68] Iremakova D, Master's thesis, Institut de Ciència de Materials de Barcelona (CSIC). On the comparative stability of li and na metal anode interfaces in conventional alkyl carbonate electrolytes, 2015.
- [69] Man *et al.* Universality in oxygen evolution electrocatalysis on oxide surfaces. *Chem-CatChem*, 3(7):1159–1165, 2011.
- [70] NIST Mass Spec Data Center. Infrared Spectra. In S.E. Stein, director, editor, *NIST Chemistry WebBook, NIST Standard Reference Database Number 69, Eds. P.J. Linstrom and W.G. Mallard*. <http://webbook.nist.gov>, Accessed 2016-04-21.
- [71] J. Clark. Chemistry of Vanadium, 2013. [http://chemwiki.ucdavis.edu/Core/Inorganic\\_Chemistry/Descriptive\\_Chemistry/Elements\\_Organized\\_by\\_Block/3\\_d-Block\\_Elements/Group\\_05%3A\\_Transition\\_Metals/Chemistry\\_of\\_Vanadium](http://chemwiki.ucdavis.edu/Core/Inorganic_Chemistry/Descriptive_Chemistry/Elements_Organized_by_Block/3_d-Block_Elements/Group_05%3A_Transition_Metals/Chemistry_of_Vanadium), accessed 2016-05-13.
- [72] S. Tasker, R. D. Chambers, and J. P. S. Badyal. Surface defluorination of PTFE by sodium atoms. *J. Phys. Chem.*, 98(47):12442–12446, 1994.

# A

## Industrial Uses of Glymes With R=Me and n=1-4

Glyme name	Solvent feature	Industrial applications
Monoglyme	<ul style="list-style-type: none"> <li>• Low b.p. (85.2 °C)</li> <li>• High stability</li> </ul>	<ul style="list-style-type: none"> <li>• Production of active ingredients</li> <li>• Metal-organics</li> <li>• Electrolyte solvent for sealed Li-ion batteries</li> <li>• entrainer</li> <li>• Chromium electroplating</li> <li>• Cyanoacrylate based adhesives</li> <li>• Etching of printed circuit boards</li> <li>• Treating aluminum surfaces.</li> </ul>
Diglyme	<ul style="list-style-type: none"> <li>• High solubility for Na/K alloys</li> <li>• Chelate ligand for cations</li> <li>• Excellent stability both at high and low pH-values</li> <li>• Good solvent for Grignard reactions</li> </ul>	<ul style="list-style-type: none"> <li>• API production</li> <li>• Reaction solvent for organometallic reagents</li> <li>• Entrainer for azeotropic distillation</li> <li>• Battery electrolyte</li> <li>• Conducting thermoplastic paste</li> <li>• Solvent for teflon etchants</li> <li>• A suspension of sodium and naphthalene in G2 for destruction of polychlorinated biphenyls in transformer oil</li> <li>• Solvent in a formulation to improve the bonding of tire cord to rubber</li> <li>• Solvent in printing and inkjet inks and inkjet cartridges</li> <li>• Brake fluid</li> <li>• Paints and other coatings</li> <li>• Plastics</li> <li>• Adhesives and sealants</li> </ul>

**Table A.1:** Industrial uses of Mono- and diglyme. Directly adapted from [9]

## A. Industrial Uses of Glymes With R=Me and n=1-4

---

Glyme name	Solvent feature	Industrial applications
Triglyme	<ul style="list-style-type: none"> <li>• High b.p (218 °C)</li> <li>• Chemically inert</li> </ul>	<ul style="list-style-type: none"> <li>• Solvent for Teflon etching</li> <li>• High boiling and inert solvent for organic reactions</li> <li>• Solvent in consumer adhesives and paints</li> <li>• Components of brake fluids and paint/graffiti removers</li> </ul>
Tetraglyme	<ul style="list-style-type: none"> <li>• High b.p (275 °C)</li> <li>• High stability</li> <li>• High solubility of organic salts</li> </ul>	<ul style="list-style-type: none"> <li>• Flue gas cleaning systems</li> <li>• Solvents for production of binders for paints</li> <li>• Coalescing agent in paint formulations</li> <li>• Adhesives production</li> <li>• Electrodeposition</li> <li>• Manufacture of soldering fluxes/solder pastes</li> <li>• Adsorption liquid and gas scrubbing</li> <li>• Formulations of paint strippers and adhesive removers</li> <li>• Extraction of volatile organic compounds from solid wastes</li> <li>• Inert additive for fixation of methylated methylomelamine resins in durable-press cotton and cellulosic fabrics, an HFC/CFC lubricant</li> </ul>

**Table A.2:** Industrial uses of glymes. Directly adapted from [9]

# B

## Details of CVs From Half Cells

A from the CV of NVPF in a half cell vs. Na cycled 5 times up to 4.9 V using a EC<sub>50</sub>:DMC<sub>50</sub>/ 1M NaPF<sub>6</sub> electrolyte shows three different peaks (Figure B.1).

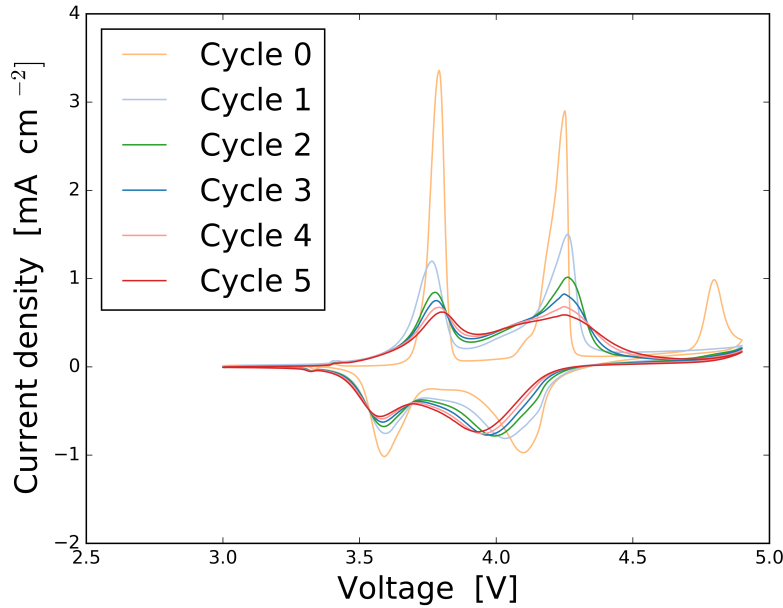


**Figure B.1:** Cyclic voltammogram from cycling an EC<sub>50</sub>:DMC<sub>50</sub>/NaPF<sub>6</sub> electrolyte beyond the third peak five times

The two first peaks are related to reversible extraction of Na. The third peak, however, is equal in shape (although not in height) but only appears on the first cycle. The fact that the capacity loss is so large after passing this peak indicates that the material undergoes an irreversible phase transformation leading to the fade. This points strongly towards the third peak being associated with the extraction of the final sodium in the NVPF. This sodium is the third atom left in the stoichiometry of the compound after the other two have been extracted.

# C

## Full Cell Reconstructions

To estimate what potentials (vs.  $\text{Na}^+/\text{Na}^\circ$ ) that each electrode in a full cell took at a specific full cell voltage, a cell reconstruction for the first cycle was employed. Such a reconstruction was done by realising that both the half cell voltages for NVPF and HC can be expressed as function of the reached specific ( $C_s$ ) or total capacities ( $C$ ), that are simply related as:

$$V_{vs.\text{Na}^+/\text{Na}^\circ} = f(C_s) = g(C_s m) = g(C) \quad (\text{C.1})$$

, where  $m$  is the mass of the electrode which was used. By interpolating the measurement data for half cells using a set of quadratic splines, thus approximating the functions  $f$  and  $g$  for both the electrodes, the full cell voltage could be recovered according to:

$$V_{reconst} = g(C^{\text{NVPF}}) - g(C^{\text{HC}}) \quad (\text{C.2})$$

where the masses used to scale the specific capacities are now those of the full cell electrodes, respectively. The scaled functions  $g(C^{\text{HC}})$  and  $g(C^{\text{NVPF}})$  can for one reconstruction be seen in Figure C.1 **A**). The resulting full cell reconstruction can instead be seen in Figure C.1 **B**), where the x-axis has been scaled back to the specific capacity, now only using the mass of NVPF.

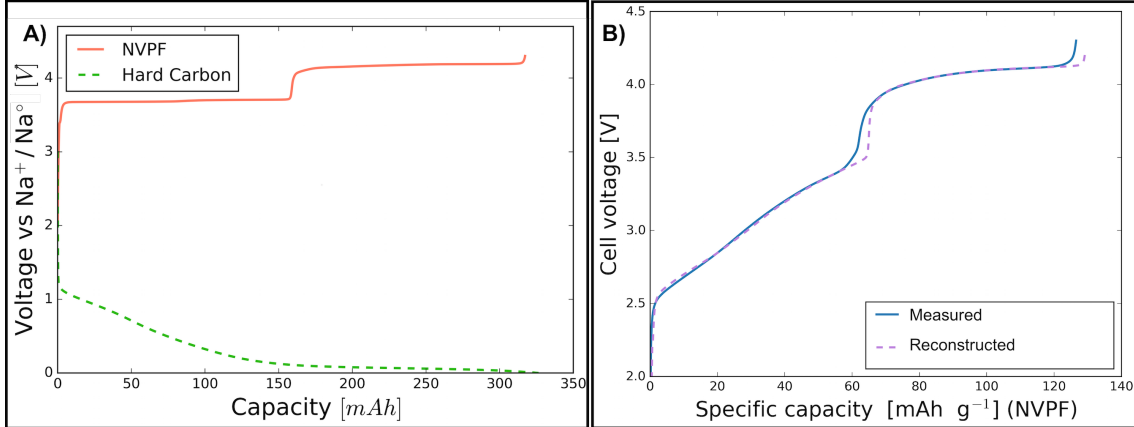


**Figure C.1:** Capacity curves

# D

## Reduction Schemes for PVDF Binder

Taking into account that both PVDF and PFTE are similar fluorinated polymers, a reduction scheme for PVDF binder was constructed based on previous work done by Tasker *et al.* on PTFE [72]. The main product predicted to be formed during reduction is NaF (Top of Figure D.1 ). The resulting radicals on the polymer chain can further in different fashions, splitting the polymers.

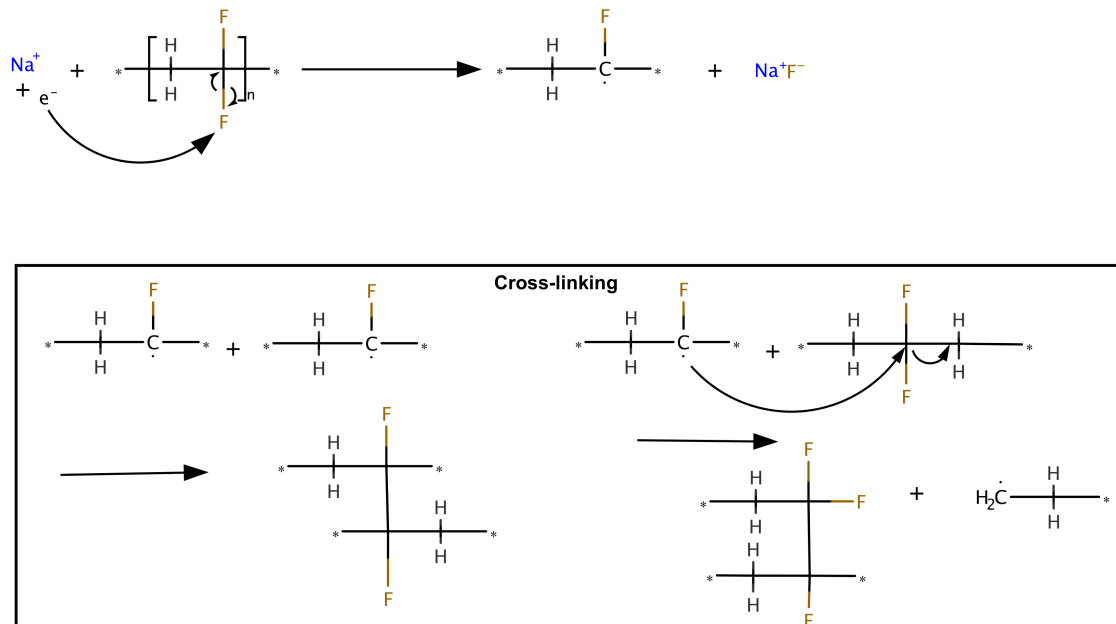
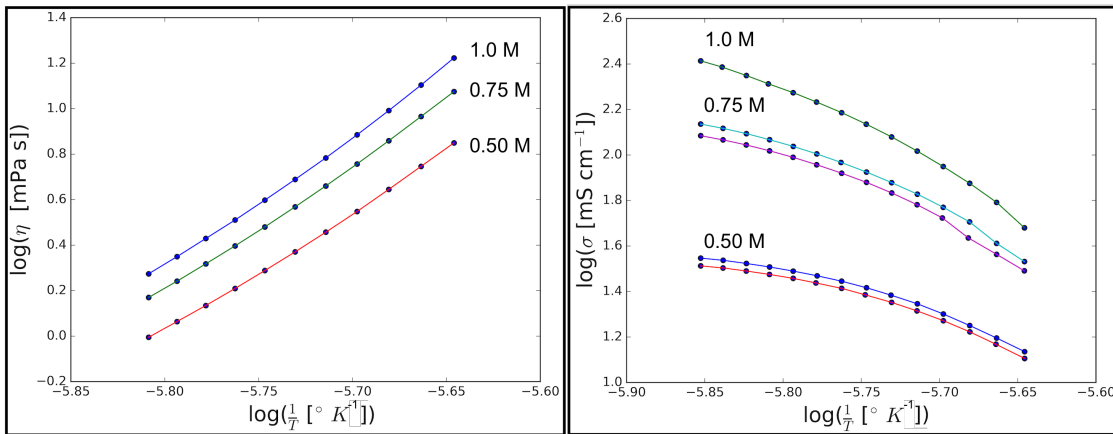


Figure D.1: Reduction scheme for PVDF binder.

# E

## Ionic Conductivity and Viscosity Data

In figure E.1 the measured values of viscosity and ionic conductivity for the different concentrations of  $\text{NaPF}_6$  in diglyme can be found as a reference.

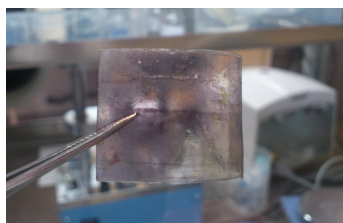


**Figure E.1:** Measured temperature dependence of Ionic conductivity and Viscosity for a G2  $\text{NaPF}_6$  electrolyte. In the case of ionic conductivity the 1 M electrolyte has only been measured once due to lack of availability.

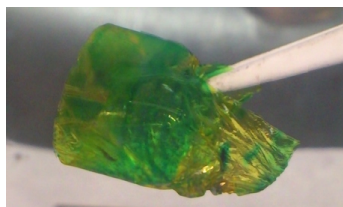
# F

## Images of Swagelok Insulating Polymers After Cycling

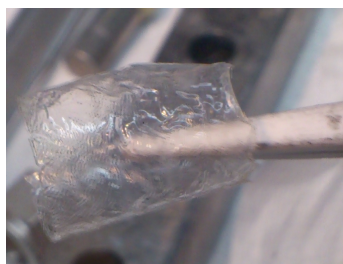
Early indications were given that full cell performance in Swagelok cells was not satisfactory when compared to equivalent coin cells. The reason for this was thought to lie in the polymer films used for insulating the cell. Both Mylar<sup>®</sup> and Kapton<sup>®</sup> films experienced a grave discolouration of purple and green, respectively, when recovered after cycling (Figure F.1, a), b) ). The nylon foil, however, showed little such discolouration (Figure F.1, c) ) indicating that this might be a better alternative for use in full cells. A rapid capacity loss was, however, still experienced for the all three types of polymer films.



(a) Mylar



(b) Kapton



(c) Nylon laminate

**Figure F.1:** Different types of polymers used as insulation in Swagelok cells comprising NVPF and HC with a G2 1M NaPF<sub>6</sub> electrolyte. Films are recovered under glovebox conditions after cycling.